IEEE Open Journal of Vehicular Technology

Received 20 October 2022; accepted 9 November 2022. Date of publication 15 November 2022;
date of current version 7 December 2022. The review of this article was coordinated by Prof. Chenhao Qi.

Digital Object Identifier 10.1109/OJVT.2022.3222187

Physical Layer Security Performance of NOMA-Aided Vehicular Communications Over Nakagami-*m* Time-Selective Fading Channels With Channel Estimation Errors

NEHA JAISWAL [1] (Student Member, IEEE), ANSHUL PANDEY [2] (Member, IEEE), SUNEEL YADAV [1] (Senior Member, IEEE), NEETESH PUROHIT [1] (Senior Member, IEEE), AND DEVENDRA SINGH GURJAR [3] (Senior Member, IEEE)

[1]Department of Electronics and Communication Engineering, Indian Institute of Information Technology Allahabad, Prayagraj 211015, India
[2]Secure Systems Research Center, Technology Innovation Institute, Abu Dhabi 9639, UAE
[3]Department of Electronics and Communication Engineering, National Institute of Technology Silchar, Cachar 788010, India

CORRESPONDING AUTHOR: ANSHUL PANDEY (e-mail: anshul@ssrc.tii.ae)

ABSTRACT This paper considers a single-input-multiple-output non-orthogonal multiple access enabled vehicular communication system, and investigates its secrecy performance over time-selective fading and channel estimation errors. We formulate two scenarios considering the decoding ability at eavesdropper, viz., 1) Scenario I: when it has sufficient decoding capability, and 2) Scenario II: when its decoding capability can be the same as the legitimate vehicles. Under such a realistic system setup, we derive the secrecy outage probability (SOP) and ergodic secrecy capacity expressions for both legitimate vehicles and the overall system under both Scenarios I and II over Nakagami-*m* fading channels. We then analyze the asymptotic SOP limits of both legitimate vehicles under Scenarios I and II, by formulating cases based on the average transmit signal-to-noise ratio and average channel gains associated with the main links and wiretap link. From the asymptotic analysis under these cases, it is observed that both legitimate vehicles do not achieve any secrecy diversity order even after leveraging the benefits of fading severity parameters and multiple antennas. We also formulate several special cases of interest to reveal some more insightful information about the system's secrecy performance. Finally, we corroborate our analytical and theoretical findings via simulation results.

INDEX TERMS Channel estimation errors, Nakagami-*m* fading channels, non-orthogonal multiple access (NOMA), physical layer security, time-varying errors, vehicular communications.

I. INTRODUCTION

The rapid proliferation of autonomous vehicles enabled with integrated communication and sensing capabilities has led to a surge in lucrative intelligent transportation system (ITS) applications [1], [2]. The ITS applications can offer better on-road safety and traffic management, infotainment services, vehicle platooning, and data services. Realizing the immense potential of ITS applications, vehicle-to-vehicle (V2V) communications form an integral part of fifth generation and beyond communication networks [3]. However, the dynamic and decentralized communication framework, along with the massive connectivity requirements in V2V networks face various challenges in the form of spectrum scarcity, estimating wireless channels, and security [4]. Recently, non-orthogonal multiple access (NOMA) technique has emerged as a potential solution to achieve efficient spectrum utilization for V2V communication networks [5], [6]. NOMA exploits power-domain multiplexing at the transmitter side to superimpose multiple user signals having power allocations in accordance to their channel conditions, and transmit the resultant signal over the

same time and frequency resources [7]. After that successive interference cancellation (SIC) technique is implemented at the receiver side to decode the superimposed signal [8]. NOMA has been shown to outperform orthogonal multiple access in terms of latency, data-rate, user fairness, and spectrum utilization [9]. However, the broadcast nature of wireless channels make the transmitted information vulnerable to various security threats, such as jamming and eavesdropping. The security concerns are further aggravated as the dynamic and decentralized architecture of such networks bring several challenges in implementing the traditional key-based cryptography infrastructure at the upper layers [10], [11].

To this end, physical layer security (PLS) can be a promising solution to complement the existing cryptographic framework. Operating independently of the existing key-based security infrastructure, PLS exploits the inherent random behavior of the physical channel (multipath fading, interference, propagation delay etc.) and uses various coding, signal design, and signal processing techniques to realize the key-less secure transmissions [11], [12], [13]. Moreover, the wireless channels become time-varying due to vehicle's mobility (Doppler spread effect) and hence experience the time-varying errors. Also, with time-varying channels, estimating the accurate channel state information (CSI) becomes complex which is an essential recipe to design reliable and secure communication schemes. However, the efforts to investigate PLS performance of NOMA-enabled V2V communications considering the time-varying channel impairments, are scarce and challenging. Accordingly, this paper investigates PLS performance of a NOMA-enabled V2V communication system under the joint impact of imperfect channel estimates and nodes' mobility.

A. RELATED WORKS

PLS performance for the power-domain NOMA-enabled communication systems has been thoroughly investigated in the literature [14], [15], [16], [17], [18], [19], [20], [21], [22], [23], [24], [25], [26], [27], [28], [29], [30], [31], [32], [33], [34], [35], [36], [37], [38], [39], [40]. Specifically, the authors in [14] have investigated the ergodic secrecy capacity (ESC) performance of NOMA systems over Rayleigh fading channels. The authors in [15] have considered the outage constraint to study the secrecy performance of a downlink NOMA system under Rayleigh fading channels. Moreover, the authors in [16] have studied the impact of imperfect SIC on the security performance of NOMA systems. The authors in [17] have studied the PLS performance of a large scale network deployment scenario comprising randomly distributed users. Recently, the authors in [18] have analyzed the security performance of NOMA-enabled Internet-of-Things (IoT) network where the users have both delay-sensitive and security requirements. The authors in [19] have studied the security performance of a NOMA network where a trusted and an untrusted user are paired together. The authors in [20] and [21] have considered the instantaneous phase shifts associated with each user and Quality-of-Service (QoS) constraints, respectively, to design a PLS scheme for the NOMA systems. Furthermore, the authors in [22], [23], [24] have proposed jamming based PLS schemes to enhance the security of NOMA systems. Moreover, artificial noise assisted PLS schemes were exploited to secure NOMA systems in [25], [26]. Moreover, the authors in [27], [28], [29], [30] have exploited the benefits of antenna selection at the base station to improve the secrecy performance of multiple-input-single-output (MISO) NOMA-enabled communication systems. Furthermore, the authors in [31] have proposed a secure beamforming strategy for MISO NOMA systems. Recently, the authors in [32] have designed a joint beamforming and power allocation scheme under Rayleigh fading channels to enhance the security of MISO NOMA system under multiple eavesdroppers. Moreover, the authors in [33], [34], [35], [36] have investigated the performance of MISO NOMA-enabled wireless networks. Also, some efforts exist in the literature to study the PLS performance of multiple-input-multiple-output enabled NOMA systems [37], [38], [39]. The authors in [40] have studied the secrecy performance of a MISO-NOMA systems under cognitive radio framework.

Albeit, all the aforesaid works [14], [15], [16], [17], [18], [19], [20], [21], [22], [23], [24], [25], [26], [27], [28], [29], [30], [31], [32], [33], [34], [35], [36], [37], [38], [39], [40] have considered non-vehicular scenario where the nodes are stationary or fixed infrastructure. To take vehicular scenario into account, the authors in [41], [42], [43], [44], [45], [46] have put some positive efforts to investigate the performance of NOMA-aided V2V systems but without considering PLS framework. Also, these works did not adopt the time-varying nature of V2V channels. Notably, the Doppler shift arising from nodes' mobility causes the channel to become time-selective, and the estimation process of such time-selective channels leads to channel estimation errors (CEE) in the system. Therefore, it is important to consider these effects while evaluating the performance of vehicular communication systems. Moreover, the authors in [47], [48], [49] have analyzed the secrecy performance of NOMA-enabled V2V systems but without taking the combined impact of nodes' mobility and CEE. Recently, the authors in [44] and [50] have considered the impact of CEE and the joint impact of nodes' mobility and CEE, respectively, but they were restricted to the non-security framework. In addition, the literature lacks an evaluation of the secrecy performance of NOMA-enabled V2V systems considering multi-antenna legitimate users and eavesdropper. Thus, it is of great interest to consider the impact of nodes' mobility and CEE and benefits of multi-antenna diversity while analyzing the PLS performance of single-input-multiple-output (SIMO) NOMA-enabled V2V communications.

B. MOTIVATION AND CHALLENGES

References [47] and [48] have studied PLS performance of a full-duplex relay assisted NOMA V2V communication networks under Rayleigh and Nakagami-m fading channels, respectively. Also, the authors in [49] have studied the intercept

TABLE 1. Comparison of Proposed NOMA-Enabled V2V Communication System With the Related Works

	Vehicular Scenario	Fading Channels	Joint Impact of CEE & Nodes' Mobility	Multi-Antenna System	PLS
[41]	V2V	Rayleigh Fading	×	✓	×
[42]	V2I	Nakagami-m Fading	×	✓	×
[43]	V2I	Rayleigh Fading	×	×	×
[44]	V2V	Cascaded Rician Fading	×	×	×
[45]	V2V	Cascaded Rayleigh Fading	×	×	×
[46]	V2V	Cascaded Nakagami-m Fading	×	✓	×
[47]	V2V	Rayleigh Fading	×	×	✓
[48]	V2I	Nakagami-m Fading	×	×	✓
[50]	V2V	Nakagami-m Fading	✓	×	×
This Paper	V2V	Nakagami-m Fading	✓	✓	✓

probability performance of NOMA-enabled V2V systems under cascaded Rayleigh channels. However, they executed their analysis by considering time-invariant V2V links with perfect CSI. On the contrary, V2V channels are time-selective and experience imperfect channel estimates during the estimation process. In addition, exploiting multiple antennas at the end users can always aid in improving the signal reception quality owing to the inherent multi-antenna diversity benefits. Additionally, Table 1 presents the comparison between our proposed work and the existing works to clearly highlight our motivation and challenges toward conducting this important and interesting study. Furthermore, Table 1 illustrates that there is an absolute scarcity of literature putting efforts into analyzing security performance of NOMA-enabled V2V communications, which are briefly described as follows.

- Several works exist in the literature studying the performance of NOMA-enabled vehicular communication systems over cascaded fading channels, however, they assumed the channel to be time-invariant.
- In addition, few works exist who have exploited the benefits of multi-antenna diversity in NOMA-aided vehicular communications, but they did not consider the joint impact of nodes' mobility and CEE under vehicular scenario.
- Also, the PLS performance investigation in NOMA-aided vehicular communications with multi-antenna diversity and combined effects of nodes' mobility and CEE is lacking.

In view of the aforementioned limitations, this work comprehensively develop an understanding of NOMA-aided V2V communications by taking following into account; 1) physical layer security aspects, 2) combined effects of nodes' mobility and CEE, 3) multi-antenna legitimate and eavesdropper vehicles, 4) different scenarios based on the eavesdropper decoding capability, and 5) Nakagami-*m* fading channels. Under such a realistic system setup, it is to be emphasized that the theoretical findings/insights of this paper are unique as they are reported first time in the literature to examine PLS performance for such NOMA-enabled V2V systems. Additionally, the presented contributions lay the foundation for analyzing PLS for the more generalized V2V communication systems employing NOMA technology.

However, at the same time, such a analysis brings several mathematical challenges which has significantly deterred researchers from thoroughly and comprehensively investigating this work in the literature. Under vehicular communications, the channels associated with V2V links lead to time-varying errors and CEE because of their time-selective (i.e., rapidly time-varying) behavior, and hence cannot be ignored while analyzing the PLS performance of considered SIMO NOMA-aided V2V communication systems. Such a consideration alongwith Nakagami-*m* fading channels and different cases of eavesdropper decoding capability impose several mathematical complications while deriving the analytical expressions for the performance measures under investigation. The analytical complexity is further aggravated with the introduction of multiple antennas at the user vehicles and eavesdropper. It is also stressed that the analytical expressions employ some numerical integration methods to simplify intractable integration, whose convergence depends upon the various involved system/channel parameters. However, the proposed analytical framework requires rigorous mathematical steps but they can be easily applied to study the PLS performance of NOMA-aided V2V systems in practical setup. Therefore, existing analytical frameworks cannot be directly incorporated into the considered system, and to the best of authors' knowledge, this is the first work which comprehensively and thoroughly investigates the PLS performance of SIMO NOMA-enabled V2V communication systems under the joint consideration of nodes' mobility and CEE over Nakagami-*m* fading channels.

C. CONTRIBUTIONS

From the above discussion and Table 1, we can conclude that there is a lack of understanding in investigating the performance of NOMA-enabled V2V communication networks by taking 1) PLS aspects, 2) combined effects of nodes' mobility and CEE, 3) multi-antenna legitimate and eavesdropper vehicles, and 4) Nakagami-*m* fading channels, into account. Therefore, the unique analytical findings of this work involves a lot of mathematical challenges and complications and lays the foundation for analyzing the PLS performance of SIMO NOMA-assisted V2V communication systems over more generalized and practical scenarios. In addition, we extend our theoretical analysis according to the decoding capabilities of

TABLE 2. Comparison of Proposed Work With Other Related Works From Different Eavesdropping Scenarios Viewpoint

	Vehicular Scenario	Eavesdropping Scenario	Joint Impact of CEE & Nodes' Mobility	Multi-Antenna System	Secrecy Metrics
[15]	×	Scenario I & II	×	×	SOP
[26]	×	Scenario I	×	✓	SOP
[27]	×	Scenario I	×	✓	Intercept Probability
[28]	×	Scenario II	×	✓	SOP
[30]	×	Scenario I	×	×	SOP
[17], [31], [34]	×	Scenario I	×	✓	SOP
[38]	×	Scenario I	×	✓	SOP
[40]	×	Scenario II	only CEE	×	SOP
[49]	✓	Scenario I & II	×	✓	Intercept Probability
This Paper	✓	Scenario I & II	✓	✓	SOP, ESC

eavesdropper, which is unique in the literature for the considered system setup. Accordingly, this paper considers a secure downlink SIMO NOMA-enabled V2V communication system, wherein a single-antenna legitimate source vehicle S (acts as an access point) exploits power-domain NOMA approach to securely share the information with two multi-antenna vehicles V_n (near vehicle) and V_f (far vehicle) in the presence of a multi-antenna eavesdropper vehicle E. We specifically consider two cases for E based on its decoding capability[1], i.e., 1) Scenario I: E has sufficient decoding capability, and 2) Scenario II: E's decoding capability is similar to the decoding capability available at V_f and V_n. For such a realistic system setup, we deduce the secrecy outage probability (SOP), asymptotic SOP, and ergodic secrecy capacity (ESC) expressions in the presence of nodes' mobility and CEE over Nakagami-m fading. We also formulate some special cases of interest to get some additional insights about the system's secrecy performance. The key contributions are summarized as follows.

1) By modeling time-varying behavior of V2V channels via first-order auto-regressive process and CSI via linear minimum mean square error estimation method, we deduce the instantaneous end-to-end signal-to-noise ratios (SNRs)/signal-to-interference-noise ratios (SINRs) by employing maximum ratio combining (MRC) scheme at both the legitimate vehicles and eavesdropper vehicle under Scenarios I and II.
2) Based on the deduced instantaneous SNRs/SINRs under joint modeling of nodes' mobility and CEE and considering Nakagami-m fading distribution, we derive the SOP expressions for the user vehicles V_f, V_n, and overall system under both Scenarios I and II. Specifically, the obtained SOP expressions can help in quantifying PLS performance of the individual legitimate vehicles and overall system, and also provides a direction to understand the implications of various system/channel parameters on the system's security performance behavior.
3) For both Scenarios I and II, we also present the asymptotic SOP analysis for V_f and V_n in the presence of time-varying errors and CEE over Nakagami-m fading channels. For the asymptotic SOP investigations, we consider three different cases of interest; i.e., 1) Case 1: when the average transmit SNR goes to infinity, 2) Case 2: when the average channel gains associated with the legitimate links go to infinity, while the average channel gain of the wiretap link is fixed, and 3) Case 3: when the average channel gains of both legitimate and eavesdropper links approaches infinity. From this analysis, we reveal some important observations into the system's secrecy diversity order. It is observed that the secrecy diversity order is zero in all three cases, which is mainly due to the negative impacts of CEE and time-varying errors.
4) We also particularize some practical cases of interest; viz., 1) when all the nodes are mobile with perfect channel estimates (i.e., no CEE), 2) when all the nodes are static with imperfect channel estimates, and 3) when all the nodes are static with perfect channel estimates, and analyze the SOP performance of the considered system. The SOP analyses for V_f and V_n under these cases (except the analysis for V_n under static nodes with perfect channel estimates scenario) show that the nodes' mobility and imperfect channel estimates have a detrimental impact on the system's secrecy performance and degrade it by introducing a secrecy floor in the SOP curves which results into a zero secrecy diversity order. However, the asymptotic analysis for V_n for static nodes with perfect channel estimates reports that a secrecy diversity order of $m_n\mathrm{N}_n$ can be achieved, where m_n is the fading severity parameter for $\mathrm{S} \rightarrow \mathrm{V}_n$ link and N_n is the number of antennas at V_n.
5) For both Scenarios I and II, we further deduce the novel closed-form exact and approximate ESC expressions for the legitimate user vehicles and the overall system under the combined impact of nodes' mobility and imperfect channel estimates over Nakagami-m fading channels. It is seen that the proposed approximate expressions are in well agreement with the exact results.

[1]Note that in this work, we consider two scenarios for eavesdropper's decoding capability, i.e., Scenario I: when E has sufficient decoding capability, and Scenario II: when E's decoding capability is same as the near and far user vehicles, to comprehensively evaluate PLS performance of the considered NOMA-enabled V2V systems. Moreover, in the context of eavesdropper decoding capabilities, we present a Table 2 to clearly highlight the differences between the proposed work and the other related works.

6) Lastly, we corroborate our analytical findings via numerical and simulation results. We also reveal several important conclusions on the system's secrecy performance by quantifying the impact of system/channel parameters, such as, correlation parameters/relative nodes' speed, fading severity parameters, CEE, time-varying errors, on the SOP and ESC performance for the considered SIMO NOMA-enabled V2V communication systems, under Scenarios I and II.

D. ORGANIZATION

The remainder of this paper is organized as follows. Section II describes our considered network setup alongwith the statistical analysis of the SINRs/SNRs at the legitimate and eavesdropper vehicles. Sections III and IV provide the exact SOP and asymptotic SOP expressions, respectively, for both V_f and V_n under Scenarios I and II. We also provide some practical cases of interest on the SOP analysis in Section V. Further, the exact and approximate ESC expressions for both V_f and V_n under Scenarios I and II are derived in Section VI. In Section VII, we present numerical and simulation results, followed by conclusions in Section VIII.

Notations: $\mathbb{E}[\cdot]$ denotes the expectation operator, $[\cdot]^{\mathrm{T}}$ denotes transpose operation, and $[\cdot]^{\mathcal{H}}$ denotes conjugate transpose operation. $|\cdot|$ and $||\cdot||$ represent absolute value and Frobenius norm, respectively. $F_X(x)$ and $f_X(x)$ denote the cumulative distribution function (CDF) and the probability density function (PDF) of a random variable (RV) X. $\Gamma(x)$ is the complete Gamma function [51, Eq. (8.310.1)], $\Gamma(n,x)$ is the upper incomplete Gamma function [51, Eq. (8.350.2)], $\Upsilon(n,x)$ is the lower incomplete Gamma function [51, Eq. (8.350.1)], and $\mathcal{G}_{p,q}^{m,n}(x|_{b_1,\ldots,b_q}^{a_1,\ldots,a_p})$ is the Meijer-$\mathcal{G}$ function [51, Eq. (9.301)]. $\Psi(a,b;z)$ denotes the tricomi confluent hypergeometric function [51].

II. SYSTEM AND CHANNEL MODELS

We consider a secure downlink SIMO NOMA-assisted V2V communication system as depicted in Fig. 1, where a legitimate source vehicle S (acts as a vehicular access point) exploits power-domain NOMA principle for sharing confidential information with two legitimate user vehicles,[2] V_f and V_n, simultaneously over the same time and frequency resources. Specifically, on the basis of distances of both user vehicles from S, we classify V_f and V_n as far user vehicle (i.e., weak user vehicle) and near user vehicle (i.e., strong user vehicle), respectively. Moreover, we assume the presence of a passive malicious user vehicle E in the vicinity of S to overhear the confidential information intended for V_f and V_n, which brings security and privacy concerns into

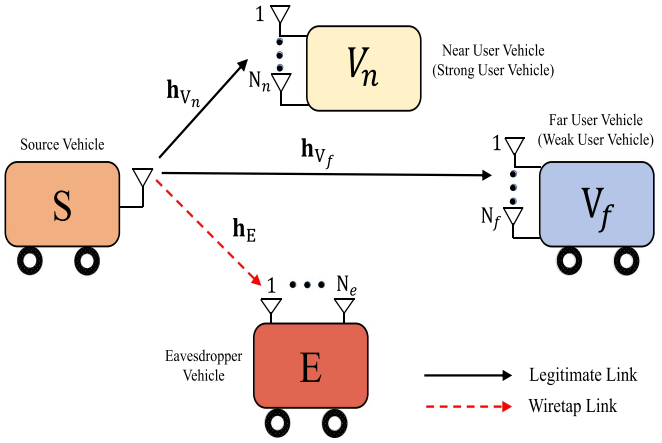

FIGURE 1. System model for secure SIMO NOMA-aided V2V communications.

the network. Also, all the nodes are assumed to operate in half-duplex mode. In addition, we consider that S is equipped with a single-antenna, while both the legitimate vehicles, V_f and V_n, and eavesdropper vehicle E are equipped with N_f, N_n, and N_e antennas, respectively. We assume the multiple antennas at V_f, V_n, and E to be uncorrelated as the antennas are having a separation greater than half wavelength and also the multi-antenna receiver vehicles in system are experiencing a high azimuthal spread [52], [53]. Accordingly, the channels for $\mathrm{S} \to \mathrm{V}_f$, $\mathrm{S} \to \mathrm{V}_n$ and $\mathrm{S} \to \mathrm{E}$ links are SIMO V2V links, therefore, the channel vectors for these links are denoted as $\mathbf{h}_{\mathrm{V}_f} = [h_{\mathrm{V}_f,1}, h_{\mathrm{V}_f,2}, \ldots, h_{\mathrm{V}_f,\mathrm{N}_f}]^{\mathrm{T}}$, $\mathbf{h}_{\mathrm{V}_n} = [h_{\mathrm{V}_n,1}, h_{\mathrm{V}_n,2}, \ldots, h_{\mathrm{V}_n,\mathrm{N}_n}]^{\mathrm{T}}$, and $\mathbf{h}_{\mathrm{E}} = [h_{\mathrm{E},1}, h_{\mathrm{E},2}, \ldots, h_{\mathrm{E},\mathrm{N}_e}]^{\mathrm{T}}$, respectively. Since all the nodes are in motion, we can model the channel coefficients for all the associated V2V links as frequency-flat time-selective independent and non-identically distributed (i.ni.d.) Nakagami-m fading.[3] Further, the noise at each receiver node is modeled as additive white Gaussian noise (AWGN) with mean zero and variance N_0.

Using power-domain multiplexing, S allocates its total transmit power P_{S} for the transmission of information symbols to both legitimate user vehicles according to their channel conditions, and as a consequence, V_f gets more power than V_n. Specifically, $\mathrm{P}_{\mathrm{V}_f} = \beta \mathrm{P}_{\mathrm{S}}$ and $\mathrm{P}_{\mathrm{V}_n} = (1-\beta)\mathrm{P}_{\mathrm{S}}$ are the transmit powers of V_f and V_n, respectively, such that $\mathrm{P}_{\mathrm{V}_f} + \mathrm{P}_{\mathrm{V}_n} = \mathrm{P}_{\mathrm{S}}$, where β is the power allocation coefficient with $\beta > 0.5$. Therefore, the received signal vector at ι-th vehicle, for $\iota \in \{\mathrm{V}_f, \mathrm{V}_n, \mathrm{E}\}$, can be given as

$$\mathbf{Y}_\iota = \mathbf{h}_\iota \left(\sqrt{\mathrm{P}_{\mathrm{V}_f}} x_{\mathrm{V}_f} + \sqrt{\mathrm{P}_{\mathrm{V}_n}} x_{\mathrm{V}_n} \right) + \mathbf{n}_\iota, \tag{1}$$

where x_{V_f} and x_{V_n} denote the information symbol of V_f and V_n, respectively. Also, $\mathbf{n}_\iota = [n_{\iota,1}, n_{\iota,2}, \ldots, n_{\iota,J}]^{\mathrm{T}}$, for

[2] In this work, we consider a two-user vehicle NOMA system where the vehicles are embedded with multiple antennas. Such a system has a significant practical relevance [40], [54], [55]. For instance, multiuser superposition transmission (MUST), is such a two user SIMO NOMA system already been proposed in the Third Generation Partnership Project Long Term Evolution Advanced (3GPP-LTE-A) standard [54].

[3] Notably, several experimental studies have found Nakagami-m fading to be a good and versatile fading model to mimic the static and small-scale fading channel behavior in V2V communications [56], [57], [58].

$(\iota, \jmath) \in \{(\mathrm{V}_f, \mathrm{N}_f), (\mathrm{V}_n, \mathrm{N}_n), (\mathrm{E}, \mathrm{N}_e)\}$ represent the AWGN noise vector at the ι-th vehicle, whose individual elements are modeled as $\mathcal{CN}(0, N_0)$.

A. MODELING OF NODES' MOBILITY AND CEE

To model the time-selective nature of the wireless links, we use the first-order auto-regressive (AR1) process [59], and consequently we can represent $\mathbf{h}_\iota$, for $\iota \in \{\mathrm{V}_f, \mathrm{V}_n, \mathrm{E}\}$ as

$$\mathbf{h}_\iota = \rho_\iota \bar{\mathbf{h}}_\iota + \sqrt{1-\rho_\iota^2}\mathbf{h}_{\epsilon_\iota}, \tag{2}$$

where $\mathbf{h}_\iota$ and $\bar{\mathbf{h}}_\iota$ denote the observed channel gains corresponding to the current transmission and immediately previous transmission, respectively. The vector $\mathbf{h}_{\epsilon_\iota} \sim \mathcal{CN}(0,\ \Omega_{\epsilon_\iota}\mathbf{I}_{\epsilon_\iota})$, for $\iota \in \{\mathrm{V}_f, \mathrm{V}_n, \mathrm{E}\}$, is the time-varying error component for $\mathrm{S} \to \iota$ link. $\rho_\iota \in [0, 1]$, for $\iota \in \{\mathrm{V}_f, \mathrm{V}_n, \mathrm{E}\}$, denotes the correlation coefficient between $\bar{\mathbf{h}}_\iota$ and $\mathbf{h}_\iota$, which can be represented using Jake's model as $\rho_\iota = J_0\left(\frac{2\pi f_c v_\iota}{Rc}\right)$, where v_ι represents the relative speed between the nodes S and ι, R is the code rate, f_c is the carrier frequency, c denotes the speed of light, and $J_0(\cdot)$ is the zeroth-order Bessel function of the first kind [51].

Additionally, assuming linear minimum mean square error estimation process, the estimated channel gain vector $\hat{\mathbf{h}}_\iota$, for $\iota \in \{\mathrm{V}_f, \mathrm{V}_n, \mathrm{E}\}$, can be written as

$$\bar{\mathbf{h}}_\iota = \hat{\mathbf{h}}_\iota + \mathbf{h}_{\delta_\iota}, \tag{3}$$

where $\mathbf{h}_{\delta_\iota} \sim \mathcal{CN}(0, \Omega_{\delta_\iota}\mathbf{I}_{\delta_\iota})$ represents the channel estimation error vector. Furthermore, substituting (3) into (2), we can express the actual channel vector $\mathbf{h}_\iota$, for $\iota \in \{\mathrm{V}_f, \mathrm{V}_n, \mathrm{E}\}$, under the joint consideration of nodes' mobility and CEE as

$$\begin{aligned}\mathbf{h}_\iota &= \rho_\iota\left(\hat{\mathbf{h}}_\iota + \mathbf{h}_{\delta_\iota}\right) + \sqrt{1-\rho_\iota^2}\mathbf{h}_{\epsilon_\iota} \\ &= \rho_\iota\hat{\mathbf{h}}_\iota + \mathbf{q}_\iota,\end{aligned} \tag{4}$$

where $\mathbf{q}_\iota = \rho_\iota\mathbf{h}_{\delta_\iota} + \sqrt{1-\rho_\iota^2}\mathbf{h}_{\epsilon_\iota}$ with variance $\Omega_{q_\iota} = \rho_\iota^2\Omega_{\delta_\iota} + \left(1-\rho_\iota^2\right)\Omega_{\epsilon_\iota}$.

B. INSTANTANEOUS END-TO-END SINR/SNR AT V_f AND V_n

Utilizing (4) into (1), the received signal vector at the ι-th user vehicle, for $\iota \in \{\mathrm{V}_f, \mathrm{V}_n, \mathrm{E}\}$, under the joint impact of nodes' mobility and CEE, can be expressed as

$$\begin{aligned}\mathbf{Y}_\iota = &\underbrace{\rho_\iota\hat{\mathbf{h}}_\iota\left(\sqrt{\beta\mathrm{P_S}}x_{\mathrm{V}_f} + \sqrt{(1-\beta)\mathrm{P_S}}x_{\mathrm{V}_n}\right)}_{\text{superimposed information signal component}} \\ &+ \underbrace{\sqrt{1-\rho_\iota^2}\mathbf{h}_{\epsilon_\iota}\left(\sqrt{\beta\mathrm{P_S}}x_{\mathrm{V}_f} + \sqrt{(1-\beta)\mathrm{P_S}}x_{\mathrm{V}_n}\right)}_{\text{time}-\text{varying error component (due to nodes' mobility)}} \\ &+ \underbrace{\rho_\iota\mathbf{h}_{\delta_\iota}\left(\sqrt{\beta\mathrm{P_S}}x_{\mathrm{V}_f} + \sqrt{(1-\beta)\mathrm{P_S}}x_{\mathrm{V}_n}\right)}_{\text{CEE component}} + \underbrace{\mathbf{n}_\iota}_{\text{AWGN}}.\end{aligned} \tag{5}$$

Furthermore, we apply MRC scheme at the receiver to combine the incoming signal components arriving at the multiple antennas. Accordingly, we can express (5) as

$$\begin{aligned}\mathbf{R}_\iota &= \mathbf{W}_\iota^{\mathcal{H}}\mathbf{Y}_\iota \\ &= \rho_\iota\mathbf{W}_\iota^{\mathcal{H}}\hat{\mathbf{h}}_\iota\left(\sqrt{\beta\mathrm{P_S}}x_{\mathrm{V}_f} + \sqrt{(1-\beta)\mathrm{P_S}}x_{\mathrm{V}_n}\right) \\ &\quad + \sqrt{1-\rho_\iota^2}\mathbf{W}_\iota^{\mathcal{H}}\mathbf{h}_{\epsilon_\iota}\left(\sqrt{\beta\mathrm{P_S}}x_{\mathrm{V}_f} + \sqrt{(1-\beta)\mathrm{P_S}}x_{\mathrm{V}_n}\right) \\ &\quad + \rho_\iota\mathbf{W}_\iota^{\mathcal{H}}\mathbf{h}_{\delta_\iota}\left(\sqrt{\beta\mathrm{P_S}}x_{\mathrm{V}_f} + \sqrt{(1-\beta)\mathrm{P_S}}x_{\mathrm{V}_n}\right) + \mathbf{W}_\iota^{\mathcal{H}}\mathbf{n}_\iota,\end{aligned} \tag{6}$$

for $\iota \in \{\mathrm{V}_f, \mathrm{V}_n, \mathrm{E}\}$, where $\mathbf{W}_\iota = \frac{\hat{\mathbf{h}}_\iota}{||\hat{\mathbf{h}}_\iota||}$ is $\jmath \times 1$, for $\jmath \in \{\mathrm{N}_f, \mathrm{N}_n, \mathrm{N}_e\}$, received beamforming vector corresponding to ι-th terminal. Moreover, we also assume that the noise samples across the different antennas are independent and can be represented via the covariance matrix $\mathbb{R}_{\mathbf{n}_\iota}$ as $\mathbb{R}_{\mathbf{n}_\iota} = \mathbb{E}\{n_{\iota,u}n_{\iota,v}^*\} = N_0\mathbf{I}_\jmath$, for $(\iota, \jmath) \in \{(\mathrm{V}_f, \mathrm{N}_f), (\mathrm{V}_n, \mathrm{N}_n), (\mathrm{E}, \mathrm{N}_e)\}$.

Next, the far (weak) user vehicle directly decodes its own signal without applying the successive interference cancellation (SIC) technique and considers the signal associated with near (strong) user vehicle as interference, and hence the instantaneous end-to-end SINR at V_f can be given as

$$\Lambda_{\mathrm{V}_f} = \frac{\beta\rho_{\mathrm{V}_f}^2\gamma\hat{X}}{(1-\beta)\rho_{\mathrm{V}_f}^2\gamma\hat{X} + \gamma\Omega_{q_{\mathrm{V}_f}} + 1}. \tag{7}$$

Moreover, the near user vehicle first detects the signal pertaining to the far user vehicle and then applies the SIC technique to decode its own message, and consequently the instantaneous end-to-end SNR at V_n can be expressed as

$$\Lambda_{\mathrm{V}_n} = \frac{(1-\beta)\rho_{\mathrm{V}_n}^2\gamma\hat{Y}}{(1-\beta)\gamma\Omega_{q_{\mathrm{V}_n}} + 1}, \tag{8}$$

where $\hat{X} = ||\hat{\mathbf{h}}_{\mathrm{V}_f}||^2 \triangleq \sum_{l=1}^{\mathrm{N}_f}|\hat{h}_{\mathrm{V}_f,l}|^2$, $\hat{Y} = ||\hat{\mathbf{h}}_{\mathrm{V}_n}||^2 \triangleq \sum_{l=1}^{\mathrm{N}_n}|\hat{h}_{\mathrm{V}_n,l}|^2$, and $\gamma = \frac{\mathrm{P_S}}{N_0}$.

C. INSTANTANEOUS END-TO-END SINRs/SNRs AT E

Here, we first formulate two scenarios by considering the decoding capability at E; 1) Scenario I: E has sufficient decoding capabilities,[4] and 2) Scenario II: E's decoding capability is same as the decoding capability of V_f and V_n, and then evaluate the SINRs/SNRs at E, in what follows.

1) SCENARIO I (E HAS SUFFICIENT DECODING CAPABILITY)

Herein, E has the ability to completely overcome the interference to V_f from V_n. Consequently, the SNRs at E for V_f's

[4]Note that the consideration of E has sufficient decoding capability indicates that E is equipped with powerful multi-user decoding capability to fully decode every user's information by exploiting the multi-user detection techniques. Also, since E's capabilities are often unknown, therefore, it is reasonable to overestimate E's multi-user decodability. In the literature, many works have focused on PLS performance of NOMA systems under such assumption (see [17], [27], [31] and the references therein), which motivates us to adopt this scenario for investigating the PLS performance in our considered NOMA-aided V2V communications.

and V_n's signals can be given, respectively, as

$$\Lambda_{\mathrm{E}_f^{\mathrm{I}}} = \frac{\beta\rho_{\mathrm{E}}^2\gamma\hat{Z}}{\beta\gamma\Omega_{q_{\mathrm{E}}}+1}, \tag{9}$$

$$\Lambda_{\mathrm{E}_n^{\mathrm{I}}} = \frac{(1-\beta)\rho_{\mathrm{E}}^2\gamma\hat{Z}}{(1-\beta)\gamma\Omega_{q_{\mathrm{E}}}+1}, \tag{10}$$

where $\hat{Z} = ||\hat{\mathbf{h}}_{\mathrm{E}}||^2 \triangleq \sum_{l=1}^{\mathrm{N}_e} |\hat{h}_{\mathrm{E}_l}|^2$.

2) SCENARIO II (E HAS SAME DECODING CAPABILITY AS V_f AND V_n)

Herein, E applies SIC to decode V_n's signal. Accordingly, the SINR at E (for V_f's signal) and the SNR at E (for V_n's signal) can be expressed, respectively, as

$$\Lambda_{\mathrm{E}_f^{\mathrm{II}}} = \frac{\beta\rho_{\mathrm{E}}^2\gamma\hat{Z}}{(1-\beta)\rho_{\mathrm{E}}^2\gamma\hat{Z}+\gamma\Omega_{q_{\mathrm{E}}}+1}, \tag{11}$$

$$\Lambda_{\mathrm{E}_n^{\mathrm{II}}} = \frac{(1-\beta)\rho_{\mathrm{E}}^2\gamma\hat{Z}}{(1-\beta)\gamma\Omega_{q_{\mathrm{E}}}+1}. \tag{12}$$

Moreover, the capacities of legitimate vehicles and eavesdropper vehicle under Scenarios I and II can be expressed as $\mathbf{C}_i = \log_2(1+\Lambda_i)$, for $i \in \{\mathrm{V}_f, \mathrm{V}_n, \mathrm{E}_f^{\mathrm{I}}, \mathrm{E}_n^{\mathrm{I}}, \mathrm{E}_f^{\mathrm{II}}, \mathrm{E}_n^{\mathrm{II}}\}$. Consequently, the instantaneous secrecy capacity for V_f and V_n can be defined as $\mathbf{C}_{\mathrm{sec},\mathrm{V}_f}^j = \max[\mathbf{C}_{\mathrm{V}_f} - \mathbf{C}_{\mathrm{E}_f^j}, 0]$ and $\mathbf{C}_{\mathrm{sec},\mathrm{V}_n}^j = \max[\mathbf{C}_{\mathrm{V}_n} - \mathbf{C}_{\mathrm{E}_n^j}, 0]$, respectively, for $j \in \{\mathrm{I}, \mathrm{II}\}$.

D. STATISTICAL ANALYSIS OF SINRs/SNRs AT V_f, V_n, AND E

For Nakagami-*m* fading channel[5] (say h), the cumulative distribution function (CDF) and the probability density function (PDF) of the channel gains, i.e., $|h|^2$, follow Gamma distribution with shape and scale parameters as m and Ω, respectively. Moreover, it is to be noted that the summation of a large number of Gamma distributed random variables, i.e., $\sum_{\ell=1}^{L} |h_\ell|^2$, results into a Gamma distribution with shape and scale parameters as mL and Ω, respectively. Following the above statement, the CDF and PDF of $\hat{X} = ||\hat{\mathbf{h}}_{\mathrm{V}_f}||^2 \triangleq \sum_{l=1}^{\mathrm{N}_f} |\hat{h}_{\mathrm{V}_{f,l}}|^2$, $\hat{Y} = ||\hat{\mathbf{h}}_{\mathrm{V}_n}||^2 \triangleq \sum_{l=1}^{\mathrm{N}_n} |\hat{h}_{\mathrm{V}_{n,l}}|^2$, and $\hat{Z} = ||\hat{\mathbf{h}}_{\mathrm{E}}||^2 \triangleq \sum_{l=1}^{\mathrm{N}_e} |\hat{h}_{\mathrm{E}_l}|^2$ can be expressed as

$$F_J(y) = \frac{1}{\Gamma(m_\kappa \mathrm{N}_\kappa)} \Upsilon\left(m_\kappa \mathrm{N}_\kappa, \frac{m_\kappa}{\Omega_\kappa} y\right), \; y > 0, \tag{13}$$

$$f_J(y) = \frac{1}{\Gamma(m_\kappa \mathrm{N}_\kappa)} \left(\frac{m_\kappa}{\Omega_\kappa}\right)^{m_\kappa \mathrm{N}_\kappa} y^{m_\kappa \mathrm{N}_\kappa - 1} \mathrm{e}^{-\frac{m_\kappa}{\Omega_\kappa} y}, y > 0, \tag{14}$$

respectively, where $(J, \kappa) \in \{(\hat{X}, f), (\hat{Y}, n), (\hat{Z}, e)\}$. Now, with the aid of (13) and (14), we evaluate the CDFs corresponding to the instantaneous SINRs/SNRs given in (7)–(12). As such, we first deduce the CDFs of Λ_{V_f} and Λ_{V_n} given in (7) and (8), respectively, as per the below proposition.

Proposition 1: The CDFs of Λ_{V_f} and Λ_{V_n} can be given, respectively, as

$$F_{\Lambda_{\mathrm{V}_f}}(y) = \begin{cases} \dfrac{\Upsilon\left(m_f \mathrm{N}_f, \frac{m_f}{\Omega_f} \frac{\left(\Omega_{q_{\mathrm{V}_f}} + \frac{1}{\gamma}\right) y}{\rho_{\mathrm{V}_f}^2 (\beta - (1-\beta) y)}\right)}{\Gamma(m_f \mathrm{N}_f)}, & y < \frac{\beta}{1-\beta} \\ 1, & y \geq \frac{\beta}{1-\beta}, \end{cases} \tag{15}$$

$$F_{\Lambda_{\mathrm{V}_n}}(y) = \frac{\Upsilon\left(m_n \mathrm{N}_n, \frac{m_n}{\Omega_n} \frac{\left((1-\beta)\gamma\Omega_{q_{\mathrm{V}_n}} + 1\right) y}{\rho_{\mathrm{V}_n}^2 (1-\beta)\gamma}\right)}{\Gamma(m_n \mathrm{N}_n)}, \; y > 0. \tag{16}$$

Proof: With the aid of (7), the CDF of Λ_{V_f} can be expressed as $F_{\Lambda_{\mathrm{V}_f}}(y) = \Pr\left[\hat{X} < \frac{(\Omega_{q_{\mathrm{V}_f}} + \frac{1}{\gamma}) y}{\rho_{\mathrm{V}_f}^2 (\beta - (1-\beta) y)}\right]$. Now, simplifying with the help of the CDF of $\hat{X}$ presented in (13), we can easily obtain (15). Likewise, we can get the CDF $F_{\Lambda_{\mathrm{V}_n}}(y)$, as shown in (16). ■

Similar to Proposition 1, we can also derive the CDFs of $\Lambda_{\mathrm{E}_f^{\mathrm{I}}}$, $\Lambda_{\mathrm{E}_f^{\mathrm{II}}}$, $\Lambda_{\mathrm{E}_n^{\mathrm{I}}}$, and $\Lambda_{\mathrm{E}_n^{\mathrm{II}}}$ as per Proposition 2.

Proposition 2: The CDFs of $\Lambda_{\mathrm{E}_f^{\mathrm{I}}}$, $\Lambda_{\mathrm{E}_f^{\mathrm{II}}}$, $\Lambda_{\mathrm{E}_n^{\mathrm{I}}}$, and $\Lambda_{\mathrm{E}_n^{\mathrm{II}}}$ under Nakagami-*m* fading channels can be expressed as

$$F_{\Lambda_{\mathrm{E}_f^{\mathrm{I}}}}(y) = \frac{\Upsilon\left(m_e \mathrm{N}_e, \frac{m_e}{\Omega_e} \frac{(\beta\gamma\Omega_{q_{\mathrm{E}}} + 1) y}{\rho_{\mathrm{E}}^2 \beta\gamma}\right)}{\Gamma(m_e \mathrm{N}_e)}, \; y > 0, \tag{17}$$

$$F_{\Lambda_{\mathrm{E}_f^{\mathrm{II}}}}(y) = \begin{cases} \dfrac{\Upsilon\left(m_e \mathrm{N}_e, \frac{m_e}{\Omega_e} \frac{\left(\Omega_{q_{\mathrm{E}}} + \frac{1}{\gamma}\right) y}{\rho_{\mathrm{E}}^2 (\beta - (1-\beta) y)}\right)}{\Gamma(m_e \mathrm{N}_e)}, & y < \frac{\beta}{1-\beta} \\ 1, & y \geq \frac{\beta}{1-\beta}, \end{cases} \tag{18}$$

$$F_{\Lambda_{\mathrm{E}_n^{j}}}(y) = \frac{\Upsilon\left(m_e \mathrm{N}_e, \frac{m_e}{\Omega_e} \frac{\left((1-\beta)\gamma\Omega_{q_{\mathrm{E}}} + 1\right) y}{\rho_{\mathrm{E}}^2 (1-\beta)\gamma}\right)}{\Gamma(m_e \mathrm{N}_e)}, \; y > 0, \tag{19}$$

where $j \in \{\mathrm{I}, \mathrm{II}\}$. The deduced CDFs in (15)–(19) will be exploited for analytical investigation of the considered system, in what follows.

III. SECRECY OUTAGE PROBABILITY (SOP) ANALYSIS

This section analyzes the SOP performance for the considered SIMO NOMA-enabled V2V communication system under both Scenarios I and II by taking joint impact of nodes' mobility and CEE into account over Nakagami-*m* fading channels. The SOP quantifies the event probability when the instantaneous capacity difference between the ι-th legitimate user vehicle, for $\iota \in \{\mathrm{V}_f, \mathrm{V}_n\}$, and eavesdropper vehicle E falls below a predetermined secrecy target rate $\mathcal{R}_\iota$. Accordingly, we can mathematically express the SOP, for $\iota \in \{\mathrm{V}_f, \mathrm{V}_n\}$ and $j \in \{\mathrm{I}, \mathrm{II}\}$, as

$$\mathcal{P}_{\mathrm{sec},\iota}^j = \Pr\left[\mathbf{C}_{\mathrm{sec},\iota}^j < \mathcal{R}_\iota\right]. \tag{20}$$

[5]Note that parameter m can take both integer and non-integer values. When m is integer, the associated lower incomplete Gamma function can easily be expanded into a finite summation of the exponential function and power function, which then helps in obtaining the closed-form expressions for performance metrics under investigation. However, integer m may limit the application of Nakagami-*m* fading channel, but this is not a major restriction as indicated in [60], [61]. Moreover, when parameter m takes a non-integer value [62], [63], the associated lower incomplete Gamma function can be realized in terms of infinite series summation, and hence the system performance depends on the convergence of infinite series summation under different parameters setting. In the context of this work, we only consider positive integer values of parameter m.

Next, we deduce the analytical expressions of SOP for user vehicles V_f and V_n under Scenarios I and II.

A. SOP ANALYSIS UNDER SCENARIO I

Herein, we analytically derive the SOP expressions for V_f, V_n, and overall system under Scenario I.

1) SOP OF V_f

Using (20), we can express the SOP of V_f under Scenario I as

$$\mathcal{P}^{\mathrm{I}}_{\mathrm{sec},\mathrm{V}_f}(\eta_{\mathrm{V}_f}) = \mathbf{Pr}\left[\frac{1+\Lambda_{\mathrm{V}_f}}{1+\Lambda_{\mathrm{E}^{\mathrm{I}}_f}} < \eta_{\mathrm{V}_f}\right] = \mathbf{Pr}\left[\Lambda_{\mathrm{V}_f} < \eta_{\mathrm{V}_f}\Lambda_{\mathrm{E}^{\mathrm{I}}_f} + \eta_{\mathrm{V}_f} - 1\right], \quad (21)$$

where $\eta_{\mathrm{V}_f} = 2^{\mathcal{R}_{\mathrm{V}_f}}$ denotes the preset secrecy threshold at V_f. Further, the SOP expression for V_f can be evaluated as per the below theorem.

Theorem 1: For Scenario I, the SOP expression of V_f in the presence of joint impact of nodes mobility and CEE over Nakagami-m fading channels can be expressed as

$$\mathcal{P}^{\mathrm{I}}_{\mathrm{sec},\mathrm{V}_f}\left(\eta_{\mathrm{V}_f}\right) = 1 - \sum_{k=0}^{\mathrm{N}_f m_f - 1}\sum_{u=1}^{\mathcal{N}} \frac{1}{k!}\frac{\pi}{\mathcal{N}}\frac{\left(\frac{\xi}{2}\right)^{\mathrm{N}_e m_e}}{\Gamma(\mathrm{N}_e m_e)} \mathrm{e}^{-\mathcal{B}_1\left(\eta_{\mathrm{V}_f}\right)} \times \left(\frac{m_f\left(\Omega_{q_{\mathrm{V}_f}} + \frac{1}{\gamma}\right)}{\Omega_f \rho^2_{\mathrm{V}_f}}\right)^k \left(\frac{m_e\left(\beta\Omega_{q_{\mathrm{E}}} + \frac{1}{\gamma}\right)}{\Omega_e \beta \rho^2_{\mathrm{E}}}\right)^{\mathrm{N}_e m_e} \mathcal{A}_u\left(\eta_{\mathrm{V}_f}\right), \quad (22)$$

where $\xi = \frac{1}{\eta_{\mathrm{V}_f}(1-\beta)} - 1$, $t_u = \cos\left(\frac{(2u-1)\pi}{2\mathcal{N}}\right)$, $\bar{\xi}_u = \frac{\xi}{2}(t_u + 1)$, $\mathcal{N}$ denotes the number of summation terms,

$$\mathcal{A}_u(\eta_{\mathrm{V}_f}) = \frac{\sqrt{1-t_u^2}(\eta_{\mathrm{V}_f}\bar{\xi}_u + \eta_{\mathrm{V}_f} - 1)^k (t_u+1)^{\mathrm{N}_e m_e - 1}}{(\beta - (1-\beta)(\eta_{\mathrm{V}_f}\bar{\xi}_u + \eta_{\mathrm{V}_f} - 1))^k},$$

and

$$\mathcal{B}_1(\eta_{\mathrm{V}_f}) = \frac{m_f}{\Omega_f}\left(\frac{(\Omega_{q_{\mathrm{V}_f}} + \frac{1}{\gamma})(\eta_{\mathrm{V}_f}\bar{\xi}_u + \eta_{\mathrm{V}_f} - 1)}{\rho^2_{\mathrm{V}_f}(\beta - (1-\beta)(\eta_{\mathrm{V}_f}\bar{\xi}_u + \eta_{\mathrm{V}_f} - 1))}\right) + \frac{m_e(\beta\Omega_{q_{\mathrm{E}}} + \frac{1}{\gamma})\bar{\xi}_u}{\Omega_e \beta \rho^2_{\mathrm{E}}}.$$

Proof: See Appendix A for the detailed derivation. ■

Remark 1: Following important remarks can be summarized from this analysis.

1) The SOP expression presented in (22) mainly consists of finite summation and elementary functions, which can easily be evaluated by the help of Mathematica/Matlab computational software for various involved channel/system parameters. In addition, the expression consists of $\mathcal{N}$ order Gauss-Chebyshev quadrature series expansion which converges quickly and rapidly, and hence makes it for practical use. The convergence is shown numerically in Section VII.
2) Under this analysis, the SOP depends on the transmit SNR in terms of power functions and negative exponential function, i.e., $\left(\Omega_{q_{\mathrm{V}_f}} + \frac{1}{\gamma}\right)^k (\beta\Omega_{q_{\mathrm{E}}} + \frac{1}{\gamma})^{\mathrm{N}_e m_e} \mathrm{e}^{-\mathcal{B}_1(\bar{\xi}_u)}$. When γ is small, the power terms increase with varying $k = 0$ to $\mathrm{N}_f m_f - 1$ and $\mathrm{N}_e m_e$, while exponential term decreases with γ, and hence results into a lower SOP. On the other hand, as γ grows large, the terms may have the negligible impact of γ and hence the SOP exhibits a saturation floor. This behavior is further analytically elaborated in Section IV, and numerically demonstrated in Section VII.
3) We can also observe that the SOP is significantly dependent on Ω_f, from which large Ω_f results in lower SOP because of the dominance of exponential term $\mathrm{e}^{-\mathcal{B}_1(\eta_{\mathrm{V}_f})}$ compared to $\left(\frac{1}{\Omega_f}\right)^k$ with varying $k = 0$ to $\mathrm{N}_f m_f - 1$. This behavior is also reported numerically in Section VII. Similarly, we can analytically show the impact of various other involved parameters, such as, number of antennas, fading severity parameters, CEE, time-varying errors, wiretap link's channel quality, and secrecy target rate, on the SOP performance.

2) SOP OF V_n

From (20), the SOP expression for the near user vehicle V_n under Scenario I can be expressed as

$$\mathcal{P}^{\mathbf{I}}_{\mathrm{sec},\mathrm{V}_n}(\eta_{\mathrm{V}_n}) = \mathbf{Pr}\left[\Lambda_{\mathrm{V}_n} < (\eta_{\mathrm{V}_n}\Lambda_{\mathrm{E}^{\mathrm{I}}_n} + \eta_{\mathrm{V}_n} - 1)\right], \quad (23)$$

where $\eta_{\mathrm{V}_n} = 2^{\mathcal{R}_{\mathrm{V}_n}}$ is the predefined secrecy threshold at V_n. We can derive the novel analytical SOP expression for V_n in accordance to the following theorem.

Theorem 2: The SOP expression of V_n for Scenario I under both nodes' mobility and CEE in the presence of Nakagami-m fading channels can be expressed as

$$\mathcal{P}^{\mathrm{I}}_{\mathrm{sec},\mathrm{V}_n}(\eta_{\mathrm{V}_n}) = 1 - \sum_{r=0}^{\mathrm{N}_n m_n - 1}\sum_{p=0}^{r}\frac{1}{r!}\binom{r}{p}\left(\frac{m_n}{\Omega_n \mathcal{B}_{\mathrm{V}_n}}\right)^r \times (\eta_{\mathrm{V}_n})^p \frac{(\eta_{\mathrm{V}_n} - 1)^{r-p}}{\Gamma(\mathrm{N}_e m_e)}\left(\frac{m_e}{\Omega_e \mathcal{B}_{\mathrm{E}}}\right)^{\mathrm{N}_e m_e} \times \frac{\Gamma(\mathrm{N}_e m_e + p)}{\left(\frac{m_e}{\Omega_e \mathcal{B}_{\mathrm{E}}} + \frac{m_n \eta_{\mathrm{V}_n}}{\Omega_n \mathcal{B}_{\mathrm{V}_n}}\right)^{\mathrm{N}_e m_e + p}} \mathrm{e}^{-\frac{m_n(\eta_{\mathrm{V}_n} - 1)}{\Omega_n \mathcal{B}_{\mathrm{V}_n}}}, \quad (24)$$

where $\mathcal{B}_{\mathrm{V}_n} = \frac{(1-\beta)\rho^2_{\mathrm{V}_n}\gamma}{1+(1-\beta)\gamma\Omega_{q_{\mathrm{V}_n}}}$ and $\mathcal{B}_{\mathrm{E}} = \frac{(1-\beta)\rho^2_{\mathrm{E}}\gamma}{1+(1-\beta)\gamma\Omega_{q_{\mathrm{E}}}}$.

Proof: See Appendix B for the detailed derivation. ■

Remark 2: We can have the following key observations.

1) The SOP expression for the near user vehicle consists of finite summation and can be evaluated easily for involved channel/system parameters using Mathematica software, and hence makes it for practical use. Moreover, it can be observed that the SOP expression is strongly dependent on transmit SNR γ in terms of

power functions $(\frac{1}{\gamma}+(1-\beta)\Omega_{q_{\mathrm{V}_n}})^r$ with varying $r=0$ to $\mathrm{N}_n m_n-1$, $(\frac{1}{\gamma}+(1-\beta)\Omega_{q_{\mathrm{E}}})^{\mathrm{N}_e m_e}$, and $(\frac{m_e}{\Omega_e \mathcal{B}_{\mathrm{E}}}+\frac{m_n \eta_{\mathrm{V}_n}}{\Omega_n \mathcal{B}_{\mathrm{V}_n}})^{-\mathrm{N}_e m_e-p}$ with varying $p=0$ to r, and exponential function $\mathrm{e}^{-\frac{m_n(\eta_{\mathrm{V}_n}-1)}{\Omega_n \mathcal{B}_{\mathrm{V}_n}}}$. We can see that the impact of γ on these terms will be negligible in the higher regime of γ, and hence SOP saturates, as also reported in Section VII.

2) Also, the SOP decays fast as Ω_n increases because of the dominance of the term $(\frac{1}{\Omega_n})^r(\frac{m_e}{\Omega_e \mathcal{B}_{\mathrm{E}}}+\frac{m_n \eta_{\mathrm{V}_n}}{\Omega_n \mathcal{B}_{\mathrm{V}_n}})^{-\mathrm{N}_e m_e-p}$, with varying $p=0$ to r and $r=0$ to $\mathrm{N}_n m_n-1$, as also shown numerically in Section VII. In addition, SOP is the function of $(\eta_{\mathrm{V}_n})^p(\eta_{\mathrm{V}_n}-1)^{r-p}$ with $\eta_{\mathrm{V}_n}=2^{\mathcal{R}_{\mathrm{V}_n}}$ and varying $p=0$ to r where r varies 0 to $\mathrm{N}_n m_n-1$, which implies that SOP increases as $\mathcal{R}_{\mathrm{V}_n}$ increases.

3) The effects of other associated parameters, like, number of antennas, fading severity parameters, CEE, time-varying errors, and quality of eavesdropper link, on the SOP performance can be obtained in a similar way.

3) OVERALL SOP

The overall SOP expression of the considered SIMO NOMA-enabled V2V communication system under Scenario I can be expressed as [17], [46]

$$\mathcal{P}^{\mathrm{I}}_{\mathrm{sec,System}}=1-(1-\mathcal{P}^{\mathrm{I}}_{\mathrm{sec},\mathrm{V}_f}(\eta_{\mathrm{V}_f}))(1-\mathcal{P}^{\mathrm{I}}_{\mathrm{sec},\mathrm{V}_n}(\eta_{\mathrm{V}_n})), \quad (25)$$

where $\mathcal{P}^{\mathrm{I}}_{\mathrm{sec},\mathrm{V}_f}(\eta_{\mathrm{V}_f})$ and $\mathcal{P}^{\mathrm{I}}_{\mathrm{sec},\mathrm{V}_n}(\eta_{\mathrm{V}_n})$ are given in (22) and (24), respectively.

B. SOP ANALYSIS UNDER SCENARIO II

Here, we derive the analytical SOP expressions for V_f, V_n, and the overall system under Scenario II.

1) SOP OF V_f

Using (20), the SOP of V_f is given by

$$\mathcal{P}^{\mathrm{II}}_{\mathrm{sec},\mathrm{V}_f}(\eta_{\mathrm{V}_f})=\mathbf{Pr}\left[\Lambda_{\mathrm{V}_f}<\eta_{\mathrm{V}_f}\Lambda_{\mathrm{E}^{\mathrm{II}}_f}+\eta_{\mathrm{V}_f}-1\right], \quad (26)$$

which can be further evaluated over Nakagami-*m* fading channels according to Theorem 3.

Theorem 3: Under Scenario II, the SOP expression for the legitimate user vehicle V_f under combined effect of nodes' mobility and CEE can be expressed as

$$\mathcal{P}^{\mathrm{II}}_{\mathrm{sec},\mathrm{V}_f}(\eta_{\mathrm{V}_f})=1-\sum_{s=0}^{\mathrm{N}_f m_f-1}\sum_{w=1}^{\mathcal{M}}\frac{1}{s!}\frac{\pi}{\mathcal{M}}\frac{\beta}{\Gamma(\mathrm{N}_e m_e)}\left(\frac{\xi}{2}\right)^{\mathrm{N}_e m_e}\times\left(\frac{m_f\left(\Omega_{q_{\mathrm{V}_f}}+\frac{1}{\gamma}\right)}{\Omega_f \rho^2_{\mathrm{V}_f}}\right)^s\left(\frac{m_e\left(\Omega_{q_{\mathrm{E}}}+\frac{1}{\gamma}\right)}{\Omega_e \rho^2_{\mathrm{E}}}\right)^{\mathrm{N}_e m_e}\mathcal{A}_w(\eta_{\mathrm{V}_f}), \quad (27)$$

where $\overline{\xi}_w=\frac{\xi}{2}(t_w+1)$, $t_w=\cos\left(\frac{(2w-1)\pi}{2\mathcal{M}}\right)$, $\mathcal{M}$ denotes the number of summation terms,

$$\mathcal{A}_w(\eta_{\mathrm{V}_f})=\frac{(1-t_w^2)^{\frac{1}{2}}(\eta_{\mathrm{V}_f}\overline{\xi}_w+\eta_{\mathrm{V}_f}-1)^s}{(\beta-(1-\beta)(\eta_{\mathrm{V}_f}\overline{\xi}_w+\eta_{\mathrm{V}_f}-1))^s}\times\frac{(t_w+1)^{\mathrm{N}_e m_e-1}}{(\beta-(1-\beta)\overline{\xi}_w)^{\mathrm{N}_e m_e+1}}e^{-\mathcal{B}_2(\eta_{\mathrm{V}_f})},$$

$$\text{and } \mathcal{B}_2(\eta_{\mathrm{V}_f})=\frac{m_f}{\Omega_f}\left(\frac{\left(\Omega_{q_{\mathrm{V}_f}}+\frac{1}{\gamma}\right)(\eta_{\mathrm{V}_f}\overline{\xi}_w+\eta_{\mathrm{V}_f}-1)}{\rho^2_{\mathrm{V}_f}(\beta-(1-\beta)(\eta_{\mathrm{V}_f}\overline{\xi}_w+\eta_{\mathrm{V}_f}-1))}\right)+\frac{m_e\left(\Omega_{q_{\mathrm{E}}}+\frac{1}{\gamma}\right)\overline{\xi}_w}{\Omega_{\mathrm{e}}\rho^2_{\mathrm{E}}\left(\beta-(1-\beta)\overline{\xi}_w\right)}.$$

Proof: See Appendix C for the detailed steps. ■

2) SOP OF V_n

Notably, the SNR at E under Scenario II remains identical to Scenario I, therefore, the SOP of near user vehicle V_n is similar to the SOP expression deduced in (24), and can be expressed as

$$\mathcal{P}^{\mathrm{II}}_{\mathrm{sec},\mathrm{V}_n}(\eta_{\mathrm{V}_n})=1-\sum_{r=0}^{\mathrm{N}_n m_n-1}\sum_{p=0}^{r}\frac{1}{r!}\binom{r}{p}\left(\frac{m_n}{\Omega_n \mathcal{B}_{\mathrm{V}_n}}\right)^r\times(\eta_{\mathrm{V}_n})^p\frac{(\eta_{\mathrm{V}_n}-1)^{r-p}}{\Gamma(\mathrm{N}_e m_e)}\left(\frac{m_e}{\Omega_e \mathcal{B}_{\mathrm{E}}}\right)^{\mathrm{N}_e m_e}\times\frac{\Gamma(\mathrm{N}_e m_e+p)}{\left(\frac{m_e}{\Omega_e \mathcal{B}_{\mathrm{E}}}+\frac{m_n \eta_{\mathrm{V}_n}}{\Omega_n \mathcal{B}_{\mathrm{V}_n}}\right)^{\mathrm{N}_e m_e+p}}\mathrm{e}^{-\frac{m_n(\eta_{\mathrm{V}_n}-1)}{\Omega_n \mathcal{B}_{\mathrm{V}_n}}}. \quad (28)$$

Remark 3: The SOP expressions of V_f in (27) and V_n in (28) under Scenario II are presented in closed-form, and hence making them practically efficient and effective for use. Moreover, the impact of various channel/system parameters, such as, number of antennas at legitimate and eavesdropper terminals, fading severity parameters, CEE, time-varying errors, transmit SNR, and quality of eavesdropper and legitimate links, on the SOP performance under Scenario II can be formulated and justified in the same manner as reported in Remarks 1 and 2 for Scenario I.

3) OVERALL SOP

The overall SOP expression of the considered SIMO NOMA-enabled V2V communication system under Scenario II can be given as

$$\mathcal{P}^{\mathrm{II}}_{\mathrm{sec,System}}=1-(1-\mathcal{P}^{\mathrm{II}}_{\mathrm{sec},\mathrm{V}_f}(\eta_{\mathrm{V}_f}))(1-\mathcal{P}^{\mathrm{II}}_{\mathrm{sec},\mathrm{V}_n}(\eta_{\mathrm{V}_n})), \quad (29)$$

where $\mathcal{P}^{\mathrm{II}}_{\mathrm{sec},\mathrm{V}_f}(\eta_{\mathrm{V}_f})$ and $\mathcal{P}^{\mathrm{II}}_{\mathrm{sec},\mathrm{V}_n}(\eta_{\mathrm{V}_n})$ given in (27) and (28), respectively.

IV. ASYMPTOTIC SOP ANALYSIS

In this section, we perform the asymptotic SOP analysis of the legitimate user vehicles V_f and V_n to obtain further insights

on the achievable secrecy diversity order under both Scenarios I and II. For the considered study, we model the variance of time-varying error component as $\Omega_{\epsilon_\iota} = \Omega_{\delta_\iota} + \Omega_\kappa$, for $(\iota, \kappa) \in \{(\mathrm{V}_f, f), (\mathrm{V}_n, n), (\mathrm{E}, e)\}$. To investigate the asymptotic SOP analysis and secrecy diversity order, we consider three possible cases of interest:

1) *Case 1:* when the transmit SNR for $\mathrm{V}_f(\mathrm{V}_n)$ goes to infinity, i.e., $\gamma \to \infty$, In this case, the SNR improves simultaneously at both legitimate vehicles and eavesdropper vehicle.
2) *Case 2:* when the channel quality of legitimate vehicles is better than the eavesdropper's channel quality, i.e., $\Omega_f \to \infty, \Omega_n \to \infty$ with Ω_e as a fixed finite value. Such a situation arises practically when the eavesdropper vehicle is far away from S compared to the legitimate user vehicles.
3) *Case 3:* when the legitimate and eavesdropper vehicles have same channel strengths, i.e., $\Omega_f \to \infty, \Omega_n \to \infty, \Omega_e \to \infty$. Such a condition resembles to a situation where the legitimate and eavesdropper vehicles are moving near to the source vehicle.

Further, it is important to note that under Case 3, the legitimate vehicles V_f and V_n under Scenarios I and II will never be able to extract any secrecy diversity benefits, because all the legitimate and wiretap links experience strong channel conditions and thereby observing a perfect eavesdropping. As such, in what follows, we present the asymptotic SOP analysis under Case 1 and Case 2 for both Scenarios I and II.

Moreover, the secrecy diversity order of ι-th legitimate user vehicle, for $\iota \in \{\mathrm{V}_f, \mathrm{V}_n\}$, can be extracted from the asymptotic analysis under Scenarios I and II by exploiting the definition $\mathbb{D}^j_{\mathrm{sec},\iota} = -\lim_{\mathcal{X}\to\infty} \frac{\log \widetilde{\mathcal{P}}^j_{\mathrm{sec},\iota}}{\log \mathcal{X}}$, for $\mathcal{X} \in \{\gamma, \Omega_f, \Omega_n\}$, $\iota \in \{\mathrm{V}_f, \mathrm{V}_n\}$, $j \in \{\mathrm{I}, \mathrm{II}\}$, and $\widetilde{\mathcal{P}}^j_{\mathrm{sec},\iota}$ denotes the asymptotic SOP of legitimate vehicles.

A. ASYMPTOTIC SOP ANALYSIS UNDER SCENARIO I

1) ASYMPTOTIC SOP ANALYSIS OF V_f

Here, we present the asymptotic SOP analysis for far user vehicle V_f for Cases 1 and 2 under the joint impact of nodes' mobility and CEE in the presence of Nakagami-m fading.

Case 1: When transmit SNR approaches infinity, i.e., $\gamma \to \infty$, we can approximate the instantaneous SINR and SNR in (7) and (9) as $\Lambda_{\mathrm{V}_f} \approx \frac{\beta\rho^2_{\mathrm{V}_f}\hat{X}}{(1-\beta)\rho^2_{\mathrm{V}_f}\hat{X}+\Omega_{q_{\mathrm{V}_f}}}$ and $\Lambda_{\mathrm{E}^{\mathrm{I}}_f} \approx \frac{\rho^2_{\mathrm{E}}\hat{Z}}{\Omega_{q_{\mathrm{E}}}}$, respectively. Now, invoking these approximated SINR and SNR into (21) along with the distributions of $\hat{X}$ and $\hat{Z}$, and after some simplifications, we can express the asymptotic SOP of far user vehicle V_f as

$$\widetilde{\mathcal{P}}^{\mathrm{I,Case\ 1}}_{\mathrm{sec},\mathrm{V}_f}(\eta_{\mathrm{V}_f}) = 1 - \frac{\left(\frac{m_e\Omega_{q_{\mathrm{E}}}}{\Omega_e\rho^2_{\mathrm{E}}}\right)^{\mathrm{N}_e m_e}}{\Gamma(\mathrm{N}_e m_e)} \sum_{k=0}^{\mathrm{N}_f m_f - 1} \frac{1}{k!}\left(\frac{m_f\Omega_{q_{\mathrm{V}_f}}}{\Omega_f\rho^2_{\mathrm{V}_f}}\right)^k \times \int_0^{\xi} \frac{(\eta_{\mathrm{V}_f}x + \eta_{\mathrm{V}_f} - 1)^k x^{\mathrm{N}_e m_e - 1}\mathrm{e}^{-\mathcal{B}_3(x)}}{(\beta - (1-\beta)(\eta_{\mathrm{V}_f}x + \eta_{\mathrm{V}_f} - 1))^k}dx, \tag{30}$$

where $\mathcal{B}_3(x) = \frac{m_f}{\Omega_f}\left(\frac{\Omega_{q_{\mathrm{V}_f}}(\eta_{\mathrm{V}_f}x+\eta_{\mathrm{V}_f}-1)}{\rho^2_{\mathrm{V}_f}(\beta-(1-\beta)(\eta_{\mathrm{V}_f}x+\eta_{\mathrm{V}_f}-1))}\right) + \frac{m_e\Omega_{q_{\mathrm{E}}}}{\Omega_e\rho^2_{\mathrm{E}}}x$ and $\xi = \frac{1}{\eta_{\mathrm{V}_f}(1-\beta)} - 1$. The integral in (30) seems intractable due to its complicated form, therefore, it can be simplified by applying the Gauss-Chebyshev quadrature [66, Eq. (25.4.38)] numerical method to express $\widetilde{\mathcal{P}}^{\mathrm{I,Case\ 1}}_{\mathrm{sec},\mathrm{V}_f}(\eta_{\mathrm{V}_f})$ as

$$\widetilde{\mathcal{P}}^{\mathrm{I,Case\ 1}}_{\mathrm{sec},\mathrm{V}_f}(\eta_{\mathrm{V}_f}) = 1 - \frac{\left(\frac{m_e\Omega_{q_{\mathrm{E}}}}{\Omega_e\rho^2_{\mathrm{E}}}\right)^{\mathrm{N}_e m_e}}{\Gamma(\mathrm{N}_e m_e)} \sum_{k=0}^{\mathrm{N}_f m_f - 1} \sum_{u=1}^{\mathcal{N}} \frac{1}{k!}\frac{\pi}{\mathcal{N}} \times \left(\frac{m_f\Omega_{q_{\mathrm{V}_f}}}{\Omega_f\rho^2_{\mathrm{V}_f}}\right)^k \left(\frac{\xi}{2}\right)^{\mathrm{N}_e m_e} \mathrm{e}^{-\mathcal{B}_3(\bar{\xi}_u)}\mathcal{A}_u(\eta_{\mathrm{V}_f}), \tag{31}$$

where t_u, $\bar{\xi}_u$, and $\mathcal{A}_u(\eta_{\mathrm{V}_f})$ are given in (22).

Remark 4: The following insights can be discussed from the above analysis.

1) It can be seen from (31) that $\widetilde{\mathcal{P}}^{\mathrm{I,Case\ 1}}_{\mathrm{sec},\mathrm{V}_f}(\eta_{\mathrm{V}_f})$ is independent of transmit SNR, γ, which indicates that the achievable secrecy diversity order for V_f is zero under the high SNR regime, $\gamma \to \infty$. Such a behavior is expected as the transmit SNR at legitimate vehicle and eavesdropper vehicle improves by the same factor.
2) Also, one can easily observe that the SOP significantly depends on the quality of the wiretap channel Ω_e, and hence because of the $(\frac{1}{\Omega_e})^{\mathrm{N}_e m_e}$ function, the SOP attains its maximum when Ω_e is very large. Mathematically, $\widetilde{\mathcal{P}}^{\mathrm{I,Case\ 1}}_{\mathrm{sec},\mathrm{V}_f}(\eta_{\mathrm{V}_f}) = 1$ for $\Omega_e \to \infty$. This behavior is also depicted numerically in Section VII.

Case 2: In this case, we consider $\Omega_f \to \infty$ and Ω_e has some finite fixed value. To proceed, we first apply the well known approximation $\Upsilon(\beta, x) \underset{x\to 0}{\approx} \frac{x^\beta}{\beta}$ into (15) so as to obtain the approximate CDF expression of the SINR at V_f, i.e., $F_{\Lambda_{\mathrm{V}_f}}(y) \approx \frac{1}{\Gamma(m_f\mathrm{N}_f+1)}\left(\frac{m_f}{\Omega_f}\frac{\left(\Omega_{q_{\mathrm{V}_f}}+\frac{1}{\gamma}\right)y}{\rho^2_{\mathrm{V}_f}(\beta-(1-\beta)y)}\right)^{m_f\mathrm{N}_f}$. Then, invoking this CDF along with the PDF of $\Lambda_{\mathrm{E}^{\mathrm{I}}_f}$ into (21) and simplifying the integral via Gauss-Chebyshev quadrature numerical method [66, Eq. (25.4.38)], and ignoring the higher order infinitesimal terms for $\Omega_f \to \infty$, we can express the asymptotic SOP of V_f as

$$\widetilde{\mathcal{P}}^{\mathrm{I,Case\ 2}}_{\mathrm{sec},\mathrm{V}_f}(\eta_{\mathrm{V}_f}) = 1 - \frac{\Upsilon\left(\mathrm{N}_e m_e, \frac{m_e(\beta\Omega_{q_{\mathrm{E}}}+\frac{1}{\gamma})}{\beta\Omega_e\rho^2_{\mathrm{E}}}\xi\right)}{\Gamma(\mathrm{N}_e m_e)}. \tag{32}$$

Remark 5: From (32), we can have the following important observations:

1) The expression presented in (32) is independent of Ω_f, which indicates that the secrecy diversity order of V_f

under this case $\left(\Omega_f \to \infty \text{ with fixed } \Omega_e\right)$ is zero, as also demonstrated in Section VII.

2) By applying the relation $\Upsilon(n,x) = (n-1)![1 - \mathrm{e}^{-x}\sum_{k=0}^{n-1}\frac{x^k}{k!}]$ [51, Eq. (8.352.6)], we can represent (32) as $\widetilde{\mathcal{P}}^{\mathrm{II,Case\,2}}_{\mathrm{sec,V}_f}(\eta_{\mathrm{V}_f}) = \mathrm{e}^{-\frac{m_e(\beta\Omega_{q_\mathrm{E}}+\frac{1}{\gamma})}{\beta\Omega_e\rho^2_\mathrm{E}}\xi}$ $\sum_{r=0}^{m_e\mathrm{N}_e-1}\frac{1}{r!}\left(\frac{m_e(\beta\Omega_{q_\mathrm{E}}+\frac{1}{\gamma})}{\beta\Omega_e\rho^2_\mathrm{E}}\xi\right)^r$. From which, we can see that the SOP is directly proportional to $(m_e)^r\mathrm{e}^{-\frac{m_e(\beta\Omega_{q_\mathrm{E}}+\frac{1}{\gamma})}{\beta\Omega_e\rho^2_\mathrm{E}}\xi}$, but mainly dominated by the term $(m_e)^r$ with increasing m_e parameter for varying $r = 0$ to $m_e\mathrm{N}_e - 1$, and hence yields into a higher SOP. This is also shown numerically in Section VII.

3) The SOP is also the direct function of $(\frac{1}{\Omega_e})^r\mathrm{e}^{-\frac{m_e(\beta\Omega_{q_\mathrm{E}}+\frac{1}{\gamma})}{\beta\Omega_e\rho^2_\mathrm{E}}\xi}$, which suggests that i) the term $(\frac{1}{\Omega_e})^r$ decays with varying $r = 0$ to $m_e\mathrm{N}_e - 1$ as Ω_e increases, and ii) the negative exponential $\mathrm{e}^{-\frac{m_e(\beta\Omega_{q_\mathrm{E}}+\frac{1}{\gamma})}{\beta\Omega_e\rho^2_\mathrm{E}}\xi}$ increases rapidly to a higher value with increasing Ω_e. Overall, the exponential term dominates and hence the SOP increases as Ω_e increases, also reported numerically in Section VII.

4) Likewise, one can analytically observe the impact of CEE, time-varying errors, number of eavesdropper antennas, power allocation factor, threshold, and transmit SNR on the SOP performance.

2) ASYMPTOTIC SOP ANALYSIS OF V_n

In what follows, we discuss the asymptotic SOP analysis for near user vehicle V_n for Cases 1 and 2 under the combined effect of nodes' mobility and CEE in the presence of Nakagami-*m* fading channels.

Case 1: Under the situation when $\gamma \to \infty$, the SNRs at V_n in (8) and E in (10) can be approximated as $\Lambda_{\mathrm{V}_n} = \frac{\rho^2_{\mathrm{V}_n}\hat{Y}}{\Omega_{q_{\mathrm{V}_n}}}$ and $\Lambda^{\mathrm{I}}_{\mathrm{E}_n} = \frac{\rho^2_\mathrm{E}\hat{Z}}{\Omega_{q_\mathrm{E}}}$, respectively. Further, invoking these into (23) along with the CDF of $\hat{Y}$ and the PDF of $\hat{Z}$, and carried out the required integral by applying the identities $\Upsilon(n,x) = (n-1)![1 - \mathrm{e}^{-x}\sum_{k=0}^{n-1}\frac{x^k}{k!}]$ [51, Eq. (8.352.6)] and $\int_0^\infty z^n e^{-\mu z}dz = \frac{\Gamma(n+1)}{\mu^{n+1}}$ [51, Eq. (3.351.3)], we can express the asymptotic SOP expression of V_n for $\gamma \to \infty$ as

$$\widetilde{\mathcal{P}}^{\mathrm{I,Case\,1}}_{\mathrm{sec,V}_n}(\eta_{\mathrm{V}_n}) = 1 - \sum_{r=0}^{\mathrm{N}_n m_n-1}\sum_{p=0}^{r}\frac{1}{r!}\binom{r}{p}\left(\frac{m_n\Omega_{q_{\mathrm{V}_n}}}{\Omega_n\rho^2_{\mathrm{V}_n}}\right)^r \times (\eta_{\mathrm{V}_n})^p\frac{(\eta_{\mathrm{V}_n}-1)^{r-p}}{\Gamma(\mathrm{N}_e m_e)}\left(\frac{m_e\Omega_{q_\mathrm{E}}}{\Omega_e\rho^2_\mathrm{E}}\right)^{\mathrm{N}_e m_e} \times \mathrm{e}^{-\frac{m_n\Omega_{q_{\mathrm{V}_n}}(\eta_{\mathrm{V}_n}-1)}{\Omega_n\rho^2_{\mathrm{V}_n}}} \times \frac{\Gamma(\mathrm{N}_e m_e + p)}{\left(\frac{m_n\Omega_{q_{\mathrm{V}_n}}\eta_{\mathrm{V}_n}}{\Omega_n\rho^2_{\mathrm{V}_n}} + \frac{m_e\Omega_{q_\mathrm{E}}}{\Omega_e\rho^2_\mathrm{E}}\right)^{\mathrm{N}_e m_e+p}}. \quad (33)$$

Remark 6: From (33), we can see that the asymptotic SOP, $\mathcal{P}^{\mathrm{I,asy}}_{\mathrm{sec,V}_n}(\eta_{\mathrm{V}_n})$, is independent of transmit SNR γ and hence V_n achieves a zero secrecy diversity order. This behavior is due to the improvement in SNR at both V_n and E by the same factor. Moreover, because of the dominance of $(\frac{1}{\Omega_e})^{\mathrm{N}_e m_e}$ function, the SOP reaches to its maximum when Ω_e is very large, and even can attain $\widetilde{\mathcal{P}}^{\mathrm{I,Case\,1}}_{\mathrm{sec,V}_n}(\eta_{\mathrm{V}_n}) = 1$ when $\Omega_e \to \infty$. This deteriorating behavior of SOP is obvious because increasing Ω_e increases the eavesdropper's chances of intercepting the valid information.

Case 2: Under this case, we assume $\Omega_n \to \infty$ with fixed Ω_e. Accordingly, we can have $\Omega_{\epsilon_{\mathrm{V}_n}} = \Omega_{\delta_{\mathrm{V}_n}} + \Omega_n \approx \Omega_n$ and consequently, we get $\Omega_{q_{\mathrm{V}_n}} = \rho^2_t\Omega_{\delta_{\mathrm{V}_n}} + (1-\rho^2_{\mathrm{V}_n})\Omega_n$. Further, invoking these into (8) and simplifying for $\Omega_n \to \infty$, we can obtain the instantaneous SNR in (8) as $\Lambda_{\mathrm{V}_n} \approx \frac{\rho^2_{\mathrm{V}_n}\hat{Y}}{(1-\rho^2_{\mathrm{V}_n})\Omega_n}$. Then, invoking this into (23) along with the CDF of $\hat{Y}$ with the fact $\Upsilon(\beta,x) \underset{x\to 0}{\approx} \frac{x^\beta}{\beta}$ and the PDF of $\Lambda_{\mathrm{E}^{\mathrm{I}}_n}$, and then solving the required integral via [51, Eq. (3.351.3)], we can obtain the asymptotic SOP expression of V_n as

$$\widetilde{\mathcal{P}}^{\mathrm{I,Case\,2}}_{\mathrm{sec,V}_n}(\eta_{\mathrm{V}_n}) = \frac{\left(\frac{m_n(1-\rho^2_{\mathrm{V}_n})}{\rho^2_{\mathrm{V}_n}}\right)^{\mathrm{N}_n m_n}}{\Gamma(\mathrm{N}_n m_n+1)\Gamma(\mathrm{N}_e m_e)}\sum_{l=0}^{\mathrm{N}_n m_n}\binom{\mathrm{N}_n m_n}{l} \times (\eta_{\mathrm{V}_n})^l(\eta_{\mathrm{V}_n}-1)^{\mathrm{N}_n m_n-l} \times \frac{\Gamma(\mathrm{N}_e m_e + l)}{\left(\frac{m_e}{\Omega_e}\left(\frac{(1-\beta)\Omega_{q_\mathrm{E}}+\frac{1}{\gamma}}{(1-\beta)\rho^2_\mathrm{E}}\right)\right)^l}. \quad (34)$$

Remark 7: The following observations can be drawn from this analysis.

1) We can see that (34) is independent of Ω_n, which reflects that V_n achieves a zero secrecy diversity order when $\Omega_n \to \infty$ with fixed Ω_e.
2) The SOP expression is directly related to $(\eta_{\mathrm{V}_n})^l(\eta_{\mathrm{V}_n}-1)^{\mathrm{N}_n m_n-l}$ for varying $l = 0$ to $\mathrm{N}_n m_n$, where $\eta_{\mathrm{V}_n} = 2^{\mathcal{R}_{\mathrm{V}_n}}$, and hence the SOP increases as the target rate $\mathcal{R}_{\mathrm{V}_n}$ increases. This further implies that more power is required to support the higher secrecy capacity.
3) In addition, the SOP expression is directly proportional to $(\Omega_e)^l$ for varying $l = 0$ to $m_n\mathrm{N}_n$, and hence the SOP increases rapidly with increasing Ω_e. This behavior is expected because an improvement in the quality of the wiretap channel strengthens the eavesdropper capability to intercept the legitimate information and consequently increases the SOP.
4) Likewise, the impact of other associated parameters, such as, CEE, time-varying errors, number of antennas at the near user vehicle and eavesdropper, fading severity parameters, and SNR, on the SOP performance.

B. ASYMPTOTIC SOP ANALYSIS UNDER SCENARIO II

By following the similar approach as adopted in Scenario I to evaluate the asymptotic SOP analysis for V_f and V_n and corresponding secrecy diversity orders, we can easily analyze the asymptotic SOP and secrecy diversity orders for both legitimate user vehicles, V_f and V_n, under Cases 1 and 2. From this analysis (the detailed derivations are skipped here for brevity), we observe that both V_f and V_n achieve zero secrecy diversity order under formulated Cases 1 and 2, which is due to the several factors, such as asymptotic SOP expressions are not the function of average transmit SNR/average channel gains of the legitimate links, CEE, and time varying errors.

V. SPECIAL CASES OF INTEREST

In this section, we present some important remarks by formulating and elaborating some special cases of interest to reveal further observations and insights upon the impact of different channel/system parameters under the joint presence of nodes' mobility and CEE on the system's secrecy performance.

A. ALL MOBILE NODES WITH NO CEE

In this setting, we have $\rho_\iota \in [0, 1]$ corresponding to nodes' mobility and $\Omega_{\delta_\iota} = 0$ (no CEE or perfect channel estimates), for $\iota \in \{V_f, V_n, E\}$. Accordingly, we below present some key remarks for both V_f and V_n under Scenarios I and II.

1) *Exact SOP expression:* For all mobile nodes' and assuming perfect channel estimates, we can have $\Omega_{q_\iota} = (1 - \rho_\iota^2)\Omega_{\epsilon_\iota}$ and $\Omega_{\epsilon_\iota} = \Omega_\kappa$, for $(\iota, \kappa) \in \{(V_f, f), (E, e)\}$, for the far user vehicle V_f. Now, invoking these into (22) for Scenario I and into (27) for Scenario II, we can obtain the analytical SOP expressions for the far user vehicle V_f under this setting. Likewise, we can get the analytical SOP expressions for the near user vehicle V_n by substituting $\Omega_{q_\iota} = (1 - \rho_\iota^2)\Omega_{\epsilon_\iota}$ and $\Omega_{\epsilon_\iota} = \Omega_\kappa$, for $(\iota, \kappa) \in \{(V_n, n), (E, e)\}$ into (24) for Scenario I and into (28) for Scenario II.
2) *Asymptotic SOP limit when $\gamma \to \infty$:* We can express the SOP asymptotic limit (when $\gamma \to \infty$) for the far user vehicle V_f under Scenario I by invoking $\Omega_{q_\iota} = (1 - \rho_\iota^2)\Omega_{\epsilon_\iota}$ and $\Omega_{\epsilon_\iota} = \Omega_\kappa$, for $(\iota, \kappa) \in \{(V_f, f), (E, e)\}$ into (31). Moreover, the SOP asymptotic limit for near user vehicle V_n under Scenario I can be obtained by setting $\Omega_{q_\iota} = (1 - \rho_\iota^2)\Omega_{\epsilon_\iota}$ and $\Omega_{\epsilon_\iota} = \Omega_\kappa$, for $(\iota, \kappa) \in \{(V_n, n), (E, e)\}$, into (33). Likewise, one can also obtain the asymptotic SOP limit (when $\gamma \to \infty$) for V_f and V_n under Scenario II.

   Remark 8: Under this setting, we can note that the SOP curves of both V_f and V_n under Scenarios I and II achieve a secrecy floor phenomenon, which is due to the SOP expressions being independent of γ and the performance is limited by time-varying errors introduced by the nodes' mobility, as also reported numerically in Section VII.
3) *Asymptotic SOP limit for $\Omega_f, \Omega_n \to \infty$ with fixed Ω_e:* The SOP asymptotic limits for V_f and V_n when $\Omega_f, \Omega_n \to \infty$ with fixed Ω_e under Scenario I can be expressed by substituting $\Omega_{q_\iota} = (1 - \rho_\iota^2)\Omega_{\epsilon_\iota}$ and $\Omega_{\epsilon_\iota} = \Omega_\kappa$, for $(\iota, \kappa) \in \{(V_f, f), (V_n, n), (E, e)\}$ into (32) and (34), respectively. Similarly, we can obtain the SOP asymptotic limits of V_f and V_n for Scenario II under this setting.

   Remark 9: Notably, from this analysis, the SOP curves for both legitimate user vehicles exhibit a saturation floor even after they experience a better channel quality than the wiretap channels. This is owing to the dual impediments of time-varying errors and interference from the near user for V_f, while due to the impact of time-varying errors for V_n. Such a behavior is demonstrated numerically in Section VII.

The analytical findings under this setting are further demonstrated numerically in Section VII.

B. ALL STATIC NODES WITH CEE

In this setting, we have $\rho_\iota = 1$ (i.e., all nodes are stationary), and $\Omega_{\delta_\iota} \neq 0$ (with CEE or imperfect channel estimates), for $\iota \in \{V_f, V_n, E\}$. Under Scenarios I and II, we can have the following observations for both legitimate user vehicles.

1) *Exact SOP expression:* For all static nodes' (i.e., $\rho_\iota = 1$) with CEE, we can have $\Omega_{q_\iota} = \Omega_{\delta_\iota}$, for $\iota \in \{V_f, V_n, E\}$. For far user vehicle V_f, substituting $\Omega_{q_\iota} = \Omega_{\delta_\iota}$ and $\rho_\iota = 1$, for $\iota \in \{V_f, E\}$ into (22) for Scenario I and into (27) for Scenario II, we can obtain the analytical SOP expressions under this setting. Moreover, for near user vehicle V_n, inserting $\Omega_{q_\iota} = \Omega_{\delta_\iota}$ and $\rho_\iota = 1$, for $\iota \in \{V_n, E\}$ into (24) for Scenario I and into (28) for Scenario II, we can derive the SOP expressions.

   Remark 10: From this analysis, we can conclude that the SOP expressions of V_f and V_n under both scenarios become independent of time-varying errors and are limited by the CEEs. Hence, the SOP performance will be negatively influenced by the CEE.
2) *Asymptotic SOP limit when $\gamma \to \infty$:* For $\gamma \to \infty$ under Scenario I, substituting the modified relation $\Omega_{q_\iota} = \Omega_{\delta_\iota}$ and $\rho_\iota = 1$, for $\iota \in \{V_f, V_n, E\}$, into (31) and (33), we can get the asymptotic SOP limits for V_f and V_n, respectively. Likewise, we can obtain the asymptotic SOP limit ($\gamma \to \infty$) for V_f and V_n under Scenario II.

   Remark 11: From these asymptotic limits, it is worthwhile to note that the SOP exhibits a saturation floor (no diversity benefits) for V_f and V_n under both Scenarios I and II, even when they are independent of time-varying errors. This saturation is because of the presence of CEE.
3) *Asymptotic SOP limit for $\Omega_f, \Omega_n \to \infty$ with fixed Ω_e:* The SOP asymptotic limit (when $\Omega_f, \Omega_n \to \infty$ with fixed Ω_e) under Scenario I for V_f and V_n can be obtained by substituting $\Omega_{q_\iota} = \Omega_{\delta_\iota}$ and $\rho_\iota = 1$, for $\iota \in \{V_f, V_n, E\}$, into (32) and (34), respectively. Likewise,

we can also get the SOP asymptotic limit for V_f and V_n under Scenario II.

Remark 12: We can reveal from this analysis that the asymptotic limits for V_f and V_n under both scenarios are independent of time-varying errors. However, the system still achieves a zero secrecy diversity order, which is owing to the presence of CEE and interference for V_f, and only CEE for V_n.

We also illustrate the theoretical findings under this setting via numerical results in Section VII.

C. ALL STATIC NODES WITH NO CEE

Under this setting, we have $\rho_\iota = 1$ (i.e., static nodes) and $\Omega_{\delta_\iota} = 0$ (no CEE or perfect channel estimates), for $\iota \in \{\mathrm{V}_f, \mathrm{V}_n, \mathrm{E}\}$. We next draw some key observations pertaining to the SOP of V_f and V_n for Scenarios I and II.

1) *Exact SOP expression:* By setting $\rho_\iota = 1$ and $\Omega_{q_\iota} = 0$, for $\iota \in \{\mathrm{V}_f, \mathrm{V}_n, \mathrm{E}\}$ into (22) and (24), we can easily obtain the SOP expressions for V_f and V_n, respectively, for Scenario I. Likewise, invoking $\rho_\iota = 1$ and $\Omega_{q_\iota} = 0$, for $\iota \in \{\mathrm{V}_f, \mathrm{V}_n, \mathrm{E}\}$ into (27) and (28), we can also deduce the SOP expressions for V_f and V_n, respectively, under Scenario II.
2) *Asymptotic SOP limit when $\gamma \to \infty$:*
   - Utilizing $\rho_\iota = 1$ and $\Omega_{q_\iota} = 0$, for $\iota \in \{\mathrm{V}_f, \mathrm{E}\}$, we can express the instantaneous SNRs at V_f in (7) and E in (9) under Scenario I as $\Lambda_{\mathrm{V}_f} = \frac{\beta\gamma\hat{X}}{(1-\beta)\gamma\hat{X}+1}$ and $\Lambda_{\mathrm{E}_f^{\mathrm{I}}} = \beta\gamma\hat{Z}$, respectively. Further, invoking these into (21) along with the PDF of $\hat{Z}$ and the CDF of $\hat{X}$ with the high SNR approximation ($\gamma \to \infty$), i.e., $\Upsilon(\beta, x) \underset{x\to 0}{\approx} \frac{x^\beta}{\beta}$, and then simplifying the resultant integral via Gauss-Chebyshev quadrature numerical method [66, Eq. (25.4.38)], we can express the SOP asymptotic limit (for $\gamma \to \infty$) of V_f as

$$\widetilde{\mathcal{P}}^{\mathrm{I}}_{\mathrm{sec},\mathrm{V}_f}(\eta_{\mathrm{V}_f}) = 1 - \frac{\Upsilon\left(\mathrm{N}_e m_e, \frac{m_e}{\Omega_e\beta\gamma}\xi\right)}{\Gamma(\mathrm{N}_e m_e)} + \frac{\left(\frac{m_e\xi}{2\Omega_e\beta\gamma}\right)^{\mathrm{N}_e m_e}}{\Gamma(\mathrm{N}_e m_e)} \frac{\left(\frac{m_f}{\gamma\Omega_f}\right)^{\mathrm{N}_f m_f}}{\Gamma(\mathrm{N}_f m_f + 1)} \frac{\pi}{\mathcal{N}} \sum_{u=1}^{\mathcal{N}} \mathrm{e}^{-\frac{m_e\overline{\xi}_u}{\Omega_e\beta\gamma}} \times \frac{\sqrt{1-t_u^2}(\eta_{\mathrm{V}_f}\overline{\xi}_u + \eta_{\mathrm{V}_f} - 1)^{\mathrm{N}_f m_f}(t_u+1)^{\mathrm{N}_e m_e - 1}}{(\beta - (1-\beta)(\eta_{\mathrm{V}_f}\overline{\xi}_u + \eta_{\mathrm{V}_f} - 1))^{\mathrm{N}_f m_f}}. \quad (35)$$

Following the same approach, we can also deduce the SOP asymptotic limit of V_f for Scenario II, which is skipped here for brevity.

Remark 13: We can see from the SOP asymptotic limit in (35) that the far user vehicle V_f achieves zero secrecy diversity order, even for the scenario where all nodes are stationary and there is no CEE. This is due to the reason that i) the improved benefits of transmit SNR are equally exploited at V_f and E, and ii) the interference imposed on V_f from V_n.

- Furthermore, for the near user vehicle V_n with $\rho_\iota = 1$ and $\Omega_{q_\iota} = 0$, for $\iota \in \{\mathrm{V}_n, \mathrm{E}\}$, we can express the instantaneous SNRs at V_n and E as $\Lambda_{\mathrm{V}_n} = (1-\beta)\gamma\hat{Y}$ and $\Lambda_{\mathrm{E}_n^j} = (1-\beta)\gamma\hat{Z}$, respectively, for $\iota \in \{\mathrm{V}_n, \mathrm{E}\}$ and $j \in \{\mathrm{I}, \mathrm{II}\}$. Invoking these into the definition of SOP, i.e., $\widetilde{\mathcal{P}}_{\mathrm{sec},\mathrm{V}_n}(\eta_{\mathrm{V}_n}) = \mathbf{Pr}\left[\frac{1+\Lambda_{\mathrm{V}_n}}{1+\Lambda_{\mathrm{E}_n^j}} < \eta_{\mathrm{V}_n}\right]$, and applying the high SNR ($\gamma \to \infty$) approximation $\frac{1+x}{1+y} \approx \frac{x}{y}$, we can get $\widetilde{\mathcal{P}}_{\mathrm{sec},\mathrm{V}_n}(\eta_{\mathrm{V}_n}) \approx \mathbf{Pr}[\frac{\hat{Y}}{\hat{Z}} \leq \eta_{\mathrm{V}_n}] = \int_0^\infty F_{\hat{Y}}(\eta_{\mathrm{V}_n} z) f_{\hat{Z}}(z) dz$. Invoking the required CDF and PDF and simplifying the integral, we can express the SOP asymptotic limit (when $\gamma \to \infty$) for near user vehicle, V_n, under Scenarios I and II as

$$\widetilde{\mathcal{P}}_{\mathrm{sec},\mathrm{V}_n}(\eta_{\mathrm{V}_n}) \underset{\gamma\to\infty}{\approx} 1 - \frac{\left(\frac{m_e}{\Omega_e}\right)^{\mathrm{N}_e m_e}}{\Gamma(\mathrm{N}_e m_e)} \sum_{k=0}^{\mathrm{N}_n m_n - 1} \frac{1}{k!} \times \left(\frac{m_n}{\Omega_n}\right)^k (\eta_{\mathrm{V}_n})^k \frac{\Gamma(\mathrm{N}_e m_e + k)}{\left(\frac{m_n\eta_{\mathrm{V}_n}}{\Omega_n} + \frac{m_e}{\Omega_e}\right)^{\mathrm{N}_e m_e + k}}. \quad (36)$$

Remark 14: From (36), some important observations are as follows: 1) we can see that the SOP asymptotic limit of V_n is independent of γ. This affirms the fact that V_n also fails to extract any secrecy diversity benefits, and 2) for $k = 0$, $\widetilde{\mathcal{P}}_{\mathrm{sec},\mathrm{V}_n}(\eta_{\mathrm{V}_n})$ can be approximated as $\widetilde{\mathcal{P}}_{\mathrm{sec},\mathrm{V}_n}(\eta_{\mathrm{V}_n}) = 1 - \frac{1}{(1+\frac{m_n\Omega_e\eta_{\mathrm{V}_n}}{m_e\Omega_n})^{\mathrm{N}_e m_e}} \approx \frac{m_n\eta_{\mathrm{V}_n}\mathrm{N}_e\Omega_e}{\Omega_n}$, from which we can conclude that for fixed m_n and η_{V_n}; i) SOP increases with an increase in N_e and/or Ω_e, as expected, and ii) SOP decays quickly as Ω_n increases.

3) *Asymptotic SOP limit for $\Omega_f, \Omega_n \to \infty$ with fixed Ω_e:*
   - By following the similar approach as adopted to obtain the SOP asymptotic limit when $\gamma \to \infty$, we can get the asymptotic limit on the SOP performance of V_f when $\Omega_f \to \infty$ with finite Ω_e for Scenarios I and II.

   Remark 15: From this analysis, we can observe that V_f achieves a zero secrecy diversity order, even when the associated average channel gain Ω_f is better than Ω_e. This is due to the reason that the signal received at V_f is interfered by V_n.
   - Furthermore, for Scenarios I and II, we can express the SOP asymptotic limit of V_n when $\Omega_n \to \infty$ for fixed Ω_e as

$$\widetilde{\mathcal{P}}_{\mathrm{sec},\mathrm{V}_n}(\eta_{\mathrm{V}_n}) \underset{\Omega_n\to\infty}{\approx} \left(\frac{\eta_{\mathrm{V}_n} m_n}{\Omega_n}\right)^{\mathrm{N}_n m_n} \left(\frac{m_e}{\Omega_e}\right)^{\mathrm{N}_e m_e} \times \frac{1}{\Gamma(\mathrm{N}_e m_e)(\mathrm{N}_n m_n)!} \frac{\Gamma(\mathrm{N}_n m_n + \mathrm{N}_e m_e)}{\left(\frac{m_n\eta_{\mathrm{V}_n}}{\Omega_n} + \frac{m_e}{\Omega_e}\right)^{\mathrm{N}_n m_n + \mathrm{N}_e m_e}}. \quad (37)$$

Remark 16: From (37), it is important to note that 1) the near user vehicle V_n can achieve a secrecy diversity order of $\mathrm{N}_n m_n$ for the case when $\Omega_n \to \infty$ with fixed Ω_e under the setting of static nodes and perfect channel estimates, and 2) the SOP decaying rate is mathematically fastened as Ω_n increases because of the dominance of $\left(\frac{1}{\Omega_n}\right)^{\mathrm{N}_n m_n}$ function, as also demonstrated in Section VII.

All the analytical findings obtained above are also corroborated via numerical results in Section VII.

VI. ERGODIC SECRECY CAPACITY (ESC) ANALYSIS

The secrecy capacity is the maximum rate below which legitimate source and destination users can communicate securely. The instantaneous secrecy capacity can be defined as the difference between the channel capacities pertaining to the legitimate link and the wiretap link, for $\kappa \in \{f, n\}$ and $j \in \{\mathrm{I}, \mathrm{II}\}$, and can be expressed mathematically for the considered system as [67]

$$\mathbf{C}^{j}_{\mathrm{sec},\mathrm{V}_\kappa} = \left[\log_2(1+\Lambda_{\mathrm{V}_\kappa}) - \log_2(1+\Lambda_{\mathrm{E}^j_\kappa})\right]^{+}, \tag{38}$$

where $[x]^{+} = \max(x, 0)$. By averaging the instantaneous secrecy capacity over the distributions of the instantaneous SNRs $\Lambda_{\mathrm{V}_\kappa}$ and $\Lambda_{\mathrm{E}^j_\kappa}$, we can express the ESC as

$$\overline{\mathbf{C}}^{j}_{\mathrm{sec},\mathrm{V}_\kappa} = \mathbb{E}\left[\mathbf{C}^{j}_{\mathrm{sec},\mathrm{V}_\kappa}(\Lambda_{\mathrm{V}_\kappa}, \Lambda_{\mathrm{E}^j_\kappa})\right]. \tag{39}$$

A. EXACT ESC ANALYSIS

Using (39), the ESC for both user vehicles under Scenarios I and II can be expressed as

$$\overline{\mathbf{C}}^{j,\mathrm{Exact}}_{\mathrm{sec},\mathrm{V}_\kappa} = \frac{1}{\ln(2)}\int_0^\infty \frac{F_{\Lambda_{\mathrm{E}^j_\kappa}}(y)}{1+y}\left(1 - F_{\Lambda_{\mathrm{V}_\kappa}}(y)\right)dy, \tag{40}$$

where $\kappa \in \{f, n\}$ and $j \in \{\mathrm{I}, \mathrm{II}\}$.

1) EXACT ESC ANALYSIS UNDER SCENARIO I

Here, we provide the ESC analysis of both user vehicles V_f and V_n under Scenario I with joint impact of nodes' mobility and CEE over Nakagami-m fading channels.

a) ESC of V_f: The ESC for V_f under Scenario I using (40) can be given as

$$\overline{\mathbf{C}}^{\mathrm{I},\mathrm{Exact}}_{\mathrm{sec},\mathrm{V}_f} = \frac{1}{\ln(2)}\int_0^\infty \frac{F_{\Lambda_{\mathrm{E}^{\mathrm{I}}_f}}(y)}{1+y}\left(1 - F_{\Lambda_{\mathrm{V}_f}}(y)\right)dy. \tag{41}$$

Invoking the CDF $F_{\Lambda_{\mathrm{V}_f}}(y)$ from (15) and the CDF $F_{\Lambda_{\mathrm{E}^{\mathrm{I}}_f}}(y)$ from (17) into (41), we can express $\overline{\mathbf{C}}^{\mathrm{I},\mathrm{Exact}}_{\mathrm{sec},\mathrm{V}_f}$ as

$$\overline{\mathbf{C}}^{\mathrm{I},\mathrm{Exact}}_{\mathrm{sec},\mathrm{V}_f} = \frac{1}{\ln(2)}\int_0^{\frac{\beta}{1-\beta}} \frac{1}{1+y}\frac{\Upsilon\left(m_e\mathrm{N}_e, \frac{m_e}{\Omega_e}\frac{(\beta\gamma\Omega_{q_\mathrm{E}}+1)y}{\rho^2_\mathrm{E}\beta\gamma}\right)}{\Gamma(m_e\mathrm{N}_e)}$$
$$\times\left(1 - \frac{1}{\Gamma(m_f\mathrm{N}_f)}\Upsilon\left(m_f\mathrm{N}_f, \frac{m_f}{\Omega_f}\frac{\left(\Omega_{q_{\mathrm{V}_f}}+\frac{1}{\gamma}\right)y}{\rho^2_{\mathrm{V}_f}(\beta-(1-\beta)y)}\right)\right)dy, \tag{42}$$

which can be further simplified by applying the transformation of variables $\frac{y}{\beta-(1-\beta)y} = t$ and using the fact $\Gamma(\alpha) = \Upsilon(\alpha, x) + \Gamma(\alpha, x)$, as

$$\overline{\mathbf{C}}^{\mathrm{I},\mathrm{Exact}}_{\mathrm{sec},\mathrm{V}_f} = \frac{1}{\ln(2)}\frac{1}{\Gamma(m_e\mathrm{N}_e)}\frac{1}{\Gamma(m_f\mathrm{N}_f)}\int_0^\infty \frac{\beta}{(1+t)(1+(1-\beta)t)}$$
$$\times\Upsilon\left(m_e\mathrm{N}_e, \frac{m_e}{\Omega_e}\frac{(\beta\gamma\Omega_{q_\mathrm{E}}+1)}{\rho^2_\mathrm{E}\beta\gamma}\frac{\beta t}{1+(1-\beta)t}\right)$$
$$\times\Gamma\left(m_f\mathrm{N}_f, \frac{m_f}{\Omega_f}\frac{\left(\Omega_{q_{\mathrm{V}_f}}+\frac{1}{\gamma}\right)t}{\rho^2_{\mathrm{V}_f}}\right)dt. \tag{43}$$

The analysis of the above integral seems tedious even after utilizing the series expansions $\Upsilon(n, x) = (n-1)![1 - \mathrm{e}^{-x}\sum_{k=0}^{n-1}\frac{x^k}{k!}]$ [51, Eq. (8.352.6)] and $\Gamma(n, x) = (n-1)!\mathrm{e}^{-x}\sum_{k=0}^{n-1}\frac{x^k}{k!}$ [51, Eq. (8.352.7)], therefore, we can simplify the required integral with respect to t by applying the Gauss-Laguerre quadrature method [66], and consequently the ESC $\overline{\mathbf{C}}^{\mathrm{I},\mathrm{Exact}}_{\mathrm{sec},\mathrm{V}_f}$ can be expressed as

$$\overline{\mathbf{C}}^{\mathrm{I},\mathrm{Exact}}_{\mathrm{sec},\mathrm{V}_f} = \frac{1}{\ln(2)}\frac{1}{\Gamma(m_e\mathrm{N}_e)}\frac{1}{\Gamma(m_f\mathrm{N}_f)}\sum_{i=1}^{\mathbb{U}_1}\frac{\beta w_i e^{t_i}}{(1+(1-\beta)t_i)}$$
$$\times\frac{1}{(1+t_i)}\Upsilon\left(m_e\mathrm{N}_e, \frac{m_e}{\Omega_e}\frac{(\beta\gamma\Omega_{q_\mathrm{E}}+1)}{\rho^2_\mathrm{E}\beta\gamma}\right.$$
$$\left.\times\frac{\beta t_i}{1+(1-\beta)t_i}\right)\Gamma\left(m_f\mathrm{N}_f, \frac{m_f}{\Omega_f}\frac{\left(\Omega_{q_{\mathrm{V}_f}}+\frac{1}{\gamma}\right)t_i}{\rho^2_{\mathrm{V}_f}}\right), \tag{44}$$

where t_i is the i-th root of Gauss-Laguerre polynomial $\mathcal{L}_{\mathbb{U}_1}(t)$ [66, Eq. (25.5.45)] and the weight w_i is given by $w_i = \frac{t_i}{(\mathbb{U}_1+1)^2[\mathcal{L}_{\mathbb{U}_1+1}(t_i)]^2}$.

Remark 17: From (44), we can have the following important observations.

1) The ESC expression consists of elementary functions, upper incomplete Gamma function, and lower incomplete function which can easily be evaluated for various values of channel/system parameters with the aid of Mathematica software package. In addition, the expression depends on the $\mathbb{U}_1$-order Gauss-Laguerre series expansion that converges quickly, as shown numerically in Section VII.
2) We can see that by applying the relation $\Gamma(n, x) = (n-1)!\mathrm{e}^{-x}\sum_{k=0}^{n-1}\frac{x^k}{k!}$ [51, Eq. (8.352.7)] into (44), the ESC expression is directly related to the $(m_f)^r \mathrm{e}^{-\frac{m_f}{\Omega_f}\frac{\left(\Omega_{q_{\mathrm{V}_f}}+\frac{1}{\gamma}\right)t_i}{\rho^2_{\mathrm{V}_f}}}$, for $r = 0$ to $m_f N_f - 1$, which indicates that as m_f increases the term $(m_f)^r$ has more

dominance than the exponential term, and hence results into a better ESC performance. In addition, we can also observe that when γ is very large, i.e., $\gamma \to \infty$, the ESC expression becomes independent of γ, and hence achieve a saturation floor in the high regime of γ, as also reported in Section VII.

3) Similarly, we can discuss several analytical observations into the ESC performance against the various involved system/channel parameters.

b) ESC of V_n: Utilizing the CDFs of $\Lambda_{\mathrm{E}_n^{\mathrm{I}}}$ from (16) and Λ_{V_n} from (19) into (40), the ESC of V_n under Scenario I can be expressed as

$$\overline{\mathrm{C}}_{\mathrm{sec},\mathrm{V}_n}^{\mathrm{I,Exact}} = \frac{1}{\ln(2)} \int_0^\infty \frac{1}{1+y} \frac{\Upsilon\left(m_e \mathrm{N}_e, \frac{m_e}{\Omega_e} \frac{\left((1-\beta)\gamma\Omega_{q_{\mathrm{E}}}+1\right)y}{\rho_{\mathrm{E}}^2(1-\beta)\gamma}\right)}{\Gamma(m_e \mathrm{N}_e)} \times \frac{\Gamma\left(m_n \mathrm{N}_n, \frac{m_n}{\Omega_n} \frac{\left((1-\beta)\gamma\Omega_{q_{\mathrm{V}_n}}+1\right)y}{\rho_{\mathrm{V}_n}^2(1-\beta)\gamma}\right)}{\Gamma(m_n \mathrm{N}_n)} dy. \tag{45}$$

Now, by applying the series expansions $\Upsilon(n,x) = (n-1)![1 - \mathrm{e}^{-x}\sum_{k=0}^{n-1}\frac{x^k}{k!}]$ [51, Eq. (8.352.6)] and $\Gamma(n,x) = (n-1)!\mathrm{e}^{-x}\sum_{k=0}^{n-1}\frac{x^k}{k!}$ [51, Eq. (8.352.7)], with some simplifications, we can express $\overline{\mathrm{C}}_{\mathrm{sec},\mathrm{V}_n}^{\mathrm{I,Exact}}$ as

$$\begin{aligned}\overline{\mathrm{C}}_{\mathrm{sec},\mathrm{V}_n}^{\mathrm{I,Exact}} = \frac{1}{\ln(2)} \Bigg[& \sum_{p=0}^{m_n\mathrm{N}_n-1} \frac{1}{p!} \left(\frac{m_n}{\Omega_n} \frac{\left((1-\beta)\gamma\Omega_{q_{\mathrm{V}_n}}+1\right)}{\rho_{\mathrm{V}_n}^2(1-\beta)\gamma}\right)^p \\ & \times \int_0^\infty \frac{y^p}{1+y} e^{-\left(\frac{m_n}{\Omega_n} \frac{\left((1-\beta)\gamma\Omega_{q_{\mathrm{V}_n}}+1\right)}{\rho_{\mathrm{V}_n}^2(1-\beta)\gamma}\right)y} dy \\ & - \sum_{p=0}^{m_n\mathrm{N}_n-1} \sum_{r=0}^{m_e\mathrm{N}_e-1} \frac{1}{p!}\frac{1}{r!} \left(\frac{m_e}{\Omega_e} \frac{\left((1-\beta)\gamma\Omega_{q_{\mathrm{E}}}+1\right)}{\rho_{\mathrm{E}}^2(1-\beta)\gamma}\right)^r \\ & \times \left(\frac{m_n}{\Omega_n} \frac{\left((1-\beta)\gamma\Omega_{q_{\mathrm{V}_n}}+1\right)}{\rho_{\mathrm{V}_n}^2(1-\beta)\gamma}\right)^p \int_0^\infty \frac{1}{1+y} y^{p+r} \\ & \times \mathrm{e}^{-\left(\frac{m_n}{\Omega_n} \frac{\left((1-\beta)\gamma\Omega_{q_{\mathrm{V}_n}}+1\right)}{\rho_{\mathrm{V}_n}^2(1-\beta)\gamma} + \frac{m_e}{\Omega_e} \frac{\left((1-\beta)\gamma\Omega_{q_{\mathrm{E}}}+1\right)}{\rho_{\mathrm{E}}^2(1-\beta)\gamma}\right)y} dy \Bigg], \end{aligned} \tag{46}$$

where the integrations can be simplified by applying the fact [64, Eq. (2.3.6.9)], and accordingly the ESC expression for near user vehicle can be expressed as

$$\begin{aligned}\overline{\mathrm{C}}_{\mathrm{sec},\mathrm{V}_n}^{\mathrm{I,Exact}} = & \frac{1}{\ln(2)} \Bigg[\sum_{p=0}^{m_n\mathrm{N}_n-1} \left(\frac{m_n}{\Omega_n} \frac{\left((1-\beta)\gamma\Omega_{q_{\mathrm{V}_n}}+1\right)}{\rho_{\mathrm{V}_n}^2(1-\beta)\gamma}\right)^p \\ & \times \Psi\left(p+1, p+1; \frac{m_n}{\Omega_n} \frac{\left((1-\beta)\gamma\Omega_{q_{\mathrm{V}_n}}+1\right)}{\rho_{\mathrm{V}_n}^2(1-\beta)\gamma}\right) \\ & - \sum_{p=0}^{m_n\mathrm{N}_n-1} \sum_{r=0}^{m_e\mathrm{N}_e-1} \frac{\Gamma(r+p+1)}{p!r!} \left(\frac{m_e}{\Omega_e} \frac{\left((1-\beta)\gamma\Omega_{q_{\mathrm{E}}}+1\right)}{\rho_{\mathrm{E}}^2(1-\beta)\gamma}\right)^r \\ & \times \left(\frac{m_n}{\Omega_n} \frac{\left((1-\beta)\gamma\Omega_{q_{\mathrm{V}_n}}+1\right)}{\rho_{\mathrm{V}_n}^2(1-\beta)\gamma}\right)^p \Psi\left(p+r+1, p+r+1; \right. \\ & \left. \frac{m_n}{\Omega_n} \frac{\left((1-\beta)\gamma\Omega_{q_{\mathrm{V}_n}}+1\right)}{\rho_{\mathrm{V}_n}^2(1-\beta)\gamma} + \frac{m_e}{\Omega_e} \frac{\left((1-\beta)\gamma\Omega_{q_{\mathrm{E}}}+1\right)}{\rho_{\mathrm{E}}^2(1-\beta)\gamma}\right)\Bigg], \end{aligned} \tag{47}$$

Remark 18: From (47), we can see that the ESC expression include finite series terms with some elementary and special functions, which can be evaluated for various set of involved channel/system parameters by using Mathematica/Matlab computational software packages.

c) Overall ESC: We can express the overall exact ESC expression for the considered SIMO NOMA-assisted V2V communication system under combined consideration of nodes' mobility and CEE as

$$\overline{\mathrm{C}}_{\mathrm{sec,\ overall}}^{\mathrm{I,Exact}} = \overline{\mathrm{C}}_{\mathrm{sec},\mathrm{V}_f}^{\mathrm{I,Exact}} + \overline{\mathrm{C}}_{\mathrm{sec},\mathrm{V}_n}^{\mathrm{I,Exact}}, \tag{48}$$

where $\overline{\mathrm{C}}_{\mathrm{sec},\mathrm{V}_f}^{\mathrm{I,Exact}}$ and $\overline{\mathrm{C}}_{\mathrm{sec},\mathrm{V}_n}^{\mathrm{I,Exact}}$ are given in (44) and (47).

2) EXACT ESC ANALYSIS UNDER SCENARIO II

Here, we provide the ESC analysis of both user vehicles V_f and V_n under Scenario II in the presence of joint impact of nodes' mobility and CEE over Nakagami-*m* fading channels.

a) ESC of V_f: By invoking the CDFs of $\Lambda_{\mathrm{E}_f^{\mathrm{II}}}$ from (18) and Λ_{V_f} from (15) into (40), the ESC of V_f under Scenario II can be expressed as

$$\overline{\mathrm{C}}_{\mathrm{sec},\mathrm{V}_f}^{\mathrm{II,Exact}} = \frac{1}{\ln(2)} \int_0^\infty \frac{1}{1+y} \frac{\Upsilon\left(m_e \mathrm{N}_e, \frac{m_e}{\Omega_e} \frac{\left(\Omega_{q_{\mathrm{E}}}+\frac{1}{\gamma}\right)y}{\rho_{\mathrm{E}}^2(\beta-(1-\beta)y)}\right)}{\Gamma(m_e \mathrm{N}_e)} \times \frac{1}{\Gamma(m_f \mathrm{N}_f)} \Gamma\left(m_f \mathrm{N}_f, \frac{m_f}{\Omega_f} \frac{\left(\Omega_{q_{\mathrm{V}_f}}+\frac{1}{\gamma}\right)y}{\rho_{\mathrm{V}_f}^2(\beta-(1-\beta)y)}\right) dy. \tag{49}$$

Now, following the similar approach as used to obtain the ESC of the far user vehicle under Scenario I, we can obtain the ESC expression for the far user vehicle V_f under Scenario II as

$$\begin{aligned}\overline{\mathrm{C}}_{\mathrm{sec},\mathrm{V}_f}^{\mathrm{II,Exact}} = & \frac{1}{\ln(2)} \frac{1}{\Gamma(m_e \mathrm{N}_e)} \frac{1}{\Gamma(m_f \mathrm{N}_f)} \sum_{i=1}^{\mathbb{U}_2} \frac{\beta w_i e^{t_i}}{(1+t_i)} \\ & \times \frac{1}{(1+(1-\beta)t_i)} \Upsilon\left(m_e \mathrm{N}_e, \frac{m_e}{\Omega_e} \frac{\left(\Omega_{q_{\mathrm{E}}}+\frac{1}{\gamma}\right)}{\rho_{\mathrm{E}}^2} t_i\right) \\ & \times \Gamma\left(m_f \mathrm{N}_f, \frac{m_f}{\Omega_f} \frac{\left(\Omega_{q_{\mathrm{V}_f}}+\frac{1}{\gamma}\right)}{\rho_{\mathrm{V}_f}^2} t_i\right). \end{aligned} \tag{50}$$

TABLE 3. Difference Between Exact and Approximate Expressions for the Far User Vehicle V_f Under Scenario I

SNR (dB)	15	20	25	30	35	40
Exact $\{(m_f, N_f), (m_e, N_e)\} = \{(2,1),(1,1)\}$	1.74024	1.65436	1.50378	1.41273	1.37612	1.36356
Approximate $\{(m_f, N_f), (m_e, N_e)\} = \{(2,1),(1,1)\}$	1.74012	1.65395	1.50176	1.40793	1.36958	1.35632
Exact $\{(m_f, N_f), (m_e, N_e)\} = \{(2,2),(1,1)\}$	1.92534	1.76828	1.58688	1.48407	1.44341	1.42953
Approximate $\{(m_f, N_f), (m_e, N_e)\} = \{(2,2),(1,1)\}$	1.92534	1.76838	1.58698	1.48293	1.44122	1.42689
Exact $\{(m_f, N_f), (m_e, N_e)\} = \{(2,2),(1,1)\}$	1.73215	1.62974	1.45909	1.35458	1.31205	1.29739
Approximate $\{(m_f, N_f), (m_e, N_e)\} = \{(2,2),(1,1)\}$	1.73209	1.62959	1.45876	1.35386	1.31101	1.2962

where t_i is the i-th root of Gauss-Laguerre polynomial $\mathcal{L}_{\mathbb{U}_2}(t)$ [66, Eq. (25.5.45)] and the weight w_i is given by $w_i = \frac{t_i}{(\mathbb{U}_2+1)^2[\mathcal{L}_{\mathbb{U}_2+1}(t_i)]^2}$.

Remark 19: The ESC expression can readily be evaluated due to the involvement of finite summation imposed by Gauss-Laguerre series expansion and the presence of lower and upper incomplete Gamma functions.

b) ESC of V_n: As indicated by (19), the CDF of Λ_{E_f} under Scenarios I and II are identical, therefore, the ESC expression for the far near vehicle V_n under Scenario II is same as the one derived for Scenario I. Accordingly, we can represent the ESC expression of V_n for Scenario II as

$$\begin{aligned}
&\overline{C}^{\mathrm{II,Exact}}_{\mathrm{sec},V_n} \\
&= \frac{1}{\ln(2)}\Bigg[\sum_{p=0}^{m_nN_n-1}\left(\frac{m_n}{\Omega_n}\frac{\left((1-\beta)\gamma\Omega_{q_{V_n}}+1\right)}{\rho^2_{V_n}(1-\beta)\gamma}\right)^p \\
&\times \Psi\left(p+1, p+1; \frac{m_n}{\Omega_n}\frac{\left((1-\beta)\gamma\Omega_{q_{V_n}}+1\right)}{\rho^2_{V_n}(1-\beta)\gamma}\right) \\
&- \sum_{p=0}^{m_nN_n-1}\sum_{r=0}^{m_eN_e-1}\frac{\Gamma(r+p+1)}{p!r!}\left(\frac{m_e}{\Omega_e}\frac{\left((1-\beta)\gamma\Omega_{q_E}+1\right)}{\rho^2_E(1-\beta)\gamma}\right)^r \\
&\times \left(\frac{m_n}{\Omega_n}\frac{\left((1-\beta)\gamma\Omega_{q_{V_n}}+1\right)}{\rho^2_{V_n}(1-\beta)\gamma}\right)^p \Psi\left(p+r+1, p+r+1;\right. \\
&\left.\frac{m_n}{\Omega_n}\frac{\left((1-\beta)\gamma\Omega_{q_{V_n}}+1\right)}{\rho^2_{V_n}(1-\beta)\gamma} + \frac{m_e}{\Omega_e}\frac{\left((1-\beta)\gamma\Omega_{q_E}+1\right)}{\rho^2_E(1-\beta)\gamma}\right)\Bigg],
\end{aligned} \tag{51}$$

c) Overall ESC: We can express the overall exact ESC expression for the considered SIMO NOMA-assisted V2V communication system under combined consideration of nodes' mobility and CEE as

$$\overline{C}^{\mathrm{II,Exact}}_{\mathrm{sec,\ overall}} = \overline{C}^{\mathrm{II,Exact}}_{\mathrm{sec},V_f} + \overline{C}^{\mathrm{II,Exact}}_{\mathrm{sec},V_n}, \tag{52}$$

where $\overline{C}^{\mathrm{II,Exact}}_{\mathrm{sec},V_f}$ and $\overline{C}^{\mathrm{II,Exact}}_{\mathrm{sec},V_n}$ are given in (50) and (51).

Remark 20: From the above exact ESC analysis performed for both user vehicles under Scenarios I and II, it is observed that the ESC expressions for V_f under Scenarios I and II are dependent on the Gauss-Laguerre series expansion, this is not an issue since such series converges but require more computations to get the accurate results. In addition, the closed-form ESC expressions for the near user vehicle V_n under Scenarios I and II are heavily dependent on the finite summations and tricomi confluent hypergeometric functions, which can easily be evaluated but need more series computations as m_nN_n and m_eN_e increase. Next, we thus present approximate ESC expressions for both user vehicles under Scenarios I and II, which are quite tight with exact results for different set of parameters, as also verified numerically in Fig. 9 and the associated Tables 3–5 of Section VII.

B. APPROXIMATE ESC ANALYSIS

The approximate or conditional ESC can be given by averaging the secrecy capacity $\mathbf{C}^j_{\mathrm{sec},V_\kappa} = \log_2(1+\Lambda_{V_\kappa}) - \log_2(1+\Lambda_{E^j_\kappa})$, if $\Lambda_{V_\kappa} > \Lambda_{E^j_\kappa}$, over the distributions of Λ_{V_κ} and $\Lambda_{E^j_\kappa}$, for $\kappa \in \{f, n\}$ and $j \in \{\mathrm{I}, \mathrm{II}\}$, as

$$\overline{C}^{j,\mathrm{Approx}}_{\mathrm{sec},V_\kappa} = \mathbb{E}\left[\log_2\left(1+\Lambda_{V_\kappa}\right)\right] - \mathbb{E}\left[\log_2\left(1+\Lambda_{E^j_\kappa}\right)\right]. \tag{53}$$

1) APPROXIMATE ESC ANALYSIS UNDER SCENARIO I

Herein, we present the approximate ESC expression for V_f and V_n under Scenario I for the considered system under the joint impact of nodes' mobility and CEE.

a) ESC of V_f: The approximate ESC expression of V_f under Scenario I can be deduced in accordance to the following theorem.

Theorem 4: The ESC expression of V_f under nodes' mobility and CEE over Nakagami-m fading channels can be given as

$$\overline{C}^{\mathrm{I,Approx}}_{\mathrm{sec},V_f} = \overline{C}_{V_f} - \overline{C}_{E^{\mathrm{I}}_f}, \tag{54}$$

where

$$\begin{aligned}
\overline{C}_{V_f} = \frac{1}{\ln(2)\Gamma(N_fm_f)}\Bigg[&\mathcal{G}^{1,3}_{3,2}\left(\frac{\Omega_f\rho^2_{V_f}}{m_f\left(\Omega_{q_{V_f}}+\frac{1}{\gamma}\right)}\Bigg|^{1-N_fm_f,1,1}_{1,0}\right) \\
&-\mathcal{G}^{1,3}_{3,2}\left(\frac{\Omega_f\rho^2_{V_f}(1-\beta)}{m_f\left(\Omega_{q_{V_f}}+\frac{1}{\gamma}\right)}\Bigg|^{1-N_fm_f,1,1}_{1,0}\right)\Bigg],
\end{aligned} \tag{55}$$

$$\overline{C}_{E^{\mathrm{I}}_f} = \frac{1}{\ln(2)\Gamma(N_em_e)}\mathcal{G}^{1,3}_{3,2}\left(\frac{\Omega_e\beta\rho^2_E}{m_e\left(\beta\Omega_{q_E}+\frac{1}{\gamma}\right)}\Bigg|^{1-N_em_e,1,1}_{1,0}\right). \tag{56}$$

Proof: See Appendix D for the detailed derivation. ■

b) ESC of V_n: The approximate ESC expression of near user vehicle V_n is presented in Theorem 5.

Theorem 5: The analytical ESC expression of V_n in the presence of nodes' mobility and CEE over Nakagami-*m* fading channels can be expressed as

$$\overline{\mathbf{C}}^{\mathbf{I},\mathrm{Approx}}_{\mathrm{sec},\mathrm{V}_n} = \overline{\mathbf{C}}_{\mathrm{V}_n} - \overline{\mathbf{C}}_{\mathrm{E}^{\mathrm{I}}_n}, \tag{57}$$

where

$$\overline{\mathbf{C}}_{\mathrm{V}_n} = \frac{\mathcal{G}^{1,3}_{3,2}\left(\frac{\Omega_n(1-\beta)\rho^2_{\mathrm{V}_n}}{m_n\left((1-\beta)\Omega_{q_{\mathrm{V}_n}}+\frac{1}{\gamma}\right)}\Big|^{1-\mathrm{N}_n m_n,1,1}_{1,0}\right)}{\ln(2)\Gamma(\mathrm{N}_n m_n)}, \tag{58}$$

$$\overline{\mathbf{C}}_{\mathrm{E}^{\mathrm{I}}_n} = \frac{\mathcal{G}^{1,3}_{3,2}\left(\frac{\Omega_e(1-\beta)\rho^2_{\mathrm{E}}}{m_e\left((1-\beta)\Omega_{q_{\mathrm{E}}}+\frac{1}{\gamma}\right)}\Big|^{1-\mathrm{N}_e m_e,1,1}_{1,0}\right)}{\ln(2)\Gamma(\mathrm{N}_e m_e)}. \tag{59}$$

Proof: Using (53), we can express the ESC of V_n as

$$\overline{\mathbf{C}}^{\mathrm{I},\mathrm{Approx}}_{\mathrm{sec},\mathrm{V}_n} = \underbrace{\mathbb{E}\left[\log_2(1+\Lambda_{\mathrm{V}_n})\right]}_{\triangleq\overline{\mathbf{C}}_{\mathrm{V}_n}} - \underbrace{\mathbb{E}\left[\log_2(1+\Lambda_{\mathrm{E}^{\mathrm{I}}_n})\right]}_{\triangleq\overline{\mathbf{C}}_{\mathrm{E}^{\mathrm{I}}_n}}. \tag{60}$$

To evaluate $\overline{\mathbf{C}}_{\mathrm{V}_n}$ in (60), we first express it into its equivalent integral form and then substituting the PDF of Λ_{V_n} along with the transformation $\ln(1+z) = \mathcal{G}^{1,2}_{2,2}(z|^{1,1}_{1,0})$ [65, Eq. (01.04.26.0003.01)], and simplifying the resultant integral via [51, (7.813.1)], we can obtain $\overline{\mathbf{C}}_{\mathrm{V}_n}$ as given in (58). Likewise, we can evaluate $\overline{\mathbf{C}}_{\mathrm{E}^{\mathrm{I}}_n}$ as shown in (59). ■

Remark 21: Following important insights can be drawn from above analysis.

1) It is seen from (54) and (57) that the ESC expressions for V_f and V_n under Scenario I consist two capacity terms, which can be viewed as follows: i) $\overline{\mathbf{C}}_{\mathrm{V}_f}(\overline{\mathbf{C}}_{\mathrm{V}_n})$ represents the contribution from source for far user vehicle (near user vehicle), whereas 2) $\overline{\mathbf{C}}_{\mathrm{E}^{\mathrm{I}}_f}(\overline{\mathbf{C}}_{\mathrm{E}^{\mathrm{I}}_n})$ represents the contribution from wiretapper for far user vehicle (near user vehicle) under Scenario I.
2) Under high SNR regime, the ESC expressions become independent of SNR, suggesting that the ESC performance achieves an error floor for large SNR, as also reported in Section VII. This behavior can also be visualized as the SNR at both eavesdropper and user vehicles improve simultaneously. We further verified this with the numerical analysis in Section VII.

c) Overall ESC: We can express the overall approximate ESC expression for the considered SIMO NOMA-assisted V2V communication system under the joint consideration of nodes' mobility and CEE as

$$\overline{\mathbf{C}}^{\mathrm{I},\mathrm{Approx}}_{\mathrm{sec,\ overall}} = \overline{\mathbf{C}}^{\mathrm{I},\mathrm{Approx}}_{\mathrm{sec},\mathrm{V}_f} + \overline{\mathbf{C}}^{\mathrm{I},\mathrm{Approx}}_{\mathrm{sec},\mathrm{V}_n}, \tag{61}$$

where $\overline{\mathbf{C}}^{\mathrm{I},\mathrm{Approx}}_{\mathrm{sec},\mathrm{V}_f}$ and $\overline{\mathbf{C}}^{\mathrm{I},\mathrm{Approx}}_{\mathrm{sec},\mathrm{V}_n}$ are given in (54) and (57).

C. APPROXIMATE ESC ANALYSIS UNDER SCENARIO II

This section presents the approximate ESC expressions for V_f and V_n under Scenario II by taking joint impact of nodes' mobility and CEE into account over Nakagami-*m* fading.

a) ESC of V_f: From (53), we can express the approximate ESC expression for V_f under Scenario II as

$$\overline{\mathbf{C}}^{\mathbf{II},\mathrm{Approx}}_{\mathrm{sec},\mathrm{V}_f} = \mathbb{E}\left[\log_2(1+\Lambda_{\mathrm{V}_f})\right] - \mathbb{E}\left[\log_2(1+\Lambda_{\mathrm{E}^{\mathrm{II}}_f})\right]. \tag{62}$$

Moreover, we can note that the first expectation term in (62) is already derived and presented in (55). Whereas, the second expectation term in (62) (say $\overline{\mathbf{C}}_{\mathrm{E}^{\mathrm{II}}_f}$) can be given as

$$\overline{\mathbf{C}}_{\mathrm{E}^{\mathrm{II}}_f} = \frac{1}{\ln(2)}\int_0^\infty \ln(1+y) f_{\Lambda_{\mathrm{E}^{\mathrm{II}}_f}}(y)dy. \tag{63}$$

Invoking the PDF of $\Lambda_{\mathrm{E}^{\mathrm{II}}_f}$ from (80) into (63) and solving the resultant integral by following exactly the same steps as used to deduce (55) in Theorem 4, we can obtain $\overline{\mathbf{C}}_{\mathrm{E}^{\mathrm{II}}_f}$ as

$$\overline{\mathbf{C}}_{\mathrm{E}^{\mathrm{II}}_f} = \frac{1}{\ln(2)\Gamma(\mathrm{N}_e m_e)}\left[\mathcal{G}^{1,3}_{3,2}\left(\frac{\Omega_e\rho^2_{\mathrm{E}}}{m_e\left(\Omega_{q_{\mathrm{E}}}+\frac{1}{\gamma}\right)}\Big|^{1-\mathrm{N}_e m_e,1,1}_{1,0}\right) - \mathcal{G}^{1,3}_{3,2}\left(\frac{\Omega_e\rho^2_{\mathrm{E}}(1-\beta)}{m_e\left(\Omega_{q_{\mathrm{E}}}+\frac{1}{\gamma}\right)}\Big|^{1-\mathrm{N}_e m_e,1,1}_{1,0}\right)\right]. \tag{64}$$

Now, substituting the results obtained in (55) and (64) into (62), the closed-form ESC for V_f under Scenario II can be presented as (65), shown at the bottom of the next page.

b) ESC of V_n: The ESC expression of V_n for Scenario II is identical to the one deduced for Scenario I. Accordingly, we can express the ESC for V_n under Scenario II as

$$\overline{\mathbf{C}}^{\mathrm{II},\mathrm{Approx}}_{\mathrm{sec},\mathrm{V}_n} = \frac{\mathcal{G}^{1,3}_{3,2}\left(\frac{\Omega_n(1-\beta)\rho^2_{\mathrm{V}_n}}{m_n\left((1-\beta)\Omega_{q_{\mathrm{V}_n}}+\frac{1}{\gamma}\right)}\Big|^{1-\mathrm{N}_n m_n,1,1}_{1,0}\right)}{\ln(2)\Gamma\left(\mathrm{N}_n m_n\right)} - \frac{\mathcal{G}^{1,3}_{3,2}\left(\frac{\Omega_e(1-\beta)\rho^2_{\mathrm{E}}}{m_e\left((1-\beta)\Omega_{q_{\mathrm{E}}}+\frac{1}{\gamma}\right)}\Big|^{1-\mathrm{N}_e m_e,1,1}_{1,0}\right)}{\ln(2)\Gamma\left(\mathrm{N}_e m_e\right)}. \tag{66}$$

Remark 22: Similar to Scenario I for the far and near user vehicles, we can see from (65) and (66) that the ESC expressions for V_f and V_n under Scenario II also consist two capacity terms, which can be viewed as follows: i) $\overline{\mathbf{C}}_{\mathrm{V}_f}(\overline{\mathbf{C}}_{\mathrm{V}_n})$ represents the contribution from source for far user vehicle (near user vehicle), whereas 2) $\overline{\mathbf{C}}_{\mathrm{E}^{\mathrm{I}}_f}(\overline{\mathbf{C}}_{\mathrm{E}^{\mathrm{I}}_n})$ represents the contribution from wiretapper for far user vehicle (near user vehicle) under Scenario II. In addition, we can see as γ increases, the ESC performances improve, but attain an error floor in the high SNR regime because of the simultaneous improvement in SNR at both both eavesdropper and user vehicles, as also shown numerically in Section VII.

c) Overall ESC: We can express the overall approximate ESC expression for the considered system under the joint impact of nodes' mobility and CEE as

$$\overline{\mathbf{C}}^{\text{II,Approx}}_{\text{sec, overall}} = \overline{\mathbf{C}}^{\text{II,Approx}}_{\text{sec,V}_f} + \overline{\mathbf{C}}^{\text{II,Approx}}_{\text{sec,V}_n}, \tag{67}$$

where $\overline{\mathbf{C}}^{\text{II,Approx}}_{\text{sec,V}_f}$ and $\overline{\mathbf{C}}^{\text{II,Approx}}_{\text{sec,V}_n}$ are given in (65) and (66).

Remark 23: From the above approximate ESC analyses carried out for V_f and V_n under Scenario I and II, we can observe that the ESC expressions mainly consist of Meijer-$\mathcal{G}$ function which can efficiently be computed (with less computational overhead than the exact ESC expressions) via Mathematica computational software package. Furthermore, it is clearly observed that the ESC performance is influenced by various system/channel parameters and impacted negatively by the nodes' mobility and CEE. Moreover, it is also important to mention that the deduced closed-form ESC expressions presented for V_f and V_n under Scenario I and II under the joint impact of nodes' mobility and CEE over Nakagami-m fading channels are new.

VII. NUMERICAL RESULTS AND DISCUSSIONS

In this section, we verify our derived analytical findings for the considered SIMO NOMA-assisted V2V communication system with nodes' mobility and CEE via MATLAB simulations. For numerical investigations, we set $\mathcal{N} = \mathcal{M} = 200$ as number of summation terms (beyond which there is no change in the first three decimal places of the results) for Gauss-Chebyshev series expansion to get accurate results. Also, we model time-varying error variance as $\Omega_{\epsilon_\iota} = \Omega_{\delta_\iota} + \Omega_\kappa$, for $(\iota, \kappa) \in \{(\text{V}_f, f), (\text{V}_n, n), (\text{E}, e)\}$, and assume $(\mathcal{R}_{\text{V}_f}, \mathcal{R}_{\text{V}_n}) = (0.1, 0.5)$ bps/Hz, $\beta = 0.8$, $R = 9.6$ kbps, $f_c = 1.9 \times 10^9$ Hz, and $c = 3 \times 10^8$ m/s, unless otherwise stated.

A. SECRECY OUTAGE PROBABILITY

Fig. 2 shows the SOP performance of V_f and V_n as a function of transmit SNR γ for different values of fading severity parameters and number of antennas, under Scenarios I and II. In particular, Fig. 2(a) and (b) illustrate the SOP performance versus γ of V_f and V_n, respectively, under various sets of (m_f, N_f) and (m_e, N_e) for V_f and (m_n, N_n) and (m_e, N_e) for V_n. Here, we set $\Omega_{\text{V}_f} = 0$ dB, $\Omega_{\text{V}_n} = 10$ dB, $\Omega_e = -5$ dB, $\Omega_{\delta_{\text{V}_f}} = \Omega_{\delta_{\text{V}_n}} = \Omega_{\delta_{\text{E}}} = 0.01$, and $v_{\text{V}_f} = v_{\text{V}_n} = v_{\text{E}} = 50$ km/h.

Firstly, we can observe from these figures that the analytical and simulation results match perfectly over the entire range of γ, which validates the accuracy of our proposed analytical study. Also, the asymptotic results match well with the exact results in the medium-to-high SNR regime, and hence validating our derived asymptotic SOP expressions. In Fig. 2(a), we can observe that the SOP performance of V_f under both scenarios first improves for low values of γ and then degrades in the low-to-medium regime of γ. This is owing to the reason that as γ increases, the interference imposed by V_n over V_f increases which then dominates the SOP performance

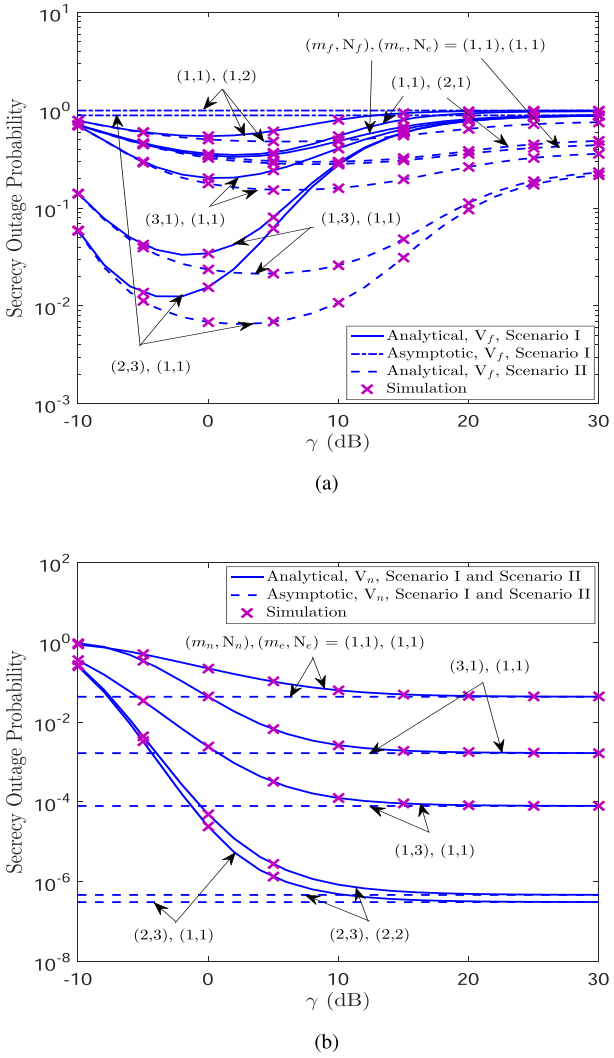

FIGURE 2. SOP performance versus γ (a) for V_f, and (b) for V_n, under Scenarios I and II.

$$\overline{\mathbf{C}}^{\text{II,Approx}}_{\text{sec,V}_f} = \frac{1}{\ln(2)\Gamma(\text{N}_f m_f)} \left[\mathcal{G}^{1,3}_{3,2}\left(\frac{\Omega_f \rho^2_{\text{V}_f}}{m_f \left(\Omega_{q_{\text{V}_f}} + \frac{1}{\gamma}\right)} \Big|^{1-\text{N}_f m_f, 1, 1}_{1,0} \right) - \mathcal{G}^{1,3}_{3,2}\left(\frac{\Omega_f \rho^2_{\text{V}_f}(1-\beta)}{m_f \left(\Omega_{q_{\text{V}_f}} + \frac{1}{\gamma}\right)} \Big|^{1-\text{N}_f m_f, 1, 1}_{1,0} \right) \right] - \frac{1}{\ln(2)\Gamma(\text{N}_e m_e)}$$
$$\times \left[\mathcal{G}^{1,3}_{3,2}\left(\frac{\Omega_e \rho^2_{\text{E}}}{m_e \left(\Omega_{q_{\text{E}}} + \frac{1}{\gamma}\right)} \Big|^{1-\text{N}_e m_e, 1, 1}_{1,0} \right) - \mathcal{G}^{1,3}_{3,2}\left(\frac{\Omega_e \rho^2_{\text{E}}(1-\beta)}{m_e \left(\Omega_{q_{\text{E}}} + \frac{1}{\gamma}\right)} \Big|^{1-\text{N}_e m_e, 1, 1}_{1,0} \right) \right]. \tag{65}$$

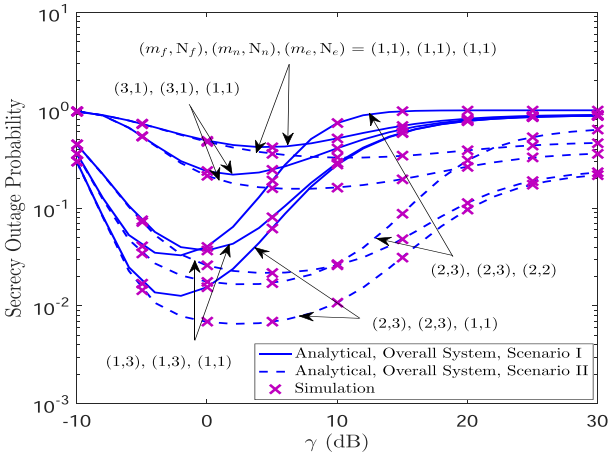

FIGURE 3. SOP performance of the overall system by varying γ, under Scenarios I and II.

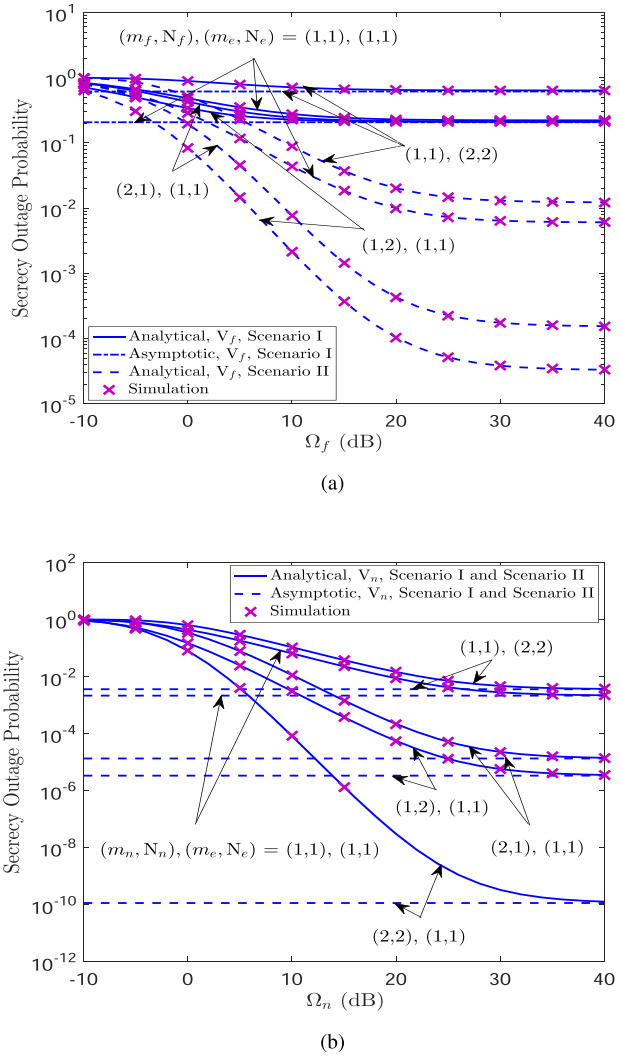

FIGURE 4. SOP performance versus (a) Ω_f for V_f, and (b) Ω_n for V_n, under Scenarios I and II.

of V_f. Furthermore, we can also see that the SOP of V_f exhibits a secrecy floor in the medium-to-high SNR regime owing to the involvement of the interference from V_n and the presence of time-varying and channel estimation errors. Also, from Fig. 2(a), it is observed that the SOP performance of V_f outperforms for Scenario II than that of Scenario I. This is due to the reason that E under Scenario II has poorer decoding capability than Scenario I. Further, in Fig. 2(b), the SOP performance of near user vehicle V_n initially improves as γ increases and then exhibits a saturation floor in the medium-to-high regime of γ. This is due to the reason that the reception capability of both V_n and E improve simultaneously with the increase in γ. In addition, the time-varying error and CEE also contribute in the secrecy floor phenomenon of the SOP curves. Moreover, from Fig. 2(a) under both scenarios, we can also see that as the value of m_f and/or N_f increases, the SOP performance of far user vehicle V_f enhances, however, it degrades as m_e and/or N_e increases. This is because of the reasons that; 1) as the value of fading severity parameter m_e increases, the fading with the associated channel reduces, and 2) increasing number of antennas at E results into a better reception quality. The similar observations can be made for near user vehicle V_n. Additionally, we can see from both the figures that the number of antennas has a more dominant impact on the SOP performance than the fading severity parameters.

Fig. 3 depicts the overall system SOP performance versus γ for various values of fading severity parameters and number of antennas for both Scenarios I and II, under the same parameters setting adopted for Fig. 2. From Fig. 3, we can see that the system SOP performance under both the scenarios first improves for low values of γ and then degrades in low-to-medium regime of γ. Further, the SOP performance of the overall system achieves a saturation floor in medium-to-high regime of γ. This is because of the reason that the SOP performance of the considered system is bottleneck by the far user vehicle V_f. Moreover, the SOP performance of the system improves as the fading severity parameters and/or the number of antennas at the legitimate user vehicles increase. On the contrary, this performance improvement degrades as m_e and/or N_e increase. On the expected lines, the system achieves better SOP performance under Scenario II compared to Scenario I.

From Figs. 2 and 3, we can conclude that the SOP performance of the user vehicles significantly deteriorated because of i) the impact of CEE and time-varying errors, ii) the simultaneous improvement in γ at both user vehicles and E, and iii) the increase in fading parameter of E and/or number of eavesdropper antennas at E. Also, SOP performance is improved under Scenario II compared to Scenario I.

Fig. 4(a) and (b) demonstrate the impact of channel strength of far user vehicle Ω_{V_f} and near user vehicle Ω_{V_n} with fixed Ω_e, respectively, on their SOP performances for various values of fading severity parameters and number of antennas under Scenarios I and II, when $\gamma = 10$ dB, $\Omega_{\delta_{\mathrm{V}_f}} = \Omega_{\delta_{\mathrm{V}_n}} = \Omega_{\delta_{\mathrm{E}}} = 0.01$, and $v_{\mathrm{V}_f} = v_{\mathrm{V}_n} = v_{\mathrm{E}} = 50$ km/h. It can be seen

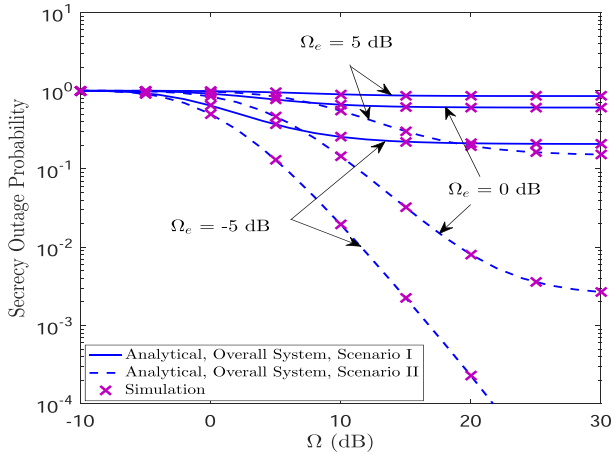

FIGURE 5. SOP performance for the overall system versus Ω, under Scenarios I and II.

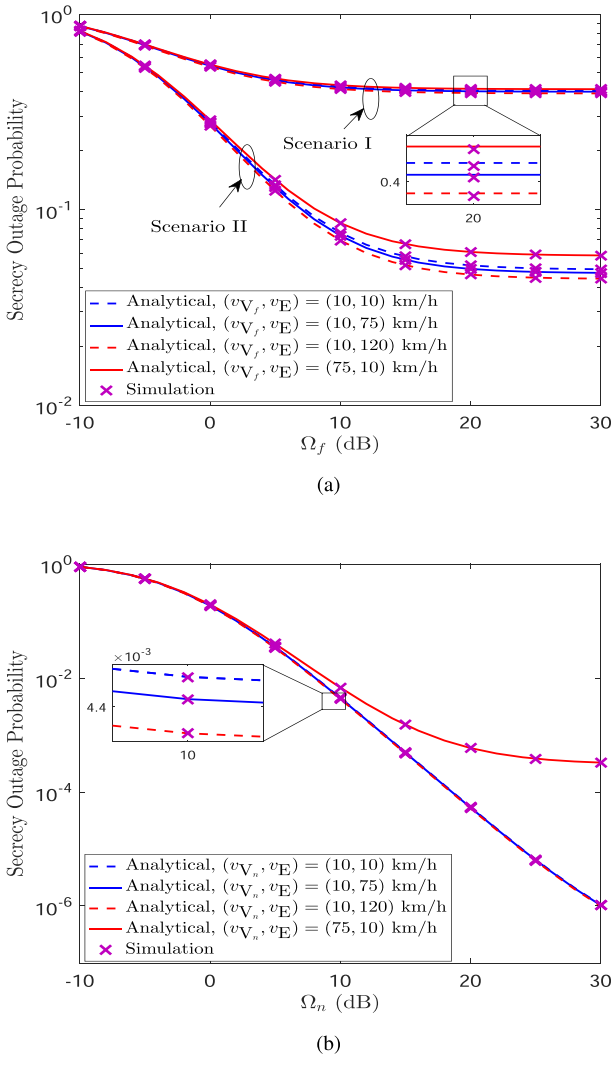

FIGURE 6. SOP performance versus (a) Ω_f for V_f, and (b) Ω_n for V_n, for various values of relative velocities.

from these figures that the exact results match perfectly with the simulation results for entire range of Ω_{V_f} for V_f and of Ω_{V_n} for V_n. Also, the asymptotic results are in well agreement with the exact ones in medium-to-high Ω_{V_f} and Ω_{V_n} regime. As expected, the SOP performance of V_f and V_n improve as their associated fading severity parameters and number of antennas increase. However, the SOP curves saturate in the high Ω_{V_f} and Ω_{V_n} regime, irrespective of m_f, m_n, N_f, and N_n. This is due to the joint impact of nodes' mobility and imperfect channel estimates, which force the SOP curves to exhibit a saturation floor. Moreover, the SOP performance improvement observed for V_f and V_n by increasing m_f, m_n, N_f, and N_n can be further deteriorated when m_e and N_e increase.

From Fig. 4, we can conclude that the system does not observe any secrecy diversity order even by varying $\Omega_f(\Omega_n)$ for fixed Ω_e, which is generally achieved when the impact of CEE and time-varying errors is ignored. This concludes that the CEE and time-varying errors play key role in diminishing the system's secrecy diversity order.

In Fig. 5, we show the impact of legitimate channel strength Ω (by setting $\Omega_{V_f} = 0.8\,\Omega$, $\Omega_{V_n} = \Omega$) on the SOP performance of overall system under Scenarios I and II for various fixed values of wiretap channel strength Ω_e, when $\gamma = 10$ dB, $(m_f, N_f) = (2, 1)$, $(m_n, N_n) = (2, 1)$, $(m_e, N_e) = (1, 1)$, $\Omega_{\delta_{V_f}} = \Omega_{\delta_{V_n}} = \Omega_{\delta_E} = 0.01$, and $v_{V_f} = v_{V_n} = v_E = 50$ km/h. We can observe from Fig. 5 that as the quality of legitimate channel improves (i.e., Ω increases), the SOP performance of overall NOMA-enabled V2V system for both scenarios improves initially, and then achieves a saturation floor in the medium-to-high regime of Ω, regardless of Ω_e. This is due to the negative effects of nodes' mobility and the presence of CEE. Moreover, the system performance is also limited by the far user vehicle for whom the interference from V_n increases with an increase in Ω. Furthermore, we can observe that as Ω_e increases the SOP performance of overall system degrades, because an increase in Ω_e improves the wiretap channel quality significantly which in turn improves the reception capability at E. As expected, the overall system gives better SOP performance under Scenario II than Scenario I due to the poorer decoding capabilities of E in Scenario II.

Fig. 5 concludes that Ω_e (i.e., E's channel quality) has very serious impact on the system performance, even the SOP performance deteriorates significantly irrespective of having $\Omega_\iota >> \Omega_e$, for $\iota \in \{f, n\}$, with other fixed channel/system parameters.

Fig. 6 depicts the impact of relative velocities of V_f, V_n, and E on the SOP performance. Specifically, we plot the SOP curves for far user vehicle V_f in Fig. 6(a) and for near user vehicle V_n in Fig. 6(b), under various setting of relative velocities (v_{V_f} for V_f and v_{V_n} for V_n) by varying the average channel strengths of V_f and V_n. For this, we set $\Omega_e = -5$ dB, $\gamma = 20$ dB, $m_f = m_n = m_e = 1$, $N_f = N_n = 2$, $N_e = 1$, and $\Omega_{\delta_{V_f}} = \Omega_{\delta_{V_n}} = \Omega_{\delta_E} = 0.1$. From Fig. 6(a), we can observe that as v_{V_f} increases the SOP performance of far user vehicle V_f decreases. Also, an increase in v_E results in improving the

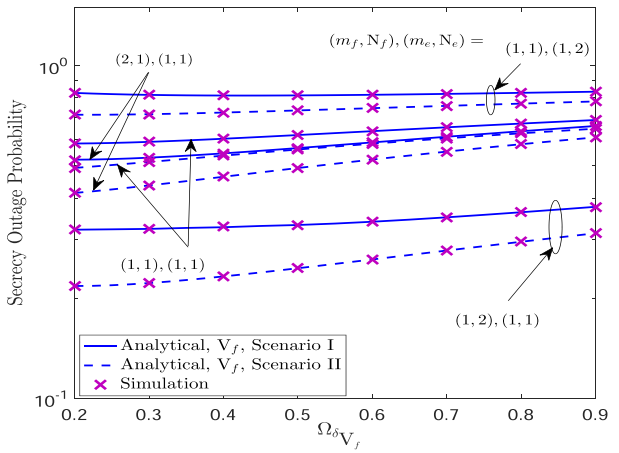

(a)

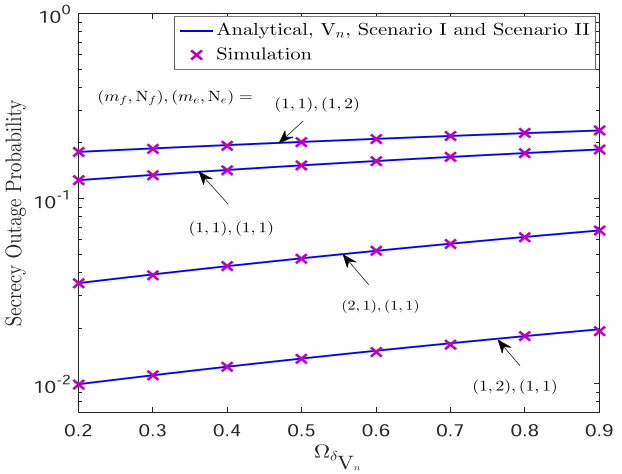

(b)

FIGURE 7. Impact of channel estimation errors on the SOP performance (a) for V_f, and (b) for V_n, under Scenarios I and II.

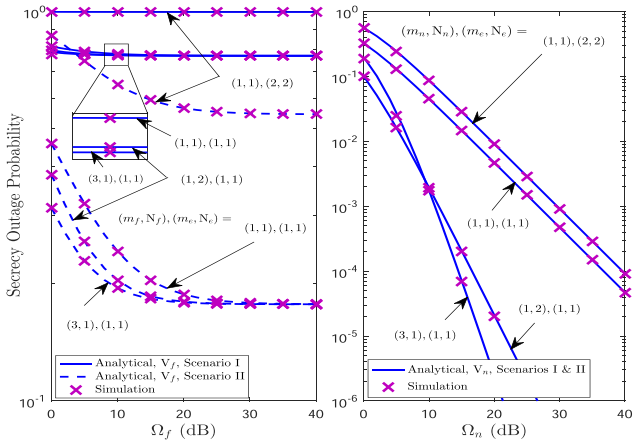

FIGURE 8. SOP performance of V_f and V_n under the special scenario of all static nodes with perfect channel estimates, when $\gamma = 20$ dB.

SOP performance of far user vehicle. Such a phenomenon can be attributed to the fact that an increase in the relative velocity causes the associated channel to becomes more time-selective. Moreover, as also seen in the previous results, the SOP performance of vehicle V_f first improves in the low-to-medium Ω_f regime and then achieves a saturation floor in the high Ω_f regime. On the same lines, we can draw the similar conclusions for the near user vehicle V_n. In addition, Fig. 6(a) shows that V_f achieves a better secrecy performance under Scenario II than the Scenario I.

Fig. 6 concludes that a higher velocity of eavesdropper vehicle is favorable for SOP improvement for legitimate user vehicles, since E's ability to intercept the legitimate information is reduced as v_{E} increases.

We demonstrate the impact of CEE, fading parameters, and number of antennas on the SOP performance of V_f in Fig. 7(a) and V_n in Fig. 7(b), for both Scenarios I and II. We set $(\mathcal{R}_{\mathrm{V}_f}, \mathcal{R}_{\mathrm{V}_n}) = (0.5, 1)$ bps/Hz, $\gamma = 10$ dB, $\Omega_{\mathrm{V}_f} = 0$ dB, $\Omega_{\mathrm{V}_n} = 10$ dB, $\Omega_e = -5$ dB, and $v_{\mathrm{V}_f} = v_{\mathrm{V}_n} = v_{\mathrm{E}} = 50$ km/h. In Fig. 7(a) for both scenarios, we can see that as m_f and/or N_f increases for fixed values of m_e and N_e, the SOP performance improves, however, as N_e increases the SOP performance reduces significantly, for all values of $\Omega_{\delta_{\mathrm{V}_f}}$. Moreover, as the error variance $\Omega_{\delta_{\mathrm{V}_f}}$ increases the SOP performance decreases, irrespective of number of antennas and fading severity parameters. This shows that the CEE and channel/system parameters associated with the wiretap link have detrimental impact of the SOP performance. As expected, V_f achieves a better SOP performance under the Scenario II compared to Scenario I, since E under Scenario II has poor decoding capability than the Scenario I. Likewise, we can draw the similar observations on the SOP performance for near user vehicle V_n in Fig. 7(b).

We can conclude from Fig. 7 that CEE has detrimental impact on the SOP performance, even when the legitimate user vehicles experience better fading conditions and/or exploit the multiple antennas diversity.

In Fig. 8, we plot the SOP performance of far user vehicle and near user vehicle by varying their average channel strengths with fixed wiretap average channel gain under the special scenario where all the nodes are static (i.e., $v_{\mathrm{V}_f} = v_{\mathrm{V}_n} = v_{\mathrm{E}} = 0$ km/h, which results into $\rho_{\mathrm{V}_f} = \rho_{\mathrm{V}_n} = \rho_{\mathrm{E}} = 1$) with perfect channel estimates (i.e., $\Omega_{\delta_{\mathrm{V}_f}} = \Omega_{\delta_{\mathrm{V}_n}} = \Omega_{\delta_{\mathrm{E}}} = 0$). We can see from this figure that the SOP performance of far user vehicle increases as m_f and/or N_f increase, however this performance improvement can be compromised when m_e and/or N_e increase. Moreover, it is observed that the SOP performance of V_f saturates as Ω_f increases for all sets of $\{(m_f, N_f), (m_e, N_e)\}$, which is due to the impact of interference imposed by V_n on V_f. This is also analytically proved in Section V-C. Furthermore, we can see from this figure that the SOP performance of the near user vehicle V_n increases as Ω_n increases, irrespective of $\{(m_n, N_n), (m_e, N_e)\}$. Interestingly, we can verify the diversity order of $m_n N_n$ for near user vehicle V_n under various values of m_n and N_n, as also analytically reported in Section V-C.

TABLE 4. Difference Between Exact and Approximate Expressions for the Far User Vehicle V_f Under Scenario II

SNR (dB)	15	20	25	30	35	40
Exact $\{(m_f, N_f), (m_e, N_e)\} = \{(2,1),(1,1)\}$	1.76648	1.74047	1.66528	1.62107	1.60367	1.59775
Approximate $\{(m_f, N_f), (m_e, N_e)\} = \{(2,1),(1,1)\}$	1.76642	1.74039	1.66527	1.62118	1.60384	1.59795
Exact $\{(m_f, N_f), (m_e, N_e)\} = \{(2,2),(1,1)\}$	1.95164	1.85468	1.74946	1.69428	1.6732	1.6661
Approximate $\{(m_f, N_f), (m_e, N_e)\} = \{(2,2),(1,1)\}$	1.95164	1.85482	1.75049	1.69617	1.67549	1.66852
Exact $\{(m_f, N_f), (m_e, N_e)\} = \{(2,2),(1,1)\}$	1.58565	1.46263	1.33079	1.26401	1.23895	1.23056
Approximate $\{(m_f, N_f), (m_e, N_e)\} = \{(2,2),(1,2)\}$	1.58541	1.46232	1.33053	1.26386	1.23886	1.23049

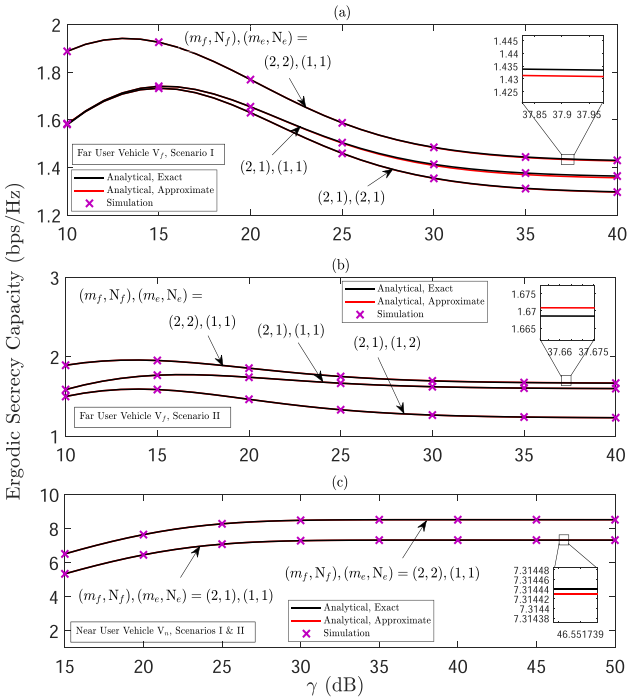

FIGURE 9. Exact and approximate ESC curves for both user vehicles under Scenarios I and II.

It is to be concluded from Fig. 8 that under the scenario when the system is free from time-varying errors and CEE (i.e., nodes are static with perfect channel estimates), the near user vehicle can achieve a full secrecy diversity order of $m_n N_n$, as also proved analytically in (37). However, the far user still fails to extract the secrecy diversity order owing to the interference imposed by the near user vehicle.

B. ERGODIC SECRECY CAPACITY

Fig. 9 demonstrates the exact (represented by solid red line) and approximate (represented by solid black line) ESC curves for varying SNR for both near user and far user vehicles under Scenarios I and II, by considering various values of m_f, N_f, m_n, N_n, m_e, and N_e, when $\Omega_{V_f} = 0$ dB, $\Omega_{V_n} = 10$ dB, $\Omega_e = -20$ dB, $\Omega_{\delta_{V_f}} = \Omega_{\delta_{V_n}} = \Omega_{\delta_E} = 0.01$, and $v_{V_f} = v_{V_n} = v_E = 50$ km/h. We also set $\mathbb{U}_1 = \mathbb{U}_2 = 50$ as number of summation terms for the Gauss-Laguerre series expansion in the exact ESC expressions to get the accurate results. Specifically, Fig. 9(a) and (b) plot the exact and approximate ESC curves for the far user vehicle under Scenario I and Scenario II, respectively, whereas Fig. 9(c) shows the exact and approximate ESC curves for near user vehicle under both Scenarios I and II. We can observe from these figures that our derived analytical approximate ESC results for both user vehicles under Scenarios I and II are perfectly matched with the derived analytical exact ESC results, which are further validated by the simulation studies. This corroborates the accuracy of the computationally efficient approximate ESC expressions. In addition, we present Tables 3, 4, and 5 corresponding to Fig. 9(a), (b), and (c), respectively, for better highlighting the difference between the exact ESC expression and approximate ESC expression, which is very small for all values of SNRs, under different sets of m_f, N_f, m_n, N_n, m_e, and N_e. In the subsequent figures, we show the impact of various parameters on the ESC performances of far user and near user vehicles under Scenarios I and II by utilizing the derived analytical approximate expressions.

In Fig. 10, we investigate the ESC performance with respect to γ for the legitimate user vehicles with different values of fading severity parameters and number of antennas under both Scenario I and II, when $\Omega_{V_f} = 0$ dB, $\Omega_{V_n} = 10$ dB, $\Omega_e = -20$ dB, $\Omega_{\delta_{V_f}} = \Omega_{\delta_{V_n}} = \Omega_{\delta_E} = 0.01$, and $v_{V_f} = v_{V_n} = v_E = 50$ km/h. Specifically, in Fig. 10(a), we show the ESC of V_f versus γ for different values of (m_f, N_f) and (m_e, N_e). From Fig. 10(a), we can see that the ESC of V_f under both scenarios first improves in low γ regime and then degrades for low-to-medium γ. This is due to the reason that as γ increases, the interfering signal component of V_n to V_f also increases. Further, we observe that the ESC curves under both the scenarios saturate in the medium-to-high regime of γ, because of the involved interference from V_n and the joint impact of time-varying and channel estimation errors. We can also make out that V_f is able to achieve better ESC performance under Scenario II than Scenario I as in the latter case E has more powerful computational capability and can decode the signals of both the legitimate user vehicles. Furthermore, Fig. 10(b) plots the ESC of V_n versus γ for different values of (m_n, N_n) and (m_e, N_e). From the plots, it can be seen that the ESC performance of V_n first improves as γ increases and then exhibits a saturation behavior with γ. This is due to the negative impact of nodes' mobility and CEE.

Moreover, from Fig. 10(a) and (b) under both Scenarios I and II, we can see that an increment in m_ι and/or N_ι values can yield into a better SOP performance of the ι-th vehicle V_ι, for $\iota \in \{f, n\}$. This is owing to the reason that a higher value of the fading severity parameter causes less severe fading and a

TABLE 5. Difference Between Exact and Approximate Expressions for the Near User Vehicle V_n Under Scenarios I and II

SNR (dB)	15	20	25	30	35	40
Exact $\{(m_f, \mathrm{N}_f), (m_e, \mathrm{N}_e)\} = \{(2,1),(1,1)\}$	5.33555	6.44923	7.07664	7.2795	7.31326	7.31525
Approximate $\{(m_f, \mathrm{N}_f), (m_e, \mathrm{N}_e)\} = \{(2,1),(1,1)\}$	5.33555	6.44923	7.07663	7.27949	7.31325	7.31524
Exact $\{(m_f, \mathrm{N}_f), (m_e, \mathrm{N}_e)\} = \{(2,2),(1,1)\}$	6.50533	7.6374	8.27096	8.4758	8.51019	8.51238
Approximate $\{(m_f, \mathrm{N}_f), (m_e, \mathrm{N}_e)\} = \{(2,2),(1,1)\}$	6.50533	7.6374	8.27096	8.4758	8.51019	8.51238

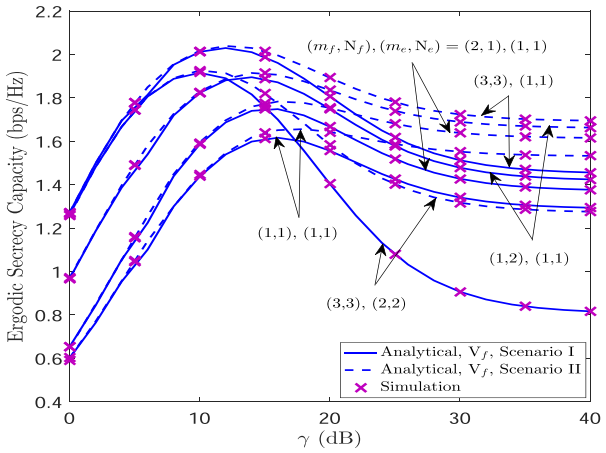

(a)

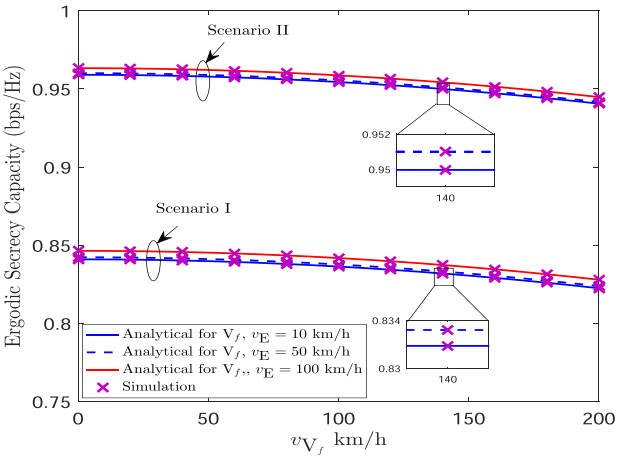

(a)

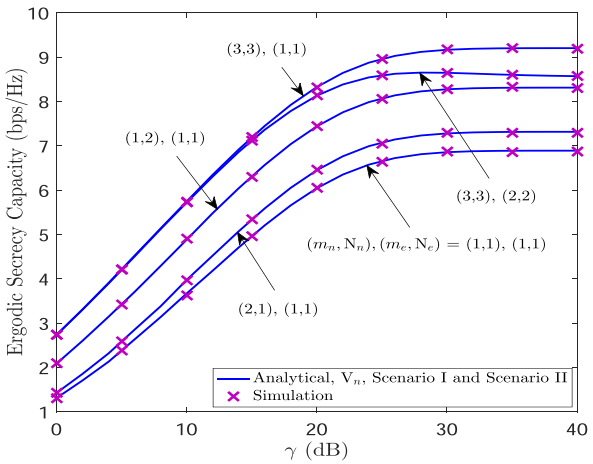

(b)

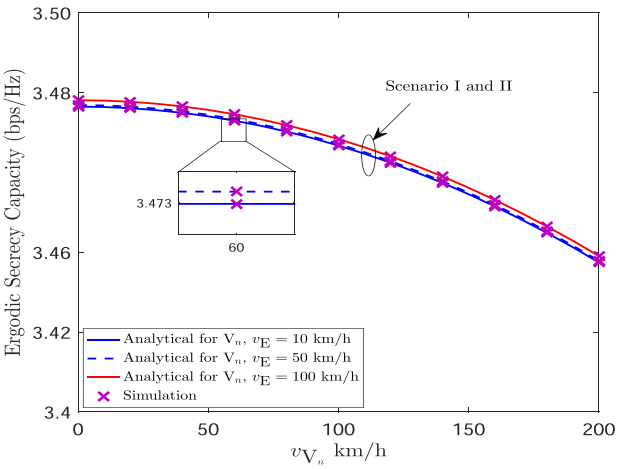

(b)

FIGURE 10. ESC performance versus γ (a) for V_f, and (b) for V_n, under Scenarios I and II.

FIGURE 11. ESC performance versus (a) v_{V_f} for V_f, and (b) v_{V_n} for V_n, under Scenarios I and II.

better channel quality. Moreover, an increase in the number of antennas at the receiver will generate better diversity coding gains. On the same lines, the SOP performance degrades as m_e and/or N_e increases for both the legitimate user vehicles under both Scenarios I and II. It is also worth noticing that the impact of number of antennas is more dominant on the SOP performance than the fading severity parameters.

From Fig. 10, we can conclude that i) the joint negative effects of nodes' mobility and CEE, and ii) an improvement in SNR at both user vehicles and E by same factor, force the ESC to exhibit a saturation floor in the high SNR. Also, the increase in fading parameter and/or number of antennas pertaining to E significantly affect the ESC performance.

In Fig. 11, we depict the ESC performance of V_f and V_n as a function of their respective relative velocities v_{V_f} and v_{V_n} (in km/h) for different fixed values of eavesdropper velocity v_{E}, when $\gamma = 10$ dB, $m_f = m_n = m_e = 1$, $\mathrm{N}_f = \mathrm{N}_n = \mathrm{N}_e = 1$, $\Omega_{\mathrm{V}_f} = 0$ dB, $\Omega_{\mathrm{V}_n} = 10$ dB, $\Omega_e = -10$ dB, and $\Omega_{\delta_{\mathrm{V}_f}} = \Omega_{\delta_{\mathrm{V}_n}} = \Omega_{\delta_{\mathrm{E}}} = 0.01$, for Scenario I and Scenario II. Fig. 11(a) plots the ESC versus v_{V_f} performance of V_f for different values of v_{E}, while Fig. 11(b) plots the ESC versus v_{V_n} performance of V_n for different fixed v_{E}. From both the

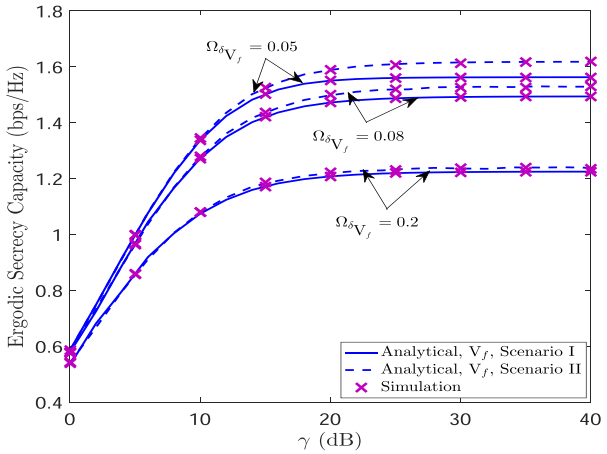

(a)

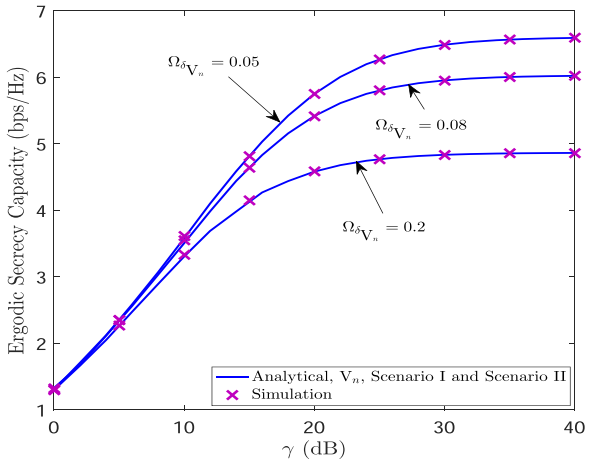

(b)

FIGURE 12. Impact of CEE on the ESC performance of (a) V_f, and (b) V_n, under Scenarios I and II.

figures, we can see that as the value of v_{V_f} (v_{V_n}) increases, the ESC performance of V_f (V_n) degrades, under both Scenarios I and II. This is because of the reason that an increasing value of v_{V_f} (v_{V_n}) also increases the time-selective nature of the legitimate fading links. Moreover, we notice that as the value of v_E increases, the ESC performance of V_f as well as V_n improves. This is expected as with increasing v_E, E's channel becomes more time-selective. Further, it can be seen that the ESC performance of V_f is better under Scenario II as compared to Scenario I owing to poorer decoding capability of E under Scenario II.

Fig. 12 illustrates the impact of CEE on the ESC performance of legitimate user vehicles, when $\Omega_{V_f} = 0$ dB, $\Omega_{V_n} = 10$ dB, $\Omega_e = -20$ dB, $m_f = m_n = m_e = 1$, $N_f = N_n = N_e = 1$, and $v_{V_f} = v_{V_n} = v_E = 50$ km/h. Specifically, Fig. 12(a) and (b) plot the ESC versus γ performance over various fixed values of $\Omega_{\delta_{V_f}}$ and $\Omega_{\delta_{V_n}}$ for legitimate user vehicles V_f and V_n, respectively. From both the figures, we can observe that as the value of CEE increases, the ESC performance of both the legitimate vehicles V_f and V_n degrade, under both Scenario I and II. Furthermore, from the plots in Fig. 12(a), we can see that the ESC performance for V_f under Scenario I underperforms than the Scenario II, because E ha sufficient decoding capability in Scenario I.

From the above description, we can conclude that the ESC performances of both user vehicles reduce with an increase in i) velocity of the legitimate user vehicles in Fig. 11, and ii) CEE associated with the legitimate user vehicles in Fig. 12, irrespective of other system/channel parameters.

VIII. CONCLUSION

In this paper, we investigated the PLS performance of SIMO NOMA-assisted vehicular communication system in the presence of nodes' mobility and CEE over Nakagami-m fading channels. Specifically, we derived the SOP and ESC expressions for both legitimate vehicles and overall system under the consideration of both Scenarios I and II formulated based on the decoding capability of eavesdropper. We further evaluated the asymptotic SOP expressions to report useful observations into the system's secrecy diversity order under three cases, i.e., 1) Case 1: when $\gamma \to \infty$, 2) Case 2: when $\Omega_f, \Omega_n \to \infty$ with fixed Ω_e, and 3) Case 3: when $\Omega_f, \Omega_n, \Omega_e \to \infty$. It is evident from this analysis that the secrecy diversity order of the considered system becomes zero under Case 1 and Case 3, since these cases provide simultaneous improvement in SNR (under Case 1) and average channel gain (under Case 3) at both legitimate user vehicles and eavesdropper vehicle, irrespective of time-varying errors due to nodes' mobility and CEE. Whereas, the zero secrecy diversity order under Case 2 is achieved due the impact of nodes' mobility and CEE. Moreover, we studied some important observations for the exact SOP and its asymptotic limits under three special cases of interest, i.e., 1) all mobile nodes with no CEE, 2) all static nodes with CEE, and 3) all static nodes with no CEE. It is observed from this analysis that the system's secrecy diversity order becomes zero for all cases, except under the setting of all static nodes with no CEE for near user vehicle where the secrecy diversity order of $m_n N_n$ can be achieved. Lastly, we verified our analytical and theoretical framework via comprehensive numerical and simulation results, and showed the impact of involved system/channel parameters on the SOP and ESC performance of the considered network setup.

APPENDIX A
PROOF OF THEOREM 1

We can express (21) into its equivalent integral form as

$$\mathcal{P}^{\mathrm{I}}_{\mathrm{sec},V_f}(\eta_{V_f}) = \int_0^\infty F_{\Lambda_{V_f}}(\eta_{V_f} x + \eta_{V_f} - 1) f_{\Lambda^{\mathrm{I}}_{E_f}}(x) dx, \quad (68)$$

which can further be expanded by invoking the CDF of Λ_{V_f} from (15) as

$$\mathcal{P}^{\mathrm{I}}_{\mathrm{sec},\mathrm{V}_f}(\eta_{\mathrm{V}_f}) = \int_0^{\xi} \frac{\Upsilon\left(m_f \mathrm{N}_f, \frac{m_f}{\Omega_f} \frac{\left(\Omega_{q_{\mathrm{V}_f}} + \frac{1}{\gamma}\right)(\eta_{\mathrm{V}_f} x + \eta_{\mathrm{V}_f} - 1)}{\rho^2_{\mathrm{V}_f}(\beta - (1-\beta)(\eta_{\mathrm{V}_f} x + \eta_{\mathrm{V}_f} - 1))}\right)}{\Gamma(m_f \mathrm{N}_f)} \times f_{\Lambda^{\mathrm{I}}_{\mathrm{E}_f}}(x)dx + \int_{\xi}^{\infty} f_{\Lambda^{\mathrm{I}}_{\mathrm{E}_f}}(x)dx, \tag{69}$$

where the limit term $\xi = \frac{1}{(1-\beta)\eta_{\mathrm{V}_f}} - 1$ can be obtained by simplifying $\eta_{\mathrm{V}_f} x + \eta_{\mathrm{V}_f} - 1 \lesseqgtr \frac{\beta}{1-\beta}$. Then, by applying the series expansion for lower incomplete Gamma function $\Upsilon(n, x)$, i.e., $\Upsilon(n, x) = (n-1)![1 - \mathrm{e}^{-x} \sum_{k=0}^{n-1} \frac{x^k}{k!}]$ [51, Eq. (8.352.6)], and after some manipulations, we can express the SOP, $\mathcal{P}^{\mathrm{I}}_{\mathrm{sec},\mathrm{V}_f}(\eta_{\mathrm{V}_f})$, in (69) as

$$\mathcal{P}^{\mathrm{I}}_{\mathrm{sec},\mathrm{V}_f}(\eta_{\mathrm{V}_f}) = \int_0^{\infty} f_{\Gamma^{\mathrm{I}}_{\mathrm{E}_f}}(x)dx - \mathcal{J}_1, \tag{70}$$

$$\text{where} \quad \mathcal{J}_1 = \sum_{k=0}^{\mathrm{N}_f m_f - 1} \frac{1}{k!} \left(\frac{m_f \left(\Omega_{q_{\mathrm{V}_f}} + \frac{1}{\gamma}\right)}{\Omega_f \rho^2_{\mathrm{V}_f}}\right)^k \times \int_0^{\xi} \frac{(\eta_{\mathrm{V}_f} x + \eta_{\mathrm{V}_f} - 1)^k}{(\beta - (1-\beta)(\eta_{\mathrm{V}_f} x + \eta_{\mathrm{V}_f} - 1))^k} \times \mathrm{e}^{-\frac{m_f}{\Omega_f}\left(\frac{\left(\Omega_{q_{\mathrm{V}_f}} + \frac{1}{\gamma}\right)\left(\eta_{\mathrm{V}_f} x + \eta_{\mathrm{V}_f} - 1\right)}{\rho^2_{\mathrm{V}_f}(\beta - (1-\beta)(\eta_{\mathrm{V}_f} x + \eta_{\mathrm{V}_f} - 1))}\right)} f_{\Lambda^{\mathrm{I}}_{\mathrm{E}_f}}(x)dx. \tag{71}$$

To simplify $\mathcal{J}_1$ in (71), we require the PDF of $\Lambda^{\mathrm{I}}_{\mathrm{E}_f}$, which can be obtained by differentiating (17) with respect to x and can be given by

$$f_{\Lambda^{\mathrm{I}}_{\mathrm{E}_f}}(x) = \frac{\left(\frac{m_e(\beta\Omega_{q_{\mathrm{E}}} + \frac{1}{\gamma})}{\Omega_e \beta \rho^2_{\mathrm{E}}}\right)^{\mathrm{N}_e m_e}}{\Gamma(\mathrm{N}_e m_e)} x^{\mathrm{N}_e m_e - 1} \mathrm{e}^{-\frac{m_e(\beta\Omega_{q_{\mathrm{E}}} + \frac{1}{\gamma})}{\Omega_e \beta \rho^2_{\mathrm{E}}} x}. \tag{72}$$

Substituting (72) into (71), we can express $\mathcal{J}_1$ as

$$\mathcal{J}_1 = \sum_{k=0}^{\mathrm{N}_f m_f - 1} \frac{1}{k!} \left(\frac{m_f \left(\Omega_{q_{\mathrm{V}_f}} + \frac{1}{\gamma}\right)}{\Omega_f \rho^2_{\mathrm{V}_f}}\right)^k \times \frac{1}{\Gamma(\mathrm{N}_e m_e)} \left(\frac{m_e(\beta\Omega_{q_{\mathrm{E}}} + \frac{1}{\gamma})}{\Omega_e \beta \rho^2_{\mathrm{E}}}\right)^{\mathrm{N}_e m_e} \times \int_0^{\xi} \frac{(\eta_{\mathrm{V}_f} x + \eta_{\mathrm{V}_f} - 1)^k x^{\mathrm{N}_e m_e - 1}}{(\beta - (1-\beta)(\eta_{\mathrm{V}_f} x + \eta_{\mathrm{V}_f} - 1))^k} e^{-\mathcal{B}_1(x)} dx, \tag{73}$$

where $\mathcal{B}_1(x) = \frac{m_f}{\Omega_f}\left(\frac{\left(\Omega_{q_{\mathrm{V}_f}} + \frac{1}{\gamma}\right)\left(\eta_{\mathrm{V}_f} x + \eta_{\mathrm{V}_f} - 1\right)}{\rho^2_{\mathrm{V}_f}(\beta - (1-\beta)(\eta_{\mathrm{V}_f} x + \eta_{\mathrm{V}_f} - 1))}\right) + \frac{m_e(\beta\Omega_{q_{\mathrm{E}}} + \frac{1}{\gamma})}{\Omega_e \beta \rho^2_{\mathrm{E}}} x$. It can be observed from (73) that the solution of the involved integral in closed-form is very tedious and intractable to obtain, therefore, we apply the Gauss-Chebyshev quadrature numerical method [66, Eq. (25.4.38)] to evaluate a tractable solution of $\mathcal{J}_1$ as

$$\mathcal{J}_1 = \sum_{k=0}^{\mathrm{N}_f m_f - 1} \sum_{u=1}^{\mathcal{N}} \frac{1}{k!} \frac{\pi}{\mathcal{N}} \left(\frac{m_f \left(\Omega_{q_{\mathrm{V}_f}} + \frac{1}{\gamma}\right)}{\Omega_f \rho^2_{\mathrm{V}_f}}\right)^k \left(\frac{\xi}{2}\right)^{\mathrm{N}_e m_e} \times \frac{1}{\Gamma(\mathrm{N}_e m_e)} \left(\frac{m_e(\beta\Omega_{q_{\mathrm{E}}} + \frac{1}{\gamma})}{\Omega_e \beta \rho^2_{\mathrm{E}}}\right)^{\mathrm{N}_e m_e} \mathcal{A}_u(\eta_{\mathrm{V}_f}). \tag{74}$$

Then, we substitute $\mathcal{J}_1$ from (74) along with the fact that $\int_0^{\infty} f_{\Gamma^{\mathrm{I}}_{\mathrm{E}_f}}(x)dx = 1$ into (70) to obtain the SOP, $\mathcal{P}^{\mathrm{I}}_{\mathrm{sec},\mathrm{V}_f}(\eta_{\mathrm{V}_f})$, as presented in (22).

APPENDIX B
PROOF OF THEOREM 2

We can express $\mathcal{P}^{\mathrm{I}}_{\mathrm{sec},\mathrm{V}_n}(\eta_{\mathrm{V}_n})$ in (23) into its equivalent integral form as

$$\mathcal{P}^{\mathrm{I}}_{\mathrm{sec},\mathrm{V}_n}(\eta_{\mathrm{V}_n}) = \int_0^{\infty} F_{\Lambda_{\mathrm{V}_n}}(\eta_{\mathrm{V}_n} x + \eta_{\mathrm{V}_n} - 1) f_{\Lambda^{\mathrm{I}}_{\mathrm{E}_n}}(x)\, dx. \tag{75}$$

To solve (75), we first substitute the CDF of Λ_{V_n} from (16) with the aid of relation $\Upsilon(n, x) = (n-1)![1 - \mathrm{e}^{-x} \sum_{k=0}^{n-1} \frac{x^k}{k!}]$ [51, Eq. (8.352.6)] and the PDF of $\Lambda^{\mathrm{I}}_{\mathrm{E}_n}$ (can be obtained by differentiating (19) with respect to x) into (75) with the use of binomial expansion to obtain

$$\mathcal{P}^{\mathrm{I}}_{\mathrm{sec},\mathrm{V}_n}(\eta_{\mathrm{V}_n}) = 1 - \sum_{r=0}^{\mathrm{N}_n m_n - 1} \sum_{p=0}^{r} \frac{1}{r!} \binom{r}{p} \left(\frac{m_n}{\Omega_n \mathcal{B}_{\mathrm{V}_n}}\right)^r \times (\eta_{\mathrm{V}_n} - 1)^{r-p} \frac{(\eta_{\mathrm{V}_n})^p}{\Gamma(\mathrm{N}_e m_e)} \left(\frac{m_e}{\Omega_e \mathcal{B}_E}\right)^{\mathrm{N}_e m_e} \times e^{-\frac{m_n(\eta_{\mathrm{V}_n} - 1)}{\Omega_n \mathcal{B}_{\mathrm{V}_n}}} \int_0^{\infty} x^{(\mathrm{N}_e m_e + p - 1)} \times \mathrm{e}^{-\left(\frac{m_e}{\Omega_e \mathcal{B}_E} + \frac{m_n \eta_{\mathrm{V}_n}}{\Omega_n \mathcal{B}_{\mathrm{V}_n}}\right)x} dx, \tag{76}$$

and then with the help of the identity $\int_0^{\infty} z^n e^{-\mu z} dz = \frac{\Gamma(n+1)}{\mu^{n+1}}$, we can simplify the integral in (76), and deduce the SOP expression of V_n as presented in (24).

APPENDIX C
PROOF OF THEOREM 3

Expressing (26) into its equivalent integral form, we get

$$\mathcal{P}^{\mathrm{II}}_{\mathrm{sec},\mathrm{V}_f}(\eta_{\mathrm{V}_f}) = \int_0^{\xi} F_{\Lambda_{\mathrm{V}_f}}(\eta_{\mathrm{V}_f} x + \eta_{\mathrm{V}_f} - 1) f_{\Lambda^{\mathrm{II}}_{\mathrm{E}_f}}(x)dx + \int_{\xi}^{\frac{\beta}{1-\beta}} f_{\Lambda^{\mathrm{II}}_{\mathrm{E}_f}}(x)dx. \tag{77}$$

Further, by invoking the CDF of Λ_{V_f} from (15) with the use of the identity [51, Eq. (8.352.6)], and applying the fact

$\int_0^{\frac{\beta}{1-\beta}} f_{\Lambda_{\mathrm{E}_f^{\mathrm{II}}}}(x)dx = 1$, we can express $\mathcal{P}^{\mathrm{II}}_{\mathrm{sec},\mathrm{V}_f}(\eta_{\mathrm{V}_f})$ in (77) as

$$\mathcal{P}^{\mathrm{II}}_{\mathrm{sec},\mathrm{V}_f}(\eta_{\mathrm{V}_f}) = 1 - \mathcal{J}_2, \tag{78}$$

$$\text{where } \mathcal{J}_2 = \sum_{s=0}^{\mathrm{N}_f m_f - 1} \frac{1}{s!} \left(\frac{m_f \left(\Omega_{q_{\mathrm{V}_f}} + \frac{1}{\gamma} \right)}{\Omega_f \rho^2_{\mathrm{V}_f}} \right)^s \times \int_0^{\xi} \frac{(\eta_{\mathrm{V}_f} x + \eta_{\mathrm{V}_f} - 1)^s}{(\beta - (1-\beta)(\eta_{\mathrm{V}_f} x + \eta_{\mathrm{V}_f} - 1))^s} \times \mathrm{e}^{-\frac{m_f}{\Omega_f} \left(\frac{\left(\Omega_{q_{\mathrm{V}_f}} + \frac{1}{\gamma} \right)(\eta_{\mathrm{V}_f} x + \eta_{\mathrm{V}_f} - 1)}{\rho^2_{\mathrm{V}_f}(\beta - (1-\beta)(\eta_{\mathrm{V}_f} x + \eta_{\mathrm{V}_f} - 1))} \right) x} f_{\Lambda_{\mathrm{E}_f^{\mathrm{II}}}}(x)dx. \tag{79}$$

To simplify integral in $\mathcal{J}_2$, we first require to deduce the PDF of $\Lambda_{\mathrm{E}_f^{\mathrm{II}}}$ which can be obtained by differentiating (18) with respect to x as

$$f_{\Lambda_{\mathrm{E}_f^{\mathrm{II}}}}(x) = \frac{1}{\Gamma(\mathrm{N}_e m_e)} \left(\frac{m_e \left(\Omega_{q_{\mathrm{E}}} + \frac{1}{\gamma} \right)}{\Omega_e \rho^2_{\mathrm{E}}} \right)^{\mathrm{N}_e m_e} \times \frac{\beta x^{\mathrm{N}_e m_e - 1}}{(\beta - (1-\beta)x)^{\mathrm{N}_e m_e + 1}} \mathrm{e}^{-\frac{m_e \left(\Omega_{q_{\mathrm{E}}} + \frac{1}{\gamma} \right)}{\Omega_e \rho^2_{\mathrm{E}} (\beta - (1-\beta)x)} x}. \tag{80}$$

Invoking (80) into $\mathcal{J}_2$, we can obtain

$$\mathcal{J}_2 = \sum_{s=0}^{\mathrm{N}_f m_f - 1} \frac{1}{s!} \left(\frac{m_f \left(\Omega_{q_{\mathrm{V}_f}} + \frac{1}{\gamma} \right)}{\Omega_f \rho^2_{\mathrm{V}_f}} \right)^s \frac{\beta}{\Gamma(\mathrm{N}_e m_e)} \times \left(\frac{m_e \left(\Omega_{q_{\mathrm{E}}} + \frac{1}{\gamma} \right)}{\Omega_e \rho^2_{\mathrm{E}}} \right)^{\mathrm{N}_e m_e} \int_0^{\xi} \frac{1}{(\beta - (1-\beta)x)^{\mathrm{N}_e m_e + 1}} \times \frac{(\eta_{\mathrm{V}_f} x + \eta_{\mathrm{V}_f} - 1)^s x^{\mathrm{N}_e m_e - 1}}{(\beta - (1-\beta)(\eta_{\mathrm{V}_f} x + \eta_{\mathrm{V}_f} - 1))^s} e^{-\mathcal{B}_2(x)} dx, \tag{81}$$

where $\mathcal{B}_2(x) = \frac{m_f}{\Omega_f} \left(\frac{\left(\Omega_{q_{\mathrm{V}_f}} + \frac{1}{\gamma} \right)(\eta_{\mathrm{V}_f} x + \eta_{\mathrm{V}_f} - 1)}{\rho^2_{\mathrm{V}_f}(\beta - (1-\beta)(\eta_{\mathrm{V}_f} x + \eta_{\mathrm{V}_f} - 1))} \right) + \frac{m_e \left(\Omega_{q_{\mathrm{E}}} + \frac{1}{\gamma} \right)}{\Omega_e \rho^2_{\mathrm{E}} (\beta - (1-\beta)x)} x.$

Similar to (73), the closed-form expression of the integral in (81) is intractable and tedious to obtain, therefore, for tractability, we use the Gauss-Chebyshev quadrature method [66, Eq. (25.4.38)] to simplify the integral in $\mathcal{J}_2$. Then, substituting the result into (78), we get $\mathcal{P}^{\mathrm{II}}_{\mathrm{sec},\mathrm{V}_f}(\eta_{\mathrm{V}_f})$ as presented in (27).

APPENDIX D
PROOF OF THEOREM 4

From (53), we can express the ESC of V_f as

$$\overline{\mathbf{C}}^{\mathrm{I,\,Approx}}_{\mathrm{sec},\mathrm{V}_f} = \underbrace{\mathbb{E}\left[\log_2(1+\Lambda_{\mathrm{V}_f})\right]}_{\triangleq \overline{\mathbf{C}}_{\mathrm{V}_f}} - \underbrace{\mathbb{E}\left[\log_2(1+\Lambda_{\mathrm{E}_f^{\mathrm{I}}})\right]}_{\triangleq \overline{\mathbf{C}}_{\mathrm{E}_f^{\mathrm{I}}}}. \tag{82}$$

where $\overline{\mathbf{C}}_{\mathrm{V}_f}$ can be expressed as

$$\overline{\mathbf{C}}_{\mathrm{V}_f} = \frac{1}{\ln(2)} \int_0^{\infty} \ln(1+y) f_{\Lambda_{\mathrm{V}_f}}(y)dy. \tag{83}$$

To solve the integral in (83), we first evaluate the PDF of Λ_{V_f} by differentiating (15) with respect to y as

$$f_{\Lambda_{\mathrm{V}_f}}(y) = \frac{\beta}{\Gamma(\mathrm{N}_f m_f)} \left(\frac{m_f}{\Omega_f} \frac{1}{\rho^2_{\mathrm{V}_f}} \left(\Omega_{q_{\mathrm{V}_f}} + \frac{1}{\gamma} \right) \right)^{\mathrm{N}_f m_f} \times \frac{y^{\mathrm{N}_f m_f - 1}}{(\beta - (1-\beta)y)^{\mathrm{N}_f m_f + 1}} \mathrm{e}^{-\frac{m_f}{\Omega_f} \frac{\left(\Omega_{q_{\mathrm{V}_f}} + \frac{1}{\gamma} \right) y}{\rho^2_{\mathrm{V}_f}(\beta - (1-\beta)y)}}. \tag{84}$$

Then, invoking $f_{\Lambda_{\mathrm{V}_f}}(y)$ from (84) into (83) followed by the substitution $\frac{y}{\beta-(1-\beta)y} = t$ and with some simplifications, we can express (83) as

$$\overline{\mathbf{C}}_{\mathrm{V}_f} = \frac{1}{\ln(2)\Gamma(\mathrm{N}_f m_f)} \left(\frac{m_f}{\Omega_f} \frac{1}{\rho^2_{\mathrm{V}_f}} \left(\Omega_{q_{\mathrm{V}_f}} + \frac{1}{\gamma} \right) \right)^{\mathrm{N}_f m_f} \times \left[\int_0^{\infty} \ln(1+t)\, \mathrm{e}^{-\frac{m_f}{\Omega_f \rho^2_{\mathrm{V}_f}} \left(\Omega_{q_{\mathrm{V}_f}} + \frac{1}{\gamma} \right) t} t^{\mathrm{N}_f m_f - 1} dt - \int_0^{\infty} \ln(1+(1-\beta)t)\, \mathrm{e}^{-\frac{m_f}{\Omega_f \rho^2_{\mathrm{V}_f}} \left(\Omega_{q_{\mathrm{V}_f}} + \frac{1}{\gamma} \right) t} t^{\mathrm{N}_f m_f - 1} dt \right]. \tag{85}$$

The above integrals can be evaluated by first applying the transformation $\ln(1+z) = \mathcal{G}^{1,2}_{2,2}(z|^{1,1}_{1,0})$ [65, Eq. (01.04.26.0003.01)], and thereafter, simplifying the resultant integrals with the aid of [51, Eq. (7.813.1)], to obtain $\overline{\mathbf{C}}_{\mathrm{V}_f}$ as shown in (55).

Furthermore, we can express $\overline{\mathbf{C}}_{\mathrm{E}_f^{\mathrm{I}}}$ in (82) as

$$\overline{\mathbf{C}}_{\mathrm{E}_f^{\mathrm{I}}} = \frac{1}{\ln(2)} \int_0^{\infty} \ln(1+y) f_{\Lambda_{\mathrm{E}_f^{\mathrm{I}}}}(y)dy. \tag{86}$$

By substituting the PDF of $\Lambda_{\mathrm{E}_f^{\mathrm{I}}}$ from (72) along with the transformation [65, Eq. (01.04.26.0003.01)] into (86), and simplifying the resultant integral with the help of [51, Eq. (7.813.1)] to get $\overline{\mathbf{C}}_{\mathrm{E}_f^{\mathrm{I}}}$ as presented in (56).

REFERENCES

[1] S. Chen et al., "Vehicle-to-everything (V2X) services supported by LTE-based systems and 5G," *IEEE Commun. Standards Mag.*, vol. 1, no. 2, pp. 70–76, 2017.

[2] B. Ji et al., "Survey on the internet of vehicles: Network architectures and applications," *IEEE Commun. Standards Mag.*, vol. 4, no. 1, pp. 34–41, Mar. 2020.

[3] "5G automotive association (5GAA)." [Online]. Available: http://5gaa.org/

[4] H. Zhou, W. Xu, J. Chen, and W. Weng, "Evolutionary V2X technologies toward the internet of vehicles: Challenges and opportunities," *Proc. IEEE*, vol. 108, no. 2, pp. 308–323, Feb. 2020.

[5] B. Di, L. Song, Y. Li, and Z. Han, "V2X meets NOMA: Non-orthogonal multiple access for 5G-enabled vehicular networks," *IEEE Wireless Commun.*, vol. 24, no. 6, pp. 14–21, Dec. 2017.

[6] K. Yang, N. Yang, N. Ye, M. Jia, Z. Gao, and R. Fan, "Non-orthogonal multiple access: Achieving sustainable future radio access," *IEEE Commun. Mag.*, vol. 57, no. 2, pp. 116–121, Feb. 2019.

[7] L. Dai, B. Wang, Z. Ding, Z. Wang, S. Chen, and L. Hanzo, "A survey of non-orthogonal multiple access for 5G," *IEEE Commun. Surv. Tut.*, vol. 20, no. 3, pp. 2294–2323, Jul.–Sep. 2018.

[8] J. Liberti, S. Moshavi, and P. Zablocky, "Successive interference cancellation," U.S. Patent 8670418, Mar. 11th 2014.

[9] B. Di, L. Song, Y. Li, and G. Y. Li, "Non-orthogonal multiple access for high-reliable and low-latency V2X communications in 5G systems," *IEEE J. Sel. Areas Commun.*, vol. 35, no. 10, pp. 2383–2397, Oct. 2017.

[10] Z. Lu, G. Qu, and Z. Liu, "A. survey on recent advances in vehicular network security, trust, and privacy," *IEEE Trans. Intel. Transp. Sys.*, vol. 20, no. 2, pp. 760–776, Feb. 2019.

[11] Z. Shu, Y. Qian, and S. Ci, "On physical layer security for cognitive radio networks," *IEEE Netw.*, vol. 27, no. 3, pp. 28–33, May/Jun. 2013.

[12] Y. Zou, J. Zhu, X. Wang, and L. Hanzo, "A survey on wireless security: Technical challenges, recent advances, and future trends," *Proc. IEEE*, vol. 104, no. 9, pp. 1727–1765, Sep. 2016.

[13] G. Anjos, D. Castanheira, A. Silva, A. Gameiro, M. Gomes, and J. P. Vilelaw, "Exploiting the reciprocal channel for discrete jamming to secure wireless communications against multiple-antenna eavesdropper," *IEEE Access*, vol. 6, pp. 33410–33420, 2018.

[14] T. M. C. Chu and H. Zepernick, "Outage probability and secrecy capacity of a non-orthogonal multiple access system," in *Proc. 11th Int. Conf. Signal Process. Commun. Syst.*, 2017, pp. 1–6.

[15] H. Lei,, R. Gao, K. -H. Park, I. S. Ansari, K. J. Kim, and M. -S. Alouini, "On secure downlink NOMA systems with outage constraint," *IEEE Trans. Commun.*, vol. 68, no. 12, pp. 7824–7836, Dec. 2020.

[16] Z. Xiang, X. Tong, and Y. Cai, "Secure transmission for NOMA systems with imperfect SIC," *China Commun.*, vol. 17, no. 11, pp. 67–78, Nov. 2020.

[17] Y. Liu, Z. Qin, M. Elkashlan, Y. Gao, and L. Hanzo, "Enhancing the physical layer security of non-orthogonal multiple access in large-scale networks," *IEEE Trans. Wireless Commun.*, vol. 16, no. 3, pp. 1656–1672, Mar. 2017.

[18] Z. Xiang, W. Yang, Y. Cai, J. Xiong, Z. Ding, and Y. Song, "Secure transmission in a NOMA-assisted IoT network with diversified communication requirements," *IEEE Internet Things J.*, vol. 7, no. 11, pp. 11157–11169, Nov. 2020.

[19] B. M. ElHalawany and K. Wu, "Physical-layer security of NOMA systems under untrusted users," in *Proc. IEEE Glob. Commun. Conf.*, 2018, pp. 1–6.

[20] A. Abushattal, S. Althunibat, M. Qaraqe, and H. Arslan, "A secure downlink NOMA scheme against unknown internal eavesdroppers," *IEEE Wireless Commun. Lett.*, vol. 10, no. 6, pp. 1281–1285, Jun. 2021.

[21] Y. Zhang, H.-M. Wang, Q. Yang, and Z. Ding, "Secrecy sum rate maximization in non-orthogonal multiple access," *IEEE Commun. Lett.*, vol. 20, no. 5, pp. 930–933, May 2016.

[22] K. Cao, B. Wang, H. Ding, L. Lv, J. Tian, and F. Gong, " On the security enhancement of uplink NOMA systems with jammer selection," *IEEE Trans. Commun*. vol. 68, no. 9, pp. 5747–5763, Sep. 2020.

[23] B. Chen, R. Li, Q. Ning, K. Lin, C. Han, and V. C. M. Leung, "Security at physical layer in NOMA relaying networks with cooperative jamming," *IEEE Trans. Veh. Technol*., vol. 71, no. 4, pp. 3883–3888, Apr. 2022. doi: 10.1109/TVT.2022.3144531.

[24] C. Zhang, F. Jia, Z. Zhang, J. Ge, and F. Gong, "On the physical layer security designs for 5G NOMA systems with a stronger near-end internal eavesdropper," *IEEE Trans. Veh. Technol.*, vol. 69, no. 11, pp. 13005–13017, Nov. 2020.

[25] C. Gong, X. Yue, Z. Zhang, X. Wang, and X. Dai, "Enhancing physical layer security with artificial noise in large-scale NOMA networks," *IEEE Trans. Veh. Technol.*, vol. 70, no. 3, pp. 2349–2361, Mar. 2021.

[26] L. Lv, Z. Ding, Q. Ni, and J. Chen, "Secure MISO-NOMA transmission with artificial noise," *IEEE Tran. Veh. Technol.*, vol. 67, no. 7, pp. 6700–6705, Jul. 2018.

[27] X. Li et al., "Security analysis of multi-antenna NOMA networks under I/Q imbalance," *Electronics*, vol. 8, Nov. 2019, Art. no. 1327.

[28] H. Lei et al., "On secure NOMA systems with transmit antenna selection schemes," *IEEE Access*, vol. 5, pp. 17450–17464, 2017.

[29] D. Deng et al., "Impact of antenna selection on physical-layer security of NOMA networks," *Wireless Commun. Mobile Comput.*, 2018, Jan. 2018, Art. no. 2390834.

[30] X. Pei, H. Yu, M. Wen, Q. Li, and Z. Ding, "Secure outage analysis for cooperative NOMA systems with antenna selection," *IEEE Trans. Veh. Technol.*, vol. 69, no. 4 pp. 4503–4507, Apr. 2020.

[31] M. Ghous et al., "Performance analysis and beamforming design of a secure cooperative MISO-NOMA network," *Sensors*, vol. 21, Jun. 2021, Art. no. 4180.

[32] K. Cao, B. Wang, H. Ding, T. Li, J. Tian, and F. Gong, "Secure transmission designs for NOMA systems against internal and external eavesdropping," *IEEE Trans. Inf. Forensics Secur.*, vol. 15, pp. 2930–2943, 2020.

[33] W. Zhang, J. Chen, Y. Kuo, and Y. Zhou, "Transmit beamforming for layered physical layer security," *IEEE Trans. Veh. Technol.*, vol. 68, no. 10, pp. 9747–9760, Oct. 2019.

[34] H.-M Wang, X. Zhang, Q. Yang, and T. A. Tsiftsis, "Secure users oriented downlink MISO NOMA," *IEEE J. Sel. Topics Signal Process.*, vol. 13, no. 3, pp. 671–684, Jun. 2019.

[35] R. M. Christopher and D. K. Borah, "Physical layer security for weak user in MISO NOMA using directional modulation (NOMAD)," *IEEE Commun. Lett.*, vol. 24, no. 5, pp. 956–960, May 2020.

[36] N. Zhao et al., "Secure transmission via joint precoding optimization for downlink MISO NOMA," *IEEE Trans. Veh. Technol.*, vol. 68, no. 8, pp. 7603–7615, Aug. 2019.

[37] Y. Qi and M. Vaezi, "Secure transmission in MIMO-NOMA networks," *IEEE Commun. Lett*. vol. 24, no. 12, pp. 2696–2700, Dec. 2020.

[38] H. Lei et al., "Secrecy outage of max-min TAS scheme in MIMO-NOMA systems," *IEEE Trans. Veh. Technol.*, vol. 67, no. 8, pp. 6981–6990, Aug. 2018.

[39] N-P. Nguyen et al., "Performance analysis and optimization of ergodic secrecy rates for downlink data transmission in massive MIMO-NOMA networks," *Wireless Netw.*, vol. 29, pp. 355–365, Jan. 2022.

[40] V. Kumar, M. F. Flanagan, D. B. Da Costa, and L.-N. Tran, "On the secrecy rate of downlink NOMA in underlay spectrum sharing with imperfect CSI: Invited paper," in *Proc. 28th Int. Conf. Telecommun.*, 2021, pp. 167–173.

[41] Y. Chen, L. Wang, Y. Ai, B. Jiao, and L. Hanzo, "Performance analysis of NOMA-SM in vehicle-to-vehicle massive MIMO channels," *IEEE J. Sel. Areas Commun.*, vol. 35, no. 12, pp. 2653–2666, Dec. 2017.

[42] D. K. Patel et al., "Performance analysis of NOMA in vehicular communications over i.n.i.d Nakagami-m fading channels," *IEEE Trans. Wireless Commun*., vol. 20, no. 10, pp. 6254–6268, Oct. 2021, doi: 10.1109/TWC.2021.3073050.

[43] Y. Sun, Z. Ding, X. Dai, K. Navaie, and D. K. C. So, "Performance of downlink NOMA in vehicular communication networks: An analysis based on poisson line Cox point process," *IEEE Trans. Veh. Technol.*, vol. 69, no. 11, pp. 14001–14006, Nov. 2020.

[44] O. Ozdemir, "Performance evaluation of NOMA-based cooperative communications over cascaded rician fading channels," in *Proc. 27th Signal Process. Commun. Appl. Conf.*, 2019, pp. 1–4.

[45] N. Jaiswal and N. Purohit, "Performance of downlink NOMA-enabled vehicular communications over double rayleigh fading channels," *IET Commun*., vol. 14, no. 20, pp. 3652–3660, Sep. 2020.

[46] N. Jaiswal and N. Purohit, "Performance analysis of NOMA-enabled vehicular communication systems with transmit antenna selection over double Nakagami-*m* fading," *IEEE Trans. Veh. Technol*, vol. 70, no. 12, pp. 12725–12741, Dec. 2021.

[47] L. Wei et al., "Secure performance analysis and optimization for FD-NOMA vehicular communications," *China Commun.*, vol. 17, no. 11, pp. 29–41, Nov. 2020.
[48] W. Xie, J. Liao, C. Yu, P. Zhu, and X. Liu, "Physical layer security performance analysis of the FD-based NOMA-VC system," *IEEE Access*, vol. 7, pp. 115568–115573, 2019.
[49] N. Jaiswal, A. Pandey, S. Yadav, and N. Purohit, "Intercept probability analysis of NOMA-enabled V2V communications over double-Rayleigh fading channels," in *Proc. IEEE Int. Black Sea Conf. Commun. Netw.*, 2022, pp. 191–196.
[50] N. Jaiswal, A. Pandey, S. Yadav, N. Purohit, L. Bariah, and S. Muhaidat, "On the performance of NOMA-enabled V2V communications under joint impact of nodes mobility and channel estimation error," in *Proc. 4th Int. Conf. Adv. Commun. Technol. Netw.*, 2021, pp. 1–9.
[51] I. S. Gradshteyn and I. M. Ryzhik, *Tables of Integrals, Series, and Products*, 6th ed. New York, NY, USA: Academic Press, 2000.
[52] J. P. Kermoal, L. Schumacher, K. I. Pedersen, P. E. Mogensen, and F. Frederiksen, "A stochastic MIMO radio channel model with experimental validation," *IEEE J. Sel. Areas Commun.*, vol. 20, no. 6, pp. 1211–1226, Aug. 2002.
[53] G. J. Foschini and M. J. Gans, "On limits of wireless communications in a fading environment when using multiple antennas," *Wireless Pers.Commun.*, vol. 6, pp. 311–335, Mar. 1998.
[54] V. Kumar, B. Cardiff, S. Prakriya, and M. F. Flanagan, "Link-layer capacity of downlink NOMA with generalized selection combining receivers," in *Proc. IEEE Int. Conf. Commun.*, 2020, pp. 1–7.
[55] C. Yan, A. Harada, A. Benjebbour, Y. Lan, A. Li, and H. Jiang, "Receiver design for downlink non-orthogonal multiple access (NOMA)," in *Proc. IEEE 81st Veh. Technol. Conf.*, 2015, pp. 1–6.
[56] R. He, A. F. Molisch, F. Tufvesson, Z. Zhong, B. Ai, and T. Zhang, "Vehicle-to-vehicle propagation models with large vehicle obstructions," *IEEE Trans. Intell. Trans. Sys.*, vol. 15, no. 5, pp. 2237–2248, Oct. 2014.
[57] A. Tassi, M. Egan, R. J. Piechocki, and A. Nix, "Modeling and design of millimeter-wave networks for highway vehicular communication," *IEEE Trans. Veh. Technol.*, vol. 66, no. 12, pp. 10676–10691, Dec. 2017.
[58] M. Suneya et al., "Fading characteristic modeling of V2V communication at 700MHz band and the system margin design," in *Proc. 20th ITS World Congr. ITS Jpn.*, 2013, pp. 1–10.
[59] Y. M. Khattabi and M. M. Matalgah, "Performance analysis of multiple-relay AF cooperative systems over Rayleigh time-selective fading channels with imperfect channel estimation," *IEEE Trans. Veh. Technol.*, vol. 65, no. 1, pp. 427–434, Jan. 2016.
[60] A. A. Abu-Dayya and N. C. Beaulieu, "Outage probabilities of cellular mobile radio systems with multiple Nakagami interferers," *IEEE Trans. Veh. Technol.*, vol. 40, no. 4, pp. 757–768, Nov. 1991.
[61] G. T. Djordjevic, K. Kansanen, and A. M. Cvetkovic, "Outage performance of decode-and-forward cooperative networks over Nakagami-*m* fading with node blockage," *IEEE Trans Wireless Commun.*, vol. 15, no. 9, pp. 5848–5860, Sep. 2016.
[62] W. Zeng, J. Zhang, S. Chen, K. P. Peppas, and B. Ai, "Physical layer security over fluctuating two-ray fading channels," *IEEE Trans. Veh. Technol.*, vol. 67, no. 9, pp. 8949–8953, Sep. 2018.
[63] J. Zhang, W. Zeng, X. Li, Q. Sun, and K. P. Peppas, "New results on the fluctuating two-ray model with arbitrary fading parameters and its applications," *IEEE Trans. Veh. Technol.*, vol. 67, no. 3, pp. 2766–2770, Mar. 2018.
[64] A. P. Prudnikov, Y. A. Brychkov, and O. I. Marichev, *Integrals and Series: Elementary Functions* vol. 1. New York, NY, USA: Gordon & Breach, 1986.
[65] "The wolfram functions site." [Online]. Available: http://functions.wolfram.com/
[66] M. Abromowitz and I. A. Stegun, *Handbook of Mathematical Functions With Formulas, Graphs, and Mathematical Tables*. New York, NY, USA: Dover, 1970.
[67] K. P. Peppas, N. C. Sagias, and A. Maras, "Physical layer security for multiple-antenna systems: A unified approach," *IEEE Trans. Commun.*, vol. 64, no. 1, pp. 314–328, Jan. 2016.

NEHA JAISWAL (Student Member, IEEE) received the B.Tech. degree in electronics and communication engineering and the M.Tech. degree in digital communications from Uttar Pradesh Technical University, Lucknow, India, in 2008 and 2016, respectively. She is currently working toward the Ph.D. degree with the Department of Electronics and Communication Engineering, Indian Institute of Information Technology Allahabad, Prayagraj, India. Her research interests include wireless communications, non-orthogonal multiple access, vehicle-to-vehicle communications, generalized fading channels, and physical layer security.

ANSHUL PANDEY (Member, IEEE) received the B.Tech. degree in electronics and communication engineering from the PDPM-Indian Institute of Information Technology Design and Manufacturing, Jabalpur, India, in 2012, the M.Tech. degree in advance networks from the ABV-Indian Institute of Information Technology and Management, Gwalior, India, in 2016, and the Ph.D. degree with the Department of Electronics and Communication Engineering, Indian Institute of Information Technology Allahabad, Allahabad, India, in 2021. He is currently a Senior Researcher with the Secure Systems Research Center, Technology Innovation Institute, Abu Dhabi, UAE. His research interests include cooperative relaying for wireless vehicular networks, physical layer security, multiple-input-multiple-output communications, and signal processing.

SUNEEL YADAV (Senior Member, IEEE) received the B.Tech. degree in electronics and communication engineering from the Meerut Institute of Engineering and Technology, Meerut, India, in 2008, the M.Tech. degree in digital communications from the ABV-Indian Institute of Information Technology and Management, Gwalior, India, in 2012, and the Ph.D. degree in discipline of electrical engineering from the Indian Institute of Technology Indore, India, in 2016. He is currently with the Department of Electronics and Communication Engineering, Indian Institute of Information and Technology Allahabad, Allahabad, India, as an Assistant Professor. He has numerous publications in peer-reviewed journals and conferences. He is a Reviewer in a number of international journals including IEEE TRANSACTIONS ON VEHICULAR TECHNOLOGY, IEEE COMMUNICATIONS LETTERS, IEEE SYSTEMS JOURNAL, IEEE ACCESS, and *Transactions on Emerging Telecommunications Technologies*. His research interests include wireless relaying techniques, cooperative communications, cognitive relaying networks, device-to-device communications, signal processing, physical layer security, and MIMO systems.

NEETESH PUROHIT (Senior Member, IEEE) received the bachelor's, master's, and Ph.D. degrees in 1998, 2001, and 2008, respectively. He is currently a Professor with the Department of Electronics and Communication Engineering, Indian Institute of Information Technology Allahabad, Allahabad, India. He has authored or coauthored several papers in reputed journals and conferences. His research interests include wireless communications, wireless sensor networks, and signal processing. He has also organized eight IEEE international conferences and two IEEE sponsored workshops.

DEVENDRA SINGH GURJAR (Senior Member, IEEE) received the B.Tech. degree in electronics and communications engineering from Uttar Pradesh Technical University, Lucknow, India, in 2011, the M.Tech. degree in wireless communications and computing from the Indian Institute of Information Technology, Allahabad, Allahabad, India, in 2013, and the Ph.D. degree in electrical engineering from the Indian Institute of Technology Indore, Indore, India, in 2017. He was with the Department of Electrical and Computer Engineering, University of Saskatchewan, Saskatoon, SK, Canada, as a Postdoctoral Research Fellow. He is currently an Assistant Professor with the Department of Electronics and Communication Engineering, National Institute of Technology Silchar, Silchar, India. He has numerous publications in peer-reviewed journals and conferences. His research interests include MIMO communication systems, cooperative relaying, device-to-device communications, smart grid communications, physical layer security, and simultaneous wireless information and power transfer. He is also a Member of the IEEE Communications Society and the IEEE Vehicular Technology Society. He was the recipient of Alain Bensoussan Fellowship, in 2019, from the European Research Consortium for Informatics and Mathematics.